

Modeling the impacts of recent climate change on ecosystem productivity across
North America

by

Zelalem Amdie Mekonnen

A thesis submitted to the Faculty of Graduate Studies and Research
in partial fulfillment of the requirements for the degree of

Doctor of Philosophy

in

Water and Land Resources

Department of Renewable Resources
University of Alberta

© Zelalem Amdie Mekonnen, 2015

Abstract

There is evidence of warming and changes in precipitation over recent decades in most regions of North America (NA) that are affecting ecosystem productivity. The impacts of these changes on land-atmosphere carbon exchange over a wide range of biomes are spatially heterogeneous and uncertain. In this study, a comprehensive mathematical process model, *ecosys*, was used to estimate the impacts of climate change and major droughts of the last three decades (1979 – 2010) on ecosystem productivity across NA. Uncertainties in model estimates subject to inherent model characteristics and external model drivers such as weather and soil were rigorously tested at selected eddy covariance (EC) flux tower sites over a wide range of biomes and climates. In a site scale test of model results, annual gross primary productivity (GPP) modeled for pixels which corresponded to the locations of 20 EC towers in diverse climate zones across NA correlated well ($R^2 = 0.76$) with annual GPP derived from the flux towers in 2005. In a continental-scale test of model results, spatial anomalies in leaf area indices (LAI) from long-term means modeled during major drought events in 1988 and 2002 agreed well with those in Normalized Difference Vegetation Index (NDVI) (geographically weighted regression, $R^2 = 0.84$ in 1988, 0.71 in 2002). GPP modeled in eastern temperate forests and most areas with lower mean annual air temperature (T_a), such as those in northern forests and Taiga, increased due to early spring and late autumn warming, and these eco-regions contributed 92% of the increases in NA GPP of the past 30 years. However, modeled GPP declined in most southwestern regions of NA (accounting >50% of the ecosystems with declining GPP), due to water stress from rising T_a and declining precipitation. Overall, NA modeled GPP increased by 5.8% in the last 30 years, with a positive trend of $+0.012 \text{ Pg C yr}^{-1}$ and a range of -1.16 to $+0.87 \text{ Pg C yr}^{-1}$ caused by interannual variability of GPP from the long-term (1980 – 2010) mean. NA modeled net ecosystem productivity (NEP) declined by 92%

(0.50 Pg C yr⁻¹) and 90% (0.49 Pg C yr⁻¹) from the long-term mean (+0.54 Pg C yr⁻¹), during droughts in 1988 and 2002 respectively. The modeled result in 2002 was corroborated with similar estimate from top-down atmospheric inversion modeling from CarbonTracker that estimated 88% (0.37 Pg C yr⁻¹) declines in 2002 carbon sink from the long-term (2000 - 2010) mean (0.42 Pg C yr⁻¹). Although NA ecosystems in the model remained a much smaller carbon sink during these two drought years, the significant drops in NEP offset 28% of the long-term carbon gains from the long-term mean over the last three decades. The long-term modeled terrestrial carbon sink was estimated to offset ~30% of the fossil fuel emissions of NA, however only 0.03 and 3.2% were offset in 1988 and 2002 leaving almost all fossil fuel emissions to the atmosphere. Interannual variabilities in modeled mid-August LAI and NDVI were the greatest in southwest of US and part of the Great Plains, which could be as a result of frequent El Niño–Southern Oscillation' events that led to major droughts. Although NA terrestrial biosphere has been modeled as a long-term carbon sink, further warming and projected dryness could enhance carbon release hence may reduce net carbon sink of the continent.

Acknowledgments

I would like to express my sincere gratitude for my supervisor Dr. Robert Grant, for his guidance, patience, continuous support and mentorship over the years and I am truly fortunate to have the opportunity of working with him. He has always been supportive and I greatly appreciate the insightful discussions we had that helped me throughout my research. I would also like to thank my committee members Dr. Derek Mackenzie, Dr. Miles Dyck and Dr. John Gamon for their guidance and constructive suggestions.

I would like to acknowledge the Multi-scale Synthesis and Terrestrial Model Intercomparison Project of the North America Carbon Program that I have been fortunate to be involved, for providing such an extensive large scale environmental model driver data. This work also required extensive computational facilities which were provided by WestGrid supercomputing infrastructure without which the project would not have been realized. Many thanks to University of Alberta AICT staffs: Denise Thornton, Dr. Masao Fujinaga, Dr. Jon Johansson for providing continuous support and putting up with the huge computing time and resources I took of this project and special thanks to Henry Zhang for computational support on WestGrid.

Many thanks to my fellow lab mates Mohammad Mezbahuddin, Nilusha Welegedara, Tracy Kinch and Sanatan for never ceasing support and thorough discussions that we have had over the years. I also like to thank all my friends for all the great friendship, encouragements and they were great motivations during the ups and downs.

I am extremely grateful for the funding I received from my supervisor provided by NSERC Discovery Frontiers (DF) grant through Arctic Development and Adaptation to Permafrost in Transition (ADAPT), and for funding the several international conferences that I have attended

which helped me communicate my work to a wide range of scholars. Many thanks to the Faculty of Graduate Studies and Research and all staffs of the Department of Renewable Resources, and special thanks to Amanda Brown and Christie Nohos who are extremely helpful and always willing to extend their assistant whenever needed.

I owe my family a lot. I always feel blessed and stronger by their unconditional support and love. You are always my biggest inspirations that helped me through the ups and downs during the course of my study. I would finally like to express my sincere thanks for all who directly or indirectly contributed to the betterment of my work over the years.

Table of Contents

Chapter 1	1
Introduction	1
1.1. Evidence of Climate Change	1
1.2. Ecosystem Responses to Climate Change	4
1.3. Estimating the Impacts of Climate Change on Ecosystem Productivity	6
1.3.1. Approaches in Estimating Land-atmosphere Carbon Exchange.....	6
1.3.2. Uncertainties in Estimating Land-atmosphere Carbon Exchange.....	8
1.4. Overview of the Study	10
Chapter 2	14
Sensitivity of modeled NEP to climate and soil drivers at site and regional scales: implications for upscaling ecosystem models	14
2.1. Introduction.....	14
2.2. Methods.....	17
2.2.1. Model Description	18
2.2.1.1. Effects of Canopy Water Status on GPP	18
2.2.1.2. Effects of Canopy Temperature on GPP	19
2.2.1.3. Effects of Nutrient Status on GPP	19
2.2.1.4. Effects of Temperature on R_a and R_h	19
2.2.2. Measured and Gridded Weather and Soil	20
2.2.2.1. Measured Weather and Soil Inputs.....	20
2.2.2.2. Gridded Weather and Soil Inputs	20

2.2.3. Simulation Design.....	21
2.3. Results.....	23
2.3.1. Comparison of Gridded vs. Measured Weather and Soil.....	23
2.3.2. Sensitivity of NEP to Gridded Climate and Soil.....	24
2.4. Discussion.....	29
2.4.1. Uncertainties in Gridded Weather and Soil.....	29
2.4.2. Gridded Weather Attributes that Caused Differences in Modeled NEP.....	31
2.4.3. Gridded Soil Attributes that Control NEP Deviations	33
2.5. Conclusions.....	34
Chapter 3	54
Contrasting changes in gross primary productivity of different regions of North America as affected by recent warming.....	54
3.1. Introduction.....	54
3.2. Materials and Methods.....	57
3.2.1. Model Description.....	57
3.2.1.1. Direct Effects.....	57
3.2.1.2. Indirect Effects	58
3.2.2. Model Drivers	60
3.2.3. Model Runs and Testing	62
3.2.4. Analysis of Outputs from Continental Scale Model Runs	63
3.3. Results.....	64
3.3.1. Model Testing	64

3.3.2. Continental Scale: Changes in T_a 1979 – 2010.....	65
3.3.3. Continental Scale: Changes in GPP 1980 - 2010.....	66
3.3.4. Continental Scale: Interannual Variability in T_a , Precipitation and GPP.....	68
3.4. Discussion.....	69
3.4.1. 30-year Spatial and Temporal Changes in T_a	69
3.4.2. Uncertainties in Continental Modeled GPP.....	70
3.4.3. Impacts of Warming in Recent Decades on Ecosystem Productivity.....	71
3.4.4. Interannual Variability in Ecosystem Productivity.....	74
3.5. Conclusions.....	75
Appendices: A – D.....	92
Chapter 4	101
Carbon sources and sinks of North America as affected by major drought events during the past 30 years	101
4.1. Introduction.....	101
4.2. Methods.....	104
4.2.1. Model Description.....	104
4.2.2. Simulation Design.....	108
4.2.3. Model Testing.....	108
4.2.4. Analysis of Data and Model Outputs.....	110
4.3. Results.....	111
4.3.1. Model Testing.....	111
4.3.2. Major Drought Events and Their Impacts on Productivity.....	113

4.3.2.1. Regional Impacts on GPP and LAI	113
4.3.2.2. Continental Impacts on NEP	114
4.3.3. Interannual Variability in Precipitation and Productivity 1980 – 2010	115
4.3.4. North American Terrestrial Carbon Budget.....	115
4.3.4.1. Sources and Sinks.....	115
4.3.4.2. Long-term Trends.....	117
4.4. Discussion.....	117
4.4.1. Major Drought Events and Long-term Trends in Productivity.....	117
4.4.2. Spatial and Temporal Patterns of NA Carbon Budget	119
4.5. Conclusions.....	122
Appendix: A.....	135
Definition of Variables in Appendix A.....	135
Chapter 5	137
General discussion and conclusions	137
5.1. Sensitivity of Modeled NEP to Gridded Climates and Soil.....	137
5.2. Impacts of Long-term Warming on GPP.....	140
5.3. North American Carbon Sources and Sinks Affected by Drought	142
References	145

List of Tables

Table 2-1. Eddy Covariance flux tower sites and years with contrasting weather used for site and gridded runs.....	36
Table 2-2. Model drivers used in the gridded and site simulations	37
Table 2-3. Simulation design to partition NEP sensitivity to gridded weather and soil drivers	38
Table 2-4. Measured and gridded mean annual T_a , annual total precipitation and radiation for contrasting years	39
Table 2-5. List of soil variables (maximum depth, initial available soil water and organic carbon) for measured and gridded soil inputs of the six EC flux tower sites	40
Table 2-6. Annual carbon budget of measured vs. gridded simulations and EC measurements for contrasting years for six EC flux tower sites.....	41
Table 3-1. Model drivers and their temporal resolution used to drive <i>ecosys</i>	77
Table 3-2. Location of 20 EC sites and mean annual air temperature (MAT) and annual precipitation (P) extracted from corresponding pixels of NARR for 2005	78
Table 3-3. Trends in annual and seasonal T_a ($^{\circ}\text{C decade}^{-1}$) across sub-regions of North America.....	79
Table 3-4. Long-term (1980-2010) spatial average and changes in modeled GPP, T_a and precipitation across level I eco-regions of North America	80
Table 4-1. Annual precipitation and modeled vs. EC-derived carbon fluxes of mixed grass prairie EC flux tower site in Lethbridge (CA-Let) during the 2001 (drought) vs. 2002 (non-drought) year	123
Table 4-2. Changes in spatially averaged ecosystem carbon fluxes for different sub-regions of North America modeled in 1988 and 2002	124

Table 4-3. Comparison of carbon budget estimates of different models for NA 125

List of Figures

Figure 2-1. Correlation between 3- hour air temperature of site and gridded climate datasets for six EC flux tower sites, each with two years of contrasting weather except Mead	42
Figure 2-2. Correlation between 3- hour incoming short wave radiation of site and gridded climate datasets for six EC flux tower sites, each with two years of contrasting weather except Mead	43
Figure 2-3. Correlation between monthly aggregated precipitation of site and gridded climate datasets for six EC flux tower sites, each with two years of contrasting weather except Mead	44
Figure 2-4. Taylor diagrams showing a comparison of four sets of simulated NEPs (g C day^{-1}) (s : site weather and soil, n : NARR weather and site soil, p : site weather and UNASM soil, r : NARR weather and UNASM soil) with observed NEP (NEP-EC) of six EC flux tower sites under a contrasting weather (Table 2-1). The RMSD (g C day^{-1}) between the simulated and observed NEP is the distance between a simulated values along the green line to the x-axis at NEP – EC, standard deviation (g C day^{-1}) is the distance from a point to the origin and correlation coefficient of each simulated values is shown in the blue line.....	45
Figure 2-5. Campbell river Douglas-fir forest (CA-CA1): (a1, a2, b1, b2) 3-hourly air temperature, (a3, b3) daily NEP measured at EC (black closed symbols), gap-filled from EC measurements (green closed symbols), modeled NEP using site climate and soil (blue lines) and regional climate and soil (red lines) for a cooler year 2001 and a warmer year 2004.	46
Figure 2-6. Campbell river Douglas-fir forest (CA-CA1): (a) hourly gridded (red line) and site (blue line) air temperature (T_a), (b) hourly modeled canopy stomatal conductance (g_c), modeled with site climate and soil (blue lines) and regional climate and soil (red lines) and (c) hourly modeled CO_2 flux, modeled with site climate and soil (blue lines) and regional climate and soil (red lines) at EC (black closed symbols), gap-filled from EC measurements (green closed symbols), for DOY 164 – 174 of a warmer year (2004)	47
Figure 2-7. Daring lake arctic tundra (DL): (a1, a2, b1, b2) 3-hourly air temperature, (a3, b3) daily NEP measured at EC (black closed symbols), gap-filled from EC measurements (green closed symbols), modeled NEP using site climate and soil	

(blue lines) and regional climate and soil (red lines) for the years of 2004 and 2005.....	48
Figure 2-8. Old Aspen forest (SOA): (a1, b1) daily volumetric soil water content at 15cm soil depth, (a2, b2) daily NEP measured at EC (black closed symbols), gap-filled from EC measurements (green closed symbols), modeled NEP using site climate and soil (blue lines) and gridded climate and soil (red lines) for the first (2001) and third (2003) years of a drought.....	49
Figure 2-9. Duke forest (DK3): (a1, a2, b1, b2) 3-hourly air temperature, (a3, b3) daily NEP measured at EC (black closed symbols), gap-filled from EC measurements (green closed symbols), modeled NEP using site climate and soil (blue lines) and regional climate and soil (red lines) for a pre-drought year 2001 and a drought year 2002.....	50
Figure 2-10. Quebec mature boreal black spruce forest (QFO): (a1, a2, b1, b2) 3-hourly air temperature, (a3, b3) daily NEP measured at EC (black closed symbols), gap-filled from EC measurements (green closed symbols), modeled NEP using site climate and soil (blue lines) and regional climate and soil (red lines) for a cooler year 2004 and a warmer year 2005.....	51
Figure 2-11. Mead crop land site (Mead): (a1, a2, b1, b2) 3-hourly air temperature, daily NEP measured at EC (black closed symbols), modeled NEP using site climate and soil (blue lines) and regional climate and soil (red lines) for (a3) irrigated vs. (b3) rainfed for maize in 2003	52
Figure 2-12. Mead crop land site (Mead): comparison of CO ₂ fluxes, latent heat fluxes and canopy conductance for irrigated (blue lines) vs. rainfed (red lines) for maize in 2003 modeled for runs with (a1, a2, a3) site and (b1, b2, b) gridded soil and weather inputs	53
Figure 3-1. Level-I eco-regions of North America and selected eddy covariance sites for model validation.....	81
Figure 3-2. Correlation between annual GPP for 2005 (a) derived from measurements at 20 selected EC flux tower sites (Table 3-2) vs. modeled GPP from the corresponding pixels where the EC flux towers were located (b) EC-derived vs. MODIS GPP averaged for corresponding pixels within 0.25 ⁰ x 0.25 ⁰ where the EC flux towers were located.....	82

Figure 3-3. Relationship between 2005 (a) mean annual air temperature (MAT) and (b) annual precipitation extracted from NARR vs. modeled annual GPP (closed squares) and EC derived annual GPP (open squares) for 20 EC sites across North America. The x symbols represent overlapping points.....	83
Figure 3-4. Long-term (2000 – 2010) annual average (a) modeled GPP and (b) MODIS GPP for North America.....	84
Figure 3-5. GPP anomaly for spatial average modeled vs. MODIS GPP from 2000-2010 for North America	85
Figure 3-6. Comparison of spatial patterns in modeled annual GPP (a, b) vs. MODIS GPP (c, d) for 2002 (drought) vs. 2005 (non-drought) years for North America: GWR for modeled vs. MODIS GPP $R^2 = 0.85$ for 2002 and 0.86 for 2005.....	86
Figure 3-7. Long-term (1979 – 2010) changes in (a) mean annual air temperature (b) annual precipitation across North America landmass (c) average air temperature across latitudes, and (d) average air temperature across longitudes.	87
Figure 3-8. Long-term mean (a) annual GPP (c) mid-August LAI and spatially averaged changes (average of the first 5 years (1980 – 1984) subtracted from average of the last 5 years (2006 – 2010) for (b) annual GPP and (d) mid-August LAI over the last three decades in North America. Pixels with no value in b and d represents forested stands with less than 60 years from the last stand replacing fire and pixels with forest stands in Mexico with no historical disturbance data	88
Figure 3-9. 3D Mesh graph showing the relationship among long-term (1980 – 2010) % change in modeled GPP and NARR precipitation (P) and changes in T_a for (a) northern (above 50° N), (b) south and southwest and (c) southeast parts of North America.....	89
Figure 3-10. Anomalies of annual average (a) precipitation, and (b) T_a derived from NARR, and (c) modeled GPP from the long-term mean for North America over the last three decades	90
Figure 3-11. Long-term (1980 – 2010) North America (a) GPP standard deviation, (b) GPP relative standard deviation (standard deviation / long-term mean), (c) mid-August LAI standard deviation and (d) mid-August LAI relative standard deviation.....	91

Figure 4-1. Mixed grass prairie in Lethbridge (CA-Let): comparison of hourly (a1, a2) incoming short wave radiation (R_s) from EC-measured (black) and NARR (green) and (b1, b2) canopy conductance (g_c), (c1, c2) energy fluxes (latent heat fluxes (blue), sensible heat fluxes (red)) and (d1, d2) CO_2 fluxes (modeled (black line), measured at EC (black closed dots), gap-filled from EC measurements (red open dots)) for drought year 2001(a1 – d1) vs. non-drought year 2002 (a2 – d2); +ve = influx, -ve = efflux. Measured fluxes source:(Flanagan and Adkinson, 2011) 126

Figure 4-2. Spatial patterns in standard precipitation index (SPI) for June, July and August during major drought events (1988 and 2002) of North America: precipitation data range to calculate SPI 1979 – 2010 127

Figure 4-3. Spatial changes in modeled annual GPP: values obtained by subtracting the long-term (1980 – 2010) annual average GPP from annual GPP during the drought years (1988, 2002) 128

Figure 4-4. Spatial anomalies in modeled mid-August LAI vs. AVHRR NDVI from their long-term means (equals zero) for the major drought years (1988, 2002) in North America: GWR $R^2 = 0.84$ for 1988 and 0.71 for 2002 129

Figure 4-5. Long-term anomalies and trends in spatially averaged GPP, NPP, R_h and NEP ($Pg\ C\ yr^{-1}$) from the long-term mean (equals zero) across different sub-regions of North America: (a1 - d1) North America (a2 - d2) above $45^{\circ}N$ (a3 - d3) below $45^{\circ}N$ 130

Figure 4-6. Relative standard deviation (%) for long-term (1980 – 2010) annual (a) NARR precipitation, (b) modeled mid-August LAI and (c) mid-August NDVI (1982 – 2006) 131

Figure 4-7. (a1 – d1) Standardized precipitation index (SPI) at different time scales (moving average for 3, 6, 12 and 24 months), and (a2 – d2) spatial average annual fluxes ($g\ C\ m^{-2}\ yr^{-1}$) for drought affected sub-region of North America (Great Plains, southwest US and northern Mexico)..... 132

Figure 4-8. Long-term (1980 – 2010) modeled mean annual (a) GPP, (b) RE and (c) NEP of North America: positive NEP implies sinks and negative NEP sources.

Localized red spots in (c) indicate carbon sources caused by severe disturbance effects on NEP during the modeled period 133

Figure 4-9. Long-term trends in modeled annual NEP (Black line), annual anthropogenic fossil fuel emissions (red line) and net carbon emissions (annual NEP subtracted from the annual fossil fuel emission) without considering the carbon that could be sequestered in water bodies in North America (blue line): North America fossil fuel emission data was obtained from Boden et al. (2013) 134

List of symbols and abbreviations

Symbol and abbreviations	Definition
AVHRR	Advanced Very High Resolution Radiometer
BD	bulk density
C_a	ambient CO ₂ concentration
C_b	canopy CO ₂ concentration
C_c	aqueous CO ₂ concentration in canopy chloroplasts
C_i	gaseous CO ₂ concentration in canopy leaves
D	vapor pressure deficits
DOC	dissolved organic carbon
EC	eddy covariance
E_c	canopy transpiration
ENSO	El Niño–Southern Oscillation
ERA	European reanalysis
EVI	enhanced vegetation index
fAPAR	absorbed photosynthetically active radiation
f_{ψ}	non-stomatal effects of plant water status on carboxylation
FC	field capacity
G	change in heat storage
g_c	stomatal conductance
g_s	stomatal conductance
GCMs	global circulation models

GFED	Global Fire Emission Database
GPCP	Global Precipitation Climatology Project
GPP	gross primary productivity
GWR	geographically weighted regression
H	sensible heat flux
HWSD	the Harmonized World Soil Database
IPCC	Intergovernmental Panel on Climate Change
K_c	Michaelis-Menten constant for carboxylation
K_{sat}	saturated hydraulic conductivity
LAI	leaf area index
LEDAPS	Landsat Ecosystem Disturbance Adaptive Processing System
LH	latent heat
LUE	light use efficiency
M	aqueous microbial concentrations
MAT	mean annual air temperature
M_h	heterotrophic microbial populations
MLO	Mauna Loa
MODIS	Moderate Resolution Imaging Spectroradiometer
MsTMIP	Multi-Scale Synthesis and Terrestrial Model Inter-comparison Project
NA	North America
NACP	North American Carbon Program
NAO	North Atlantic Oscillation

NARR	North American Regional Reanalysis
NASA	National Aeronautics and Space Administration
NBP	net biome productivity
NCEP	National Centers for Environmental Prediction
NDVI	normalized difference vegetation index
NEE	ecosystem exchange
NEP	net ecosystem productivity
NOAA	National Oceanic and Land Administration
NPP	net primary productivity
PDSI	Palmer Drought Severity Index
PRISM	Parameter-elevation Regressions on Independent Slopes Model
θ	soil water contents
R_a	autotrophic respiration
R_c	oxidation of nonstructural pools
r_c	canopy resistance
r_{cmin}	minimum canopy resistance
R_e	ecosystem respiration
R_g	growth respiration
R_h	heterotrophic respiration
r_l	leaf resistance
r_{lmin}	minimum leaf resistance
R_m	autotrophic maintenance respiration
RMS	central mean square

R_n	net radiation
SLC	Soil Landscapes of Canada
SOC	soil organic carbon
SON	soil organic nitrogen
SPI	Standard Precipitation Index
SPO	South Pole
SRES	special report on emission scenarios
SSURGO	Soil Survey Geographic
STATSGO	State Soil Geography
SWC	soil water holding capacity
T_a	surface air temperature
TBMs	terrestrial biosphere models
T_c	canopy temperature
T_s	soil temperatures
U	water uptake from all rooted soil layers
UNASM	Unified North America Soil Map
U_{NH_4} , U_{NO_3} and U_{PO_4}	active uptake of N and P
USGS	United States Geological Survey
V_b	CO ₂ -limited leaf carboxylation rate
V_c	leaf CO ₂ fixation rate
V_g	leaf CO ₂ diffusion
WP	wilting point
Ω_r	root hydraulic resistances

Ω_s	soil hydraulic resistances
ψ_c	canopy water potential
ψ_π	canopy osmotic water potential
ψ_t	canopy turgor potential
ψ_s	soil water potential

Chapter 1

Introduction

1.1. Evidence of Climate Change

Ice core records have indicated that the current atmospheric CO₂ concentration is the highest in the last six glacier cycles (650,000 years) which had a range of 180ppm - 300ppm (Siegenthaler et al., 2005). Other greenhouse gases such as methane (CH₄) and nitrous oxide (N₂O) in the atmosphere are also greater than the concentrations during the pre-industrial period (IPCC, 2013). CO₂ concentration has increased from pre-industrial period of 278 ppm in 1750 to a current level of 390 ppm measured in 2011 (IPCC, 2013), with fossil fuel burning and deforestation being the two main human induced sources (Baker et al., 2006). Projections show that by 2050 CO₂ concentration is expected to rise to 450 ppm (IPCC, 2007; Izaurrealde et al., 2011). The trajectory in future emissions of these greenhouse gases is subject to uncertainties (Allen et al., 2000; Webster et al., 2002) and difficult to estimate, as emission scenarios are dependent on future economic, political, technological and demographic changes (Stott and Kettleborough, 2002).

These increases in greenhouse gases have resulted in atmospheric warming by changing the radiative forcing of the atmosphere (IPCC, 2007; Jain et al., 2000). During 1971 – 2010 the energy balance of the earth has shifted to gaining more energy from the sun than leaving the atmosphere, which has consequently increased global surface temperatures and hastened the melting of the ice (IPCC, 2013; Murphy et al., 2009). Thus, global average surface temperature has increased by 0.6 ± 0.2 °C since the late 19th century and is predicted to rise by 1.4 – 5.8 °C from 1990 – 2100 in a range of 35 special report on emission scenarios (SRES) (Houghton et al., 2001) and estimated using different climate models. The second half of the 20th century was the

warmest period in the last 1300 years (IPCC, 2007). Northern hemisphere surface temperatures for 1983 – 2012 were very likely the warmest of the last 800 years and this was supported by comparison of instrumental temperature records with various estimates of proxy data (IPCC, 2013). Moreover, the past three decades have been the warmest since instrumental record of surface temperature began and the decade of the 2000's has been the warmest in particular (IPCC, 2013; Marcott et al., 2013).

Although global average temperature has increased, regional temperature changes are variable with most regions experiencing a rise in temperature but some regions experiencing cooling (Jones et al., 1999b). The amount by which temperature has changed varies in different regions (Shaver et al., 2000). Land surfaces are more likely to warm at a higher rate than the global average, particularly in higher latitude regions. Temperature rise is greater at northern higher latitudes than mid and lower latitudes (IPCC, 2007; Myneni et al., 1997). The warming in higher latitudes of North America (NA) is 40% greater than the global mean (Houghton et al., 2001). IPCC AR4 (2007) report showed that in the last century the rise in average surface air temperature (T_a) for the Arctic region was twice the global average, indicating amplified warming in the northern higher latitudes. This amplified warming is also projected to continue due to feedbacks associated with thawing of the permafrost (Lawrence and Slater, 2005) and a decline in the extent of snow and sea ice, hence a lower albedo (Serreze and Francis, 2006; Serreze et al., 2000). Permafrost temperature increases attributed to an increase in T_a over northern higher latitudes have been observed in recent decades (Hinzman et al., 2005; IPCC, 2013; Serreze et al., 2000). A decline of about 10% in snow cover since 1960s was observed from satellite data as a result of warming in higher latitudes (Walther et al., 2002).

Changes in precipitation in recent decades were spatially and temporally variable (Walther et al., 2002). However, there was an overall increase in precipitation over mid and high latitudes of the northern hemisphere (Dore, 2005; IPCC, 2013), particularly in autumn and winter (Walther et al., 2002). Under different scenarios of climate change several global model simulations have shown that global average precipitation is expected to increase during the 21st century, particularly at the higher and mid-latitudes (Houghton et al., 2001). Precipitation patterns however, would be more variable (Aguilar et al., 2005; IPCC, 2007) and higher inter-annual variations are expected (Houghton et al., 2001). However, overall confidence in precipitation change remains lower than in temperature, due to insufficient data especially prior to 1951 (IPCC, 2013).

Extreme climate events such as higher maximum and minimal temperature and reduced diurnal temperature range (Easterling et al., 1997), more intense precipitation (Groisman et al., 1999; Palmer and Räisänen, 2002), increased risk of drought and frequent fire disturbance have been observed during the latter half of the 20th century and their occurrence is very likely to increase in the 21st century (Houghton et al., 2001). Minimum temperature is increasing twice the rate of maximum temperature, hence increasing snow-free period in higher latitudes (Walther et al., 2002). In NA the frequency and intensity of heavy precipitation events have increased since 1950, although there were seasonal and regional variations (IPCC, 2013). Studies have shown that areas affected by drought have increased in the last four decades (Dai et al., 2004). The frequency and intensity of drought occurrences have also increased (Huntington, 2006) and are projected to increase under future climate change scenarios (IPCC, 2007). These changes in these extreme climate events could affect net ecosystem productivity (NEP) and the component fluxes (Gaumont-Guay et al., 2006). Fire is a dominant disturbance agent that affects ecosystem energy flow and biogeochemical cycling (Stocks et al., 2002) and current and future warming is likely to

increase the frequency of fire occurrences (Bond-Lamberty et al., 2007; Kasischke et al., 1995; Westerling et al., 2006).

1.2. Ecosystem Responses to Climate Change

There is evidence that ecosystems are responding to changes in climate in recent decades. Studies using remote sensing products such as the Normalized Difference Vegetation Index (NDVI) and the Enhanced Vegetation Index (EVI) have shown increases in the length of growing season in different regions, particularly in the higher latitudes (Churkina et al., 2005; Kim et al., 2012; McManus et al., 2012; Myneni et al., 1997; Olthof et al., 2008; Tucker et al., 2001; Verbyla, 2008; White et al., 2009; Zhang et al., 2008; Zhu et al., 2012), where warming is the most rapid in recent decades (IPCC, 2013). Ecosystem responses to warming in recent decades have been reported from several artificial warming experiments (Elmendorf et al., 2012a; Elmendorf et al., 2012b; Hill and Henry, 2011; Klady et al., 2011; Oberbauer et al., 2007; Walker et al., 2006) and long-term plot-based studies (Hudson and Henry, 2009). Thawing of the permafrost as a result of warming in higher latitudes could expose the frozen organic carbon to microbial decomposition and lead to the release of a large volume of carbon to the atmosphere (Davidson and Janssens, 2006; Dutta et al., 2006; Schuur et al., 2008). Schuur et al. (2009) estimated 40% more annual carbon losses in areas that thawed compared to areas minimally thawed over the last 15 years.

Evidence of increases in vegetation cover and northward movement of the tree line in northern higher latitudes has also been reported in several studies (Beck et al., 2011; Swann et al., 2010; Van Bogaert et al., 2011). Species distribution could also be affected by climate change through the impact on biome range shifting, and ecosystem responses could vary with species-specific tolerance to changes in temperature and precipitation (Parmesan and Yohe, 2003; Reich et al., 2015; Walther et al., 2002). Plants generally tend to shift to higher latitudes and elevation

following warming trends and dispersal success (Walther et al., 2002) and future warming may reduce biodiversity by favoring mobile species, as shifts in climate zone may surpass the speed of migration of some species (Malcolm et al., 2002). Responses of warming over a wide range of observational data (>29,000) from 75 studies have shown consistence and clear directional trends for more than 89% of the studies (IPCC, 2013), implying broader agreement from various climate change studies.

These ecosystem responses to changes in climate variables are spatially heterogeneous across different biomes and the responses are determined by the combined effects of all climatic and biophysical factors that result in complex and significant changes in ecosystem functioning (Albert et al., 2011; Dermody et al., 2007; Dieleman et al., 2012). For instance, warming can indirectly affect ecosystem responses through its effect on other factors such as changes in precipitation (Held and Soden, 2000; Huntington, 2006) and nutrient availability (Rustad et al., 2001) and disturbance (Harden et al., 2000). These combined effects of warming and changes in precipitation have strong impacts on ecosystem productivity (Albert et al., 2011).

Responses to changes in climatic variables are also dependent on the initial condition of the ecosystem (Shaver et al., 2000). For instance, in areas with higher mean annual surface T_a , as more frequently encountered in tropical and subtropical climates, warming may slow CO_2 fixation (Grant et al., 1999). However, in areas with lower T_a as in boreal climates, warming improves CO_2 fixation (Grant et al., 2009a). Climate change scenarios resulting in an increase in precipitation in water-limited regions could have positive effects on productivity. However, declines in precipitation would have adverse effects on productivity in water-limited regions as a result of increased water stress (Grant et al., 2008), but no or even beneficial effects in water-excess regions (IPCC, 2007).

1.3. Estimating the Impacts of Climate Change on Ecosystem Productivity

Measurements of land-atmosphere carbon exchange is of vital importance in understanding the global carbon cycle (Kalfas et al., 2011), hence the impacts of climate change on ecosystem productivity. Accurate estimates of ecosystem productivity under projected future climates depends on the skill of present models in simulating the productivity under the past and present climates in which model performance could be compared with observations. There are various approaches in observing ecosystem carbon exchange at different spatial and temporal scales, including eddy covariance (EC) and chambers, remote sensing techniques, atmospheric inversions, which can be used to test terrestrial biosphere models (TBMs).

1.3.1. Approaches in Estimating Land-atmosphere Carbon Exchange

Direct measurements of carbon fluxes can only be done at site scales from flux chambers and eddy covariance (EC) flux towers with footprints in order of few km² (Houborg and Soegaard, 2004; Sasai et al., 2007) and there is no direct observation that can be made at regional scales. However, several approaches have been used to estimate carbon fluxes at regional scales. Among these are techniques that use satellite remote sensing products (Myneni et al., 1997; Tucker et al., 2001; White et al., 2009), atmospheric inversions (Peters et al., 2007) and TBMs (Huntzinger et al., 2012), with each technique providing unique capability and limitations in examining land-atmosphere carbon exchange at continental and global scales.

Remote sensing techniques make use of sensors onboard different satellites to acquire spectral reflectance that can be used to estimate ecosystem productivity applied at regional to global scales. For instance, NDVI is a widely used vegetation index derived from various sensors on board satellites such as Landsat, Moderate Resolution Imaging Spectroradiometer (MODIS) and Advanced Very High Resolution Radiometer (AVHRR) based on spectral reflections

calculated as the difference between the near infrared and the visible (red) spectrum divided by their sum (Goward et al., 1991; Tucker, 1979; Tucker et al., 1991). The index ranges from -1.0 to 1.0, with more positive NDVI values indicating increasing greenness and vegetation density, and values near zero and more negative indicating non-vegetated areas, rocks, soil, water, snow and ice (Tucker, 1979). NDVI values are strongly correlated to photosynthetically active radiation absorbed by vegetation. Thus, increasing NDVI values indicate increasing vegetation density and gross primary productivity (GPP) (Box et al., 1989). In recent developments, solar-induced chlorophyll fluorescence (SFI), has been used to measured carbon uptake (Frankenberg et al., 2014; Guanter et al., 2014) and can potentially be used to test modeled GPP. Another approach is atmospheric inversions that make use of atmospheric transport models to estimate CO₂ sources and sinks from variations in observed atmospheric CO₂ concentration data measured over a wide range of networks collected from surface air samples, tall towers, aircrafts and direct satellite observation of CO₂ from the troposphere (Gurney et al., 2002; Peters et al., 2007). Estimates from this approach vary as a result of different inversion methods and transport models used to estimate carbon fluxes (Baker et al., 2006).

Although large scale carbon fluxes could be estimated using satellite products and inversions, both approaches lack attribution of the carbon fluxes to specific ecosystem processes and cannot partition component fluxes (Peters et al., 2007). Besides, these approaches do not have predictive capabilities of carbon exchange under future climates, as they rely on existing satellite or observed data to estimate fluxes. However, TBMs can simulate component fluxes of CO₂ exchange under changing environmental conditions and they can be used from site to regional and global scales (Sasai et al., 2007).

TBMs can be categorized as diagnostic and prognostic models (Huntzinger et al., 2013). Diagnostic models do not have a model structure to change state of biophysical conditions and are dependent on availability of data (Beer et al., 2010). This approach uses empirical relationships between a physical variable that can be measured at larger spatial extents with ecological processes that can be used to estimate carbon fluxes (Rastetter et al., 2003). An example of this approach is fusing satellite data with a model (Kalfas et al., 2011; Tagesson et al., 2012), the most widely used of which is the light use efficiency (LUE) model (Monteith, 1972). Several studies (Heinsch et al., 2006b; Running et al., 2004; Turner et al., 2006; Turner et al., 2005) have been using this model while others used an approach of coupling satellite outputs with other empirical models (Houborg and Soegaard, 2004). There are also studies that use a technique of parameterizing gridded information of an explanatory variable in a diagnostic model using flux tower estimates (Beer et al., 2010). On the other hand, prognostic models make use of biophysical and climatic relationships and basic physical, chemical and biological processes to estimate ecosystem productivity (Beer et al., 2010; Korzukhin et al., 1996) conferring predictive capabilities that enable simulation of future impacts of ecological controls on ecosystem productivity from changes in external forcing (Huntzinger et al., 2013).

1.3.2. Uncertainties in Estimating Land-atmosphere Carbon Exchange

Assessing the impacts of climate change is subject to uncertainties attributed to techniques for estimating carbon exchange. For instance, in modeling the impacts of climate change on land-atmosphere carbon exchange, there can be two sources of uncertainties: model structure and external model drivers (Moorcroft, 2006). Ecosystem models vary in the way they represent various ecosystem processes, parameters and external model drivers need (Huntzinger et al., 2013), resulting in uncertainties in model estimates. However, efforts are being made in formal

model intercomparison projects to identify and understand how TBMs structural differences (e.g. types of ecosystem processes, parameters and how they are formulated) could affect carbon fluxes at site (Schwalm et al., 2010a), continental (Huntzinger et al., 2012) and global (Huntzinger et al., 2013) scales. These structural uncertainties are assessed by prescribing common experimental protocols and standard spin-up procedures and the models are driven by common environmental inputs to isolate biases in estimates of carbon fluxes that were resulted from the inherent model characteristics (Huntzinger et al., 2013).

Another source of uncertainties could be associated with environmental data (e.g. climate forcing and soil) that drives the models (Serreze et al., 2000). Available model drivers particularly those used at regional scales vary in accuracy, spatial and temporal resolutions as they are generated from different data sources that use various methods to prepare gridded datasets (Zhang et al., 2014; Zhao et al., 2012). These variations in accuracy may determine the performance of a model in estimating regional scale carbon fluxes (Zhang et al., 2014). Besides, uncertainties in carbon flux estimates under future climates could also be partly associated to projections of the future climate generated by the global circulation models (GCMs) that would be used as inputs to drive TBMs, although these GCMs projections are continuously being improved (Houghton et al., 2001).

Examining uncertainties in model structure and parameters require direct comparisons of model estimates of carbon fluxes with benchmark observed data (Moorcroft, 2006). Although continental scale carbon flux observations are not available, fluxes from eddy covariance (EC) towers can be compared with model estimates from corresponding pixels where the EC towers are located. However, observed carbon fluxes such as from EC flux towers and chambers are also subject to measurement uncertainties such as EC data processing methods and gap-filling, operator

errors, sampling errors, instrumental error, and calibration error (Aubinet et al., 2012), and it is important to quantify these uncertainties, especially when the data is used to validate model estimates. Spatial and temporal patterns in continental scale model estimates such as leaf area index (LAI) could also be compared with satellite products of surface reflectance and vegetation indices such as NDVI and EVI.

1.4. Overview of the Study

In this study, we examined the impacts of climate change on land-atmosphere carbon exchange over the last three decades across NA. A comprehensive mathematical process model, *ecosys* (Grant, 2001, 2014) was used to simulate the impacts of changes in T_a and precipitation on ecosystem carbon exchange, using long-term (1979 – 2010) climate data from the NA Regional Reanalysis (NARR) (Mesinger et al., 2004) with a 3-hourly time-step, across various ecological regions (eco-regions) of NA. The model was initialized with prescribed one-time and dynamic environmental and meteorological drivers and standardized simulation protocol as part of Multi-Scale Synthesis and Terrestrial Model Inter-comparison Project (MsTMIP) of the North American Carbon Program (NACP) (Huntzinger et al., 2013) which was a multi-scale synthesis that compared outputs of participating TBMs at regional and global scales. We ran *ecosys* over a spatial domain of NA with $0.25^0 \times 0.25^0$ spatial resolution and included all grid cells with more than 50% land that make up 51,061 independently simulated grid cells. NARR inputs were interpolated linearly to 1-hour for use in *ecosys* which was spun-up with time-varying land use/ land cover dynamics, atmospheric CO_2 concentration, nitrogen deposition and disturbance for a simulation period of 1800 - 2010.

While assessing the impacts of recent climate change, how well land-atmosphere carbon exchange be simulated is partly determined by the accuracy, and the spatial and temporal

resolutions of the model drivers, besides the inherent model characteristics. Model drivers such as climate and soil were shown to exert strong controls on ecosystem productivity in several studies (Delpierre et al., 2012; Jung et al., 2007a; Jung et al., 2007b; Pan et al., 2006). Thus, if these controls are to be examined at regional to continental scales, inputs in the form of gridded climate and soil datasets are needed, although these may be less accurate than site measurements. Regional and continental scale modeling studies, however rarely reported the uncertainties in model estimates related to these gridded model drivers that may affect carbon flux estimates and its implications in regional and global carbon budget estimates.

Therefore, in Chapter 2 we examined differences in net ecosystem productivity (NEP) modeled with NARR and gridded soil against NEP modeled at selected sites for which detailed site scale measurements of weather and soil are available by comparing these fluxes with those from EC measurements across different biomes. This comparison allowed us to examine uncertainties in modeled NEP associated with coarser resolution model drivers, which may have direct implications for continental scale estimates of carbon exchange, and hence for our understanding of how the changing climate affects ecosystems across biomes of NA. Attributes of NARR and the soil datasets that need to be considered for future improvements were identified when the gridded inputs adversely affected the accuracy of the modeled fluxes. In this chapter, we rigorously tested simulations driven by gridded vs. site measured climate and soil against measurements from EC flux towers. To our knowledge we have not come across a study that systematically addressed the combined impacts of gridded weather and soil on NEP tested against EC.

At a continental scale, we examined the impacts of warming and changes in precipitation present in the NARR on ecosystem productivity over the last three decades in NA. Although

several plot-based (Hudson and Henry, 2009) and artificial warming experiments (Elmendorf et al., 2012a; Elmendorf et al., 2012b; Natali et al., 2012; Walker et al., 2006) have shown the responses of plants to warming in NA, the impacts of this warming on land-atmosphere carbon exchange over a wide range of biomes are spatially heterogeneous and uncertain, raising some key questions related to climate change in recent decades:

- (1) How do plants respond to changes in T_a and precipitation over a shorter and longer time scale across different eco-regions of NA?
- (2) How are these responses affecting the overall ecosystem productivity and carbon budget of NA?
- (3) To what extent do extreme climate events such as droughts affect continental carbon sources and sinks?

To examine these responses of recent climate change, in Chapter 3, we first analyzed the spatial and temporal variability and trends of warming and precipitation observed in NARR over the last three decades (1979 - 2010) across NA. We then examined plant responses modeled across different biomes to the observed changes in long-term NARR T_a and precipitation. We further analyzed the ecosystem processes through which this variability in climate affected the spatial and temporal changes in modeled GPP and LAI across different eco-regions of NA. In Chapter 4, we examined the impact of major droughts on ecosystem productivity of NA in recent decades. Effects of drought on carbon fluxes were modeled based on the fundamental theory of how water moves through the soil-plant-atmosphere water transfer scheme that enabled us to examine the underlying causes, ecosystem processes and the effects of drought on NEP and its component fluxes ($NEP = GPP - \text{autotrophic respiration } (R_a) - \text{heterotrophic respiration } (R_h)$). Thus, the long-term spatial and temporal trends in carbon sources and sinks and inter-annual variability in NEP as affected by

major drought events were assessed and amounts of carbon lost as a result of these droughts across NA in recent decades were estimated.

Modeled results were tested rigorously at multiple scales (site to continental) using data obtained from EC flux towers and satellite remote sensing products and atmospheric inversion studies. At site scale, modeled GPP aggregated from hourly values in pixels corresponding to the locations of EC flux towers were compared with GPP derived from measurements at EC sites for 20 selected EC sites. At continental scale, spatial and temporal patterns of average annual modeled vs. MODIS GPP for NA were compared to assess similarities in spatial pattern and temporal trends. We also compared long-term modeled annual GPP in drought year vs. normal year. Changes in spatial patterns of GPP and LAI during major drought years were compared with changes in NDVI from AVHRR. Moreover, estimates of modeled NEP were compared against other model estimates from TBMs and atmospheric transport inversions. The general conclusions from this study are summarized in Chapter 5.

Chapter 2

Sensitivity of modeled NEP to climate and soil drivers at site and regional scales: implications for upscaling ecosystem models

2.1. Introduction

Measurements of land-atmosphere carbon exchange are of vital importance in understanding the global carbon cycle (Baldocchi, 2003; Kalfas et al., 2011). Direct measurements of carbon fluxes can only be done at a site scale, for instance from eddy covariance (EC) flux towers with linear footprints 200m – 2km (Houborg and Soegaard, 2004; Sasai et al., 2007). However, terrestrial biosphere models (TBMs) can be used to estimate carbon fluxes at regional and global scales (Rastetter et al., 2003; Sasai et al., 2007). Processes-based TBMs make use of biophysical and climatic relationships and processes to estimate ecosystem productivity (Beer et al., 2010; Korzukhin et al., 1996) conferring predictive capabilities that enable simulation of future impacts of ecological controls on ecosystem productivity from changes in external forcing (Huntzinger et al., 2013). Performance of these models in estimating carbon fluxes is partly determined by the accuracy, and the spatial and temporal resolution of model inputs.

Model inputs such as climate and soil exert strong controls on modeled ecosystem productivity (Pan et al., 2006) and several studies have shown their impacts on modeled carbon exchange between the terrestrial environment and the atmosphere (Delpierre et al., 2012; Jung et al., 2007a; Jung et al., 2007b; Pan et al., 2006). If these controls are to be examined at regional to continental scales, inputs in the form of gridded climate and soil datasets are needed, although these may be less accurate than site measurements (Zhao et al., 2012). One of the challenges in

using these coarser resolution gridded datasets for regional model estimates is to capture the spatial heterogeneity within a pixel (Aertsens et al., 2012) needed to upscale site level processes. Ecosystems are spatially heterogeneous and temporally dynamic (Miller et al., 2004; van Nes and Scheffer, 2005) and upscaling site level ecosystem processes to a regional level should take the non-linearity of landscape level biophysical processes into account (Aertsens et al., 2012; Seidl et al., 2012). The spatial patterns of these variations can be complex and this can certainly influence the biophysical processes and hence the land-atmosphere carbon exchange (Anderson et al., 2003). Sub-pixel heterogeneity (e.g. climate, plant functional type, soil and topography variations within a pixel) increases at coarser spatial resolutions, although it may vary with model drivers. For instance, spatial variability in weather may be more homogeneous at grid scale compared to soil with more variability particularly where topography varies.

Existing North American climate and soil datasets vary in spatial and temporal resolutions and the geographic extent they cover. For instance, North American climate datasets such as DayMet (Thornton et al., 2012) and Parameter-elevation Regressions on Independent Slopes Model (PRISM) (Daly et al., 2012) have spatial resolution of 1km. DayMet has a daily time-step whereas PRISM has a monthly time-step and both datasets only cover lower and mid latitudes of North America. The European reanalysis (ERA-1) from European Centre for Medium-Range Weather Forecasts had global spatial coverage with temporal resolution of 6-hour and spatial resolution of $0.75^{\circ} \times 0.75^{\circ}$ (Berrisford et al., 2009). However, the North American Regional Reanalysis (NARR) has long-term, higher temporal resolution (3-hour) and covers the entire North America (Mesinger et al., 2004), thus providing an opportunity to model diurnal carbon exchange as affected by short-term weather events over a wide range of climates across the continent.

Although increasing efforts are being made to improve the accuracy, spatial and temporal resolutions of these large scale datasets, the extent to which these model drivers affect regional scale carbon estimates remains uncertain. Some studies have reported deviations in carbon flux estimates associated with coarse resolution model inputs: Zhao et al. (2012) indicated biases in carbon flux estimates caused by gridded weather inputs (mainly by downward shortwave radiation) on a daily time scale. Another study (Anisimov et al., 2007) reported deviations in carbon fluxes attributed to variations in air temperature in four regional weather datasets when compared to local meteorology. Zhang et al. (2014) reported the impact of differences in spatial resolution of soil datasets (coarser (State Soil Geography-STATSGO) vs. finer (Soil Survey Geographic-SSURGO) on model estimates of net ecosystem productivity (NEP) and found a relatively greater loss in accuracy of modeled NEP attributed to STATSGO. Although such attempts to address the impacts of coarse resolution model drivers on NEP have been made, the combined effects of gridded soil and weather vs. measured inputs on modeled carbon exchange have not been presented. Furthermore, the extent to which model estimates of carbon exchange could be affected by these gridded model inputs should be rigorously tested. Although, direct tests of modeled NEP at grid scale are not available, site level measurements (e.g. at representative EC tower sites) could be compared to modeled NEP for the corresponding pixels where the EC towers located.

Therefore, in this study we used a comprehensive mathematical model, *ecosys* (Grant (2001, 2014); Grant et al. (2012)), to examine differences in diurnal and seasonal NEP modeled with weather and soil inputs from gridded datasets vs. those from site measurements by comparing these fluxes with those from EC measurements across different biomes. Attributes of gridded weather and soil datasets that need to be considered for future improvements were identified when

gridded inputs adversely affected the accuracy of the modeled fluxes. *Ecosys* was used as the effects of weather and soil on biochemical and physical processes that control carbon fluxes in the model have been widely and rigorously tested under site level changes in weather (Grant, 2014) and soil management (Grant et al., 2001b; Grant et al., 2007a). Moreover, weather effects on seasonal and interannual variability of ecosystem productivity have also been tested in several studies using the model across different biomes: a boreal forest in a continental climate in Quebec (Wang et al., 2013), a coastal temperate forest in a maritime climate in British Columbia (Wang et al., 2011); dry grassland in a Mediterranean climate in California (Grant et al., 2012); a semi-arid grassland in a continental climate in Lethbridge, Alberta (Li et al., 2004); black spruce forests in wetlands in Saskatchewan and Manitoba (Grant et al., 2008), further summarized in testing across a transcontinental transect of forest stands in the Fluxnet-Canada Research Network (Grant et al., 2009a).

2.2. Methods

Ecosys was run at six EC sites (Table 2-1) with different climates and plant functional types (cool temperate douglas-fir forest, boreal aspen forest, boreal black spruce forest, arctic tundra, warm temperate loblolly pine forest and temperate crop land) using weather and soil inputs from site measurements vs. inputs from gridded datasets (NARR and Unified North America Soil Map (UNASM) (Liu et al., 2013)) during years with contrasting weather at each site (cooler vs. warmer, wetter vs. drier). For the crop site the effect of the gridded weather input on CO₂ exchange with respect to inputs from site measurements was tested by evaluating differences in CO₂ exchange simulated during a dry year (2003) under rainfed vs. irrigated conditions. Land use/ land cover dynamics, atmospheric CO₂ concentration, nitrogen deposition and disturbance were also used as model inputs for all simulations (Table 2-2). Biome types were the same for each site and

gridded runs and model parameterization, and spin-up were kept constant for all simulations to ensure the same simulation design and model initial conditions.

2.2.1. Model Description

A detailed description of inputs, parameters and algorithms used in *ecosys* can be found in (Grant, 2001; 2014) and (Grant et al., 2012). However, the general descriptions of the model that are most relevant to testing the effects of temperature and water status on modeled NEP = (gross primary productivity (GPP) – autotrophic respiration (R_a) – heterotrophic respiration (R_h)) by which gridded vs. site climate and soil inputs will be compared are given below.

2.2.1.1. Effects of Canopy Water Status on GPP

In *ecosys*, surface energy and water exchanges drive soil heat and water transfers, from which soil temperatures (T_s) and water contents (θ) are determined (Grant, 2004b). NEP is controlled by plant water status calculated from concurrent convergence solutions for canopy temperature (T_c) from first-order closure of the canopy energy balance, and for canopy water potential (ψ_c) from equilibrating total root water uptake (U) with transpiration (T) (Grant et al., 1999). This equilibration is accomplished by finding a common ψ_c at which T driven by T_c and constrained by canopy resistance (r_c) calculated from ψ_c equals U driven by the differences between ψ_c and soil water potential (ψ_s) across soil Ω_s and root Ω_r hydraulic resistances in each rooted soil layer (Grant et al., 2007c). The rates of T and U are affected by T_c and θ that are mainly controlled by weather inputs for surface air temperature (T_a), precipitation, radiation, humidity and wind speed, and by soil hydraulic conductivity and water holding capacity (WHC) determined by soil inputs for depth, bulk density (BD), texture, saturated hydraulic conductivity (K_{sat}), field capacity (FC) and wilting point (WP) for each soil layer. Rate of CO₂ fixation is affected by T_c , ψ_c and r_c (Grant and Flanagan, 2007b-b).

2.2.1.2. Effects of Canopy Temperature on GPP

Carboxylation is directly affected by T_c through the Arrhenius functions for light and dark reactions (Grant et al., 2007a). At leaf level, CO₂ diffusion is controlled by leaf resistance (r_l) when calculating CO₂ fixation from concurrent solutions for diffusion V_g and carboxylation V_c . The rate of CO₂ fixation is controlled by coupled schemes for gaseous diffusion and biochemical fixation as affected by plant water and nutrient status and modeled through concurrent solutions for stomatal effects (Section 2.2.1.1) on diffusion V_g and for non-stomatal effects f_v on CO₂ and light-limited carboxylation V_b (Grant et al., 2007a; Grant and Flanagan, 2007b-b).

2.2.1.3. Effects of Nutrient Status on GPP

NEP is also strongly controlled by plant N status from plant N uptake driven by net N mineralization driven in turn by decomposition of soil organic carbon (SOC) and soil organic nitrogen (SON) initialized from soil inputs (Grant, 2014). Decomposition rates of different organic matter substrates are combined functions of active biomass in heterotrophic microbial populations (M_h) and substrate concentrations, and of T_s through an Arrhenius function. These rates determine net N mineralization which controls soil mineral N contents and hence uptake through coupled algorithms for radial convection, diffusion and active uptake by root and mycorrhizal surfaces. Higher T_s driven from meteorological inputs thereby affects NEP by hastening soil N mineralization and N uptake, and hence NEP (Grant, 2014).

2.2.1.4. Effects of Temperature on R_a and R_h

Temperature-dependent oxidation of nonstructural pools (R_c), plus the energy costs of nutrient uptake, drive R_a by all branches, roots and mycorrhizae. The R_c by roots and mycorrhizae is constrained by O₂ uptake U_{O_2} (Grant, 2004), and is thus affected by soil porosity. After R_c is first used to meet the T_c dependent maintenance respiration (R_m), the remaining is used for growth

respiration (R_g) (Grant et al., 2011b). Oxidation of dissolved organic carbon (DOC) drives heterotrophic respiration ($R_m + R_g$) through the Arrhenius function of T_s . The R_m is driven by DOC oxidation through Q_{10} function of T_s and R_h remaining from R_m drives R_g (Grant, 2014). Soil warming hastens decomposition and mineralization (Grant, 2014).

2.2.2. Measured and Gridded Weather and Soil

2.2.2.1. Measured Weather and Soil Inputs

The measured weather inputs for air temperature, precipitation, downward shortwave radiation, relative humidity and wind speed were recorded at the EC flux tower sites at a half-hour time-step and averaged to hourly values in *ecosys*. Measured soil inputs for layer depth, clay/sand fraction, pH, total organic carbon and nitrogen, cation exchange capacity and bulk density were recorded from soil samples taken at specified depths at the flux tower sites (Table 2-2).

2.2.2.2. Gridded Weather and Soil Inputs

The gridded weather inputs for air temperature, precipitation, downward shortwave radiation, relative humidity and wind speed were taken from NARR, a long-term weather dataset originally produced at the National Oceanic and Land Administration (NOAA) National Centers for Environmental Prediction (NCEP) Global Reanalysis. NARR is an extension of the NCEP reanalysis, which is a combined data and model assimilation product that made use of wide networks of observational datasets across North America (Mesinger et al., 2004). For this study, we used a NARR dataset which was resampled and reprojected to 0.25 degree resolution in geographic latitude/ longitude projection made available through the Multi-Scale Synthesis and Terrestrial Model Inter-comparison Project (MsTMIP) (Huntzinger et al., 2013). NARR precipitation was rescaled using the Global Precipitation Climatology Project (GPCP) monthly gridded precipitation product which was derived from satellite and gauge measurements, to

improve biases in magnitude and frequency of large rainfall events (Wei et al., 2014). The NARR incoming shortwave radiation was rescaled using the weather simulation model MTCLIM version 4.3 (Wei et al., 2014). The NARR data used for this study was from 1979 - 2010 and temporal resolution of three hours, with linear interpolation to one hour in *ecosys*.

The gridded soil (UNASM) inputs with layer depths, clay/sand fraction, pH, total organic carbon, cation exchange capacity and bulk density were a reanalysis product of MsTMIP for North America that was prepared using three different soil databases (Liu et al., 2013). These included the United States General Soil Map, the State Soil Geographic (STATSGO2), the Soil Landscapes of Canada (SLC) versions 3.2 (agricultural) and 2.2 (non-agricultural) and the Harmonized World Soil Database (HWSD) version 1.1. However SON was not provided in the UNASM, and was therefore estimated for use in *ecosys* from gridded SOC in each soil layer and from a relationship between SOC and SON ratios fitted to the site measurements.

2.2.3. Simulation Design

In the gridded simulations, weather and soil inputs were taken from NARR and UNASM for the grid cells corresponding to the locations of the EC flux towers. Model runs for each site were spun up with time-varying weather drivers for a simulation period of 1800 - 2010. To represent historical weather at each site, NARR data selected from 1979 - 1993 were randomly distributed to form a 100-year sequence that cycled through 1801 - 1978. This enabled the model to attain a steady state condition prior to 1979. Then the real time NARR data were used for the rest of the study period (1979 - 2010) to simulate the real time ecosystem productivity as stated in MsTMIP protocol (Huntzinger et al., 2013). The soil inputs were used to initialize the soil profiles at each site, whereas land use and land cover changes, atmospheric CO₂ concentrations, and nitrogen deposition rates varied during the runs as shown in Table 2-2. The model runs and drivers used for the simulations with measured inputs were the same as those with gridded inputs, except

that they had measured soil attributes and measured weather substituted for the years which site level data were available (Table 2-1). We avoided sub-pixel heterogeneity for the runs using gridded inputs by taking the dominant land cover and plant functional type from the corresponding pixels where the EC towers were located.

Four different simulations were conducted to investigate differences in NEP modeled with measured vs. gridded weather and soil (Table 2-3). *Simulation-s* had measured inputs for both weather and soil to model NEP under the same conditions as those of the EC measurements. *Simulation-r* had gridded inputs from NARR and UNASM to model grid cell NEP for the EC flux tower area as part of gridded simulations. Differences in NEP between *simulation-s* and EC measurements were considered to be caused by uncertainties in model parameterization and measured fluxes. Differences in NEP between *simulation-r* and EC measurements that were greater than those from *simulation-s* were considered to be a reduction in model accuracy caused by substituting gridded weather and soil inputs for those measured at the site. To attribute this reduction to weather vs. soil inputs, *simulation-n* was run with weather inputs from the NARR dataset and soil inputs measured at the sites, and *simulation-p* was run with weather inputs from the site measurements and soil inputs from UNASM. Therefore, the sensitivity of modeled NEP to weather inputs from NARR vs. measurements was evaluated by comparing NEP from *simulation-s* and *simulation-n*, and the sensitivity of modeled NEP to soil inputs from UNASM vs. measurements was evaluated by comparing NEP from *simulation-p* and *simulation-s*.

These evaluations were conducted using Taylor diagrams (Taylor, 2001) of modeled vs. measured CO₂ fluxes that graphically illustrated the closeness in diurnal and seasonal patterns of the different sets of simulated NEP values to the measured benchmark NEP. The diagrams considered closeness based on correlation, central root mean square difference (RMSD) and

standard deviations (SD) between modeled and measured fluxes. Simulated values nearest to the EC values on the x-axis were considered to be the closest to observations, with highest correlation, lowest RMSD and a SD closest to the observed SD.

2.3. Results

2.3.1. Comparison of Gridded vs. Measured Weather and Soil

The agreement of grid cell weather with measured values varied among the weather attributes for each EC site. NARR 3-hour T_a was highly correlated ($R^2 > 0.87$) with measured values at all EC sites (Fig. 2-1) although it was slightly higher at CA-Qfo, US-Dk3 and DL where the y-intercept of the regression of NARR on measured values exceeded 1 °C (Fig. 2-1). NARR and measured incoming shortwave radiation were also correlated very well ($R^2 > 0.78$ in Fig. 2-2 for all sites except at US-Dk3 in 2001). However NARR 3-hourly shortwave radiation was slightly lower for most of the sites and years as the slope of the regression of NARR on measured values was less than 1 for all sites (Fig. 2-2). Total annual radiation in NARR was less than measured values particularly at DL where the NARR values were 16 and 18% lower in 2006 and 2008 respectively and at US-Dk3 in 2001 where they were 10% lower (Table 2-4).

NARR 3-hourly precipitation agreed less with measurements than did T_a and incoming shortwave radiation. However, monthly average NARR aggregated from 3-hourly precipitation was fairly well correlated with measured values (Fig. 2-3) with R^2 ranging from 0.5 - 0.9 except at DL in 2006 where NARR missed a particularly heavy rainfall event in June and at CA-Soa in 2003 where NARR had excessive precipitation in June and July during the 2001 – 2003 drought (Fig. 2-3). Total annual precipitation was generally higher in the NARR dataset at all sites, except for CA-Qfo (Table 2-4).

Measured and UNASM soil inputs differed for most of the EC sites (Table 2-5). UNASM soil depths were smaller than measured values for all sites (particularly at CA-Soa and US-Dk3) except CA-Qfo. Although there were differences in measured vs. UNASM SOC and measured vs. estimated SON, no systematic bias was observed as half of the sites (CA-Ca1, CA-Soa and DL) were shown to have smaller UNASM values than measured whereas they had larger UNASM values in the rest of the sites (CA-Qfo, US-Dk3 and Mead) (Table 2-5). There was anomalously higher UNASM SON estimated in *ecosys* from SOC inputs at CA-Qfo compared to measured values.

2.3.2. Sensitivity of NEP to Gridded Climate and Soil

The Taylor diagrams in Fig. 2-4 indicated that daily NEP in *simulation-s* had lower RMSD, higher correlation coefficients and SD closer to the measured values compared to *simulation-r* for most of the sites. Therefore, CO₂ fluxes modeled using inputs from NARR and UNASM had less accurate diurnal and season patterns than did those using measured weather and soil, when tested against NEP measured at EC flux towers. However, the loss in accuracy with gridded data varied among sites with little loss at some (e.g. CA-Ca1 in Fig. 2-4 (a, b)) and more at others (e.g. CA-Soa, CA-Qfo in Fig. 2-4 (e, f, i, j)). The lower accuracy with inputs from the NARR and UNASM databases are explained as follows:

Campbell River: Douglas-fir forest (CA-Ca1)

The Campbell river Douglas-fir forest EC site has a cool temperate climate with a dry summer. Taylor diagrams (Fig. 2-4 (a, b)) showed close clustering of the four simulations indicating only small differences among them. Daily NEP from all simulations for this site closely agreed with measured values (correlation coefficient > 0.8) during both cooler (2001) and warmer (2004) years (Fig. 2-4). Therefore, key modeled responses of net CO₂ exchange to changes in

weather were maintained when inputs from site weather and soil were replaced by those from NARR and UNASM for the grid cell in which CA-Ca1 is located. The good agreement in seasonal patterns of modeled vs. measured NEP during the cooler and warmer year allowed adverse effects of summer warming events on NEP widely found in coniferous forests to be simulated with both NARR and measured weather data. For instance, days 164 – 174 for 2004 in Fig. 2-5 (b1, b2) had particularly higher T_a (> 20 °C) that reduced NEP (Fig. 2-5b3) through the coupled hydraulic scheme for soil-root-canopy-atmosphere water transfer that lowered g_c (Fig. 2-6b), hence reduced CO_2 influxes (Fig. 2-6c). Higher T_a (Fig. 2-6a) also increased CO_2 effluxes (Fig. 2-6c) through temperature sensitivities of respiration processes as described in Sections 2.2.1.2 and 2.2.1.4. R_a and R_h increased in the warmer year (2004) above those in the cooler year (2001) in both site and gridded simulations (Table 2-6), thereby reducing the annual NEP by 192 and 133 $g\ C\ m^{-2}\ yr^{-1}$ for runs with measured and gridded inputs respectively. This modeled decline in NEP was corroborated by a similar decline of 214 $g\ C\ m^{-2}\ yr^{-1}$ in EC-measured NEP in 2004 vs. 2001 (Table 2-6).

Daring lake: Arctic Tundra

The Daring lake site is a tundra ecosystem located in the lower central Arctic at which we compared NEP during 2006, a warmer year, with that in 2008, a cooler year with similar precipitation (Fig. 2-7). NEP from *simulation-p* was closer to the measured NEP than was NEP from *simulation-n* (Fig. 2-4 (c, d)), indicating that the NARR inputs, particularly the overestimation of T_a (Table 2-4) and underestimation of shortwave radiation (Table 2-4) caused the deviations in seasonal patterns of modeled NEP from *simulation-n* and *-r* (Fig. 2-4 (c, d); Fig. 2-7 (a3, b3)) by reducing T_c and T_s , hence lower soil heat and water transfers that reduce the rate of CO_2 fixation. The NARR seasonal precipitation pattern also differed from measured values in

2006 when the NARR missed a particularly large precipitation event measured in June (Fig. 2-3c). However, spring T_a in 2006 was higher than in 2008 (Fig. 2-7 (a1, a2, b1, b2)) resulting in earlier net C uptake, thus key modeled responses of net CO_2 exchange to changes in spring warming, apparent in the EC-measured NEP, were captured in both measured and gridded simulations (Fig. 2-7 (a3, b3)). Moreover, for those summer days with T_a exceeding 20°C (e.g. days 200 and 220 for 2006 in Fig. 2-7 (a1, a2) and around day 200 for 2008 in Fig. 2-7 (b1, b2), NEP declined (Fig. 2-7 (a3, b3)) due to a decrease in CO_2 fixation and an increase in R_a and R_h , as noted earlier for Campbell river site (Fig. 2-5b3), and these responses were captured in both site and gridded simulations (Fig. 2-7 (a3, b3)).

Old Aspen forest (CA-Soa)

This site is an old Aspen forest in the boreal climate zone in which we compared NEP during 2001 and 2003, the first and third years of a major drought in central North America (Fig. 2-8). The Taylor diagrams (Fig. 2-4 (e, f)) showed that NEP modeled from both NARR and UNASM inputs differed from EC-derived values more than did NEP modeled from measured inputs. Regression of modeled on EC-derived CO_2 fluxes in *simulation-s* had a larger correlation coefficient, lower RMSD, and SD closer to SD from EC-derived values, compared to *simulation-n* and *simulation-p* for both 2001 and 2003. Variations in seasonal amplitude of NEP (Fig. 2-8) apparent as smaller SD (Table 2-4) in simulations with UNASM vs. measured soil inputs (*p* vs. *s* and *r* vs. *n* in Fig. 2-4 (e, f) were attributed to shallower UNASM vs. measured soil depth (1 vs. 3 m in Table 2-5) which reduced water holding capacity and consequently hastened soil drying. Annual NEP of *simulation-r* was therefore lower than that of *simulation-s* (Table 2-6) due to inadequate soil water in the shallow UNASM to sustain productivity during the first drought year in 2001 (Fig. 2-8a1). NEP measured and modeled with site inputs in 2001 was sustained by water

deeper in the measured soil profile carried forward from previous wetter years. This deeper water was depleted by 2003, reducing NEP (Fig. 2-8b2 vs. 2-8a2; Table 2-5). However this deeper water was absent in the UNASM soil profile in 2001, resulting in faster soil drying, lower g_c and hence CO₂ uptake rates to values much lower than EC measurements (Fig. 2-8a2) while net C uptake modeled with measured soil remained close to EC values. Excess summer NARR precipitation in July 2003 (Fig. 2-3f), however resulted in higher soil water content (Fig. 2-8b1), hence better CO₂ uptake rates, followed by rapid soil drying as a result of the shallow soil depth.

Duke loblolly pine forest (US-DK3)

Duke forest is a loblolly pine in a subtropical climate where NEP was compared during the first and second years of the 2001 – 2002 drought (Fig. 2-9). Lower correlation and greater RMSD of *simulation-n* vs. *s* than of *simulation-p* vs. *s* (Fig. 2-4 (g, h)) indicated that the simulation of NEP was more adversely affected by inputs from NARR vs. measured weather than from UNASM vs. measured soil. Although a good correlation ($R^2 = 0.86$) of NARR vs. measured incoming shortwave radiation was observed in 2002 (Fig. 2-2h), a 10% decline in NARR annual incoming shortwave radiation was observed in 2001 (Table 2-4) with $R^2 = 0.68$ (Fig. 2-2g). Also, NARR T_a was higher than measured values, especially in 2001 where the y-intercept of the regression lines was 1.76 °C (Fig. 2-1g), resulting in rapid evapotranspiration and hence soil drying, lowering g_c and hence NEP. The slight deviation of *simulation-p* vs. *s* observed in 2001/2002 could mainly be attributed to shallower UNASM soil depth that reduced soil water holding capacity (Table 2-5), hence contributed to the lower net CO₂ fixation. Decline of NEP in summer 2002 was greater than that in 2001 for both site and gridded runs (Fig. 2-9b3 vs. 2-9a3) due to lower summer precipitation (Fig. 2-3 (g, h)). The seasonal NARR precipitation pattern allowed this decline to be modeled in the gridded simulation similarly to that in the site simulation.

Quebec mature boreal black spruce forest (CA-Qfo)

CA-Qfo is a boreal black spruce forest site at which we compared 2004, a cooler year, with 2005, a warmer year. *Simulations-s* and *-n* were closer to measured NEP than were *simulations-p* and *-r* (Fig. 2-4 (i, j)) for both years, indicating that the UNASM soil input was mainly responsible for the differences in NEP. These differences were attributed to anomalously low SON measured at the CA-Qfo site (Table 2-5) which was less than that estimated from general SOC:SON relationships used with the UNASM inputs. This lower site SON resulted in slower root N uptake hence lower NEP than those with gridded soil inputs (Table 2-6), which was more consistent with EC values (Fig. 2-10). However, key seasonal variations in NEP were simulated with both NARR and measured weather. Earlier spring warming in 2005 vs. 2004 caused a 10-day earlier increase in net CO₂ uptake (Fig. 2-10b3 vs. 2-10a3) which was captured in both site and gridded simulations. Despite increased earlier carbon uptake, more frequent summer warming events during 2005 (e.g. DOY 180, 240) vs. 2004 (e.g. DOY 185) caused declines in NEP when T_a was higher than 20 °C through processes described in Sections 2.2.1.1 and 2.2.1.4 and demonstrated in Fig. 2-6.. Diurnal variations in NARR T_a allowed the effects of these events on NEP to be represented similarly to those with measured inputs (Fig. 2-10).

Mead Crop site

This site had an irrigated vs. rainfed maize soybean rotation where in 2003 maize was simulated with and without irrigation. The Taylor diagrams (Fig. 2-4 (k, l)) showed that NEP from *simulation-n* were closer to the EC values than were those of *simulation-p*, indicating that the slight differences were mainly attributed to the UNASM soil inputs (UNASM soil depth (1.5m) compared to site soil depth (2m)). However, key responses of earlier decline in modeled NEP to water stress effects during soil drying in the rainfed vs. irrigated runs were captured in both

simulation-s and $-r$ (Fig. 2-11) indicating sufficient accuracy in NARR to model crop water stress effects in the Mead region. The rainfed simulations were shown to have faster soil drying, causing more rapid declines in ψ_s , ψ_c , and g_c , hence lower CO₂ influxes (Fig. 2-12; Table 2-6) than the irrigated simulations for both runs with site and gridded inputs. These declines were apparent in declines of latent heat (LH) and CO₂ fluxes within the rainfed vs. irrigated simulations. These declines reduced productivity for the rainfed simulations, in both the site and gridded simulations (Fig. 2-11), allowing water stress in the rainfed run to be simulated consistent with fluxes from EC measurements (Fig. 2-12).

2.4. Discussion

2.4.1. Uncertainties in Gridded Weather and Soil

Differences in modeled NEP using gridded vs. measured inputs at site scale (Fig. 2-4) could be an important indicator in quantifying sources of uncertainty in NEP when such gridded model inputs are used to estimate continental carbon balances. In aggregating carbon exchange from site to regional scales uncertainties could originate from inaccuracies in (1) the model, (2) the model drivers (Moorcroft, 2006), and (3) the measured fluxes at EC towers used to test model values. Uncertainty in modeled NEP attributed to model structure and parameterization were shown by testing NEP simulated with measured inputs against EC values, with which the model results had generally a good agreement (Fig. 2-4; Table 2-6). This agreement demonstrated the ability of the model to simulate land-atmosphere carbon exchange across different climatic zones with varied plant functional types, under contrasting weather. In earlier studies *ecosys* has been tested rigorously under a wide range of climates and biomes as described in the introduction. Moreover, the model performed very well in the North American Carbon Program site synthesis- model intercomparison study (Schaefer et al., 2012; Schwalm et al., 2010a) where the skill of the model

to simulate carbon exchange over several EC sites across North America was compared with more than 22 participating models. It should also be noted that estimating uncertainties from inherent model structure, by comparing NEP from site simulations with EC-derived values, should also consider some uncertainties that might be associated with the measured benchmark data itself (e.g. EC data processing methods and gap-filling) which we have not accounted for in this study.

Uncertainties in the quality of gridded model drivers were assessed in the Taylor diagrams (Fig. 2-4) that illustrated differences in NEP modeled with inputs from gridded vs. measured weather and soil when compared to EC-derived NEP. These differences were larger for NEP modeled with gridded inputs than with measured inputs at most of the sites (Fig. 2-4) indicating that agreement of NEP modeled in those grid cells with EC-derived values was adversely affected by gridded inputs, particularly during years with extreme climate events such as drought, as in CA-Soa site in 2001/ 2003 (Fig. 2-8). However, the magnitude of these differences in NEP varied among sites (Fig. 2-4) with relatively little differences at some sites (e. g. Fig. 2-4 (a, b)) and greater differences at others (e. g. Fig. 2-4 (e, f)). Overall, NEP from the gridded simulations tended to deviate from EC-NEP more than did those from the site simulations (Table 2-6). These effects of gridded model drivers on NEP could have important implications in estimating the impacts of climate change on land-atmosphere carbon exchange at regional and continental scales, particularly as affected by extreme events such as heat waves and droughts.

These uncertainties associated with the quality of NARR and UNASM could be attributed to different causes. Uncertainties from NARR could be attributed to variations in the density of the networks of observational datasets that were used to construct the gridded dataset (Mesinger et al., 2004). For instance, sparse distribution of weather stations, especially in higher latitudes of NA could affect the accuracy of the gridded product. Uncertainties from UNASM could be

attributed to spatial heterogeneity within a $0.25^0 \times 0.25^0$ pixel, as soil properties vary at much smaller spatial scales which makes it difficult to assess how well the measured or gridded soil represents the diverse soils of a grid cell. Uncertainties associated with sub-pixel heterogeneity could partly be improved by increasing the spatial and temporal resolutions of model inputs and implementing cohorts of multiple plant functional types at a grid cell level. Furthermore, UNASM was a product from the fusion of three different soil datasets (STATSGO2, SLC version 2.2 and HWSD version 1.1) that were constructed using different inputs and methods of upscaling across different regions of North America. These products had different spatial resolutions and a certain loss of accuracy can be expected while harmonizing these products thereby affecting the skill of the model in simulating land-atmosphere carbon exchange.

2.4.2. Gridded Weather Attributes that Caused Differences in Modeled NEP

NARR 3-hourly T_a had generally better fits with measurements than did NARR incoming shortwave radiation and precipitation (Fig. 2-1; Table 2-4). However, the accuracy of gridded T_a was spatially and temporally variable, being slightly overestimated for some sites compared to measured values (Fig. 2-1), resulting in more adverse impacts of warming with NARR weather in some sites (e. g. DK3 2001) by hastening rapid soil drying, lowering g_c hence NEP (Table 2-6). Nevertheless, for most of the sites NARR T_a was accurate enough that the effects of diurnal and seasonal changes in T_a under contrasting weather (cool vs. warm years) on NEP, shown in the site simulations, were mostly captured in the gridded simulations (e.g. Fig. 2-5). NARR enabled simulation of key model responses to changes in seasonal weather, such as earlier spring warming that caused earlier increases in net CO_2 uptake as shown in DL 2006 (Fig. 2-7) and CA-Qfo 2005 (Fig. 2-10) and the impacts of intense warming events that reduced CO_2 uptake and increased respiration as shown in CA-Ca1 (Fig. 2-5).

The NARR incoming shortwave radiation and precipitation that we used in this study were rescaled from the original NARR datasets (Mesinger et al., 2004) to improve their quality (Wei et al., 2014). Comparison of original NARR incoming shortwave radiation with measurements from 23 EC sites has shown that NARR values were overestimated (Wei et al., 2014). A comparison of the original NARR precipitation with measurements has shown that the amount and frequency of large rainfall events in NARR precipitation were underestimated (Sun and Barros, 2010). Although the rescaled NARR incoming shortwave radiation and precipitation were shown to improve the original NARR, in this study we identified biases at some of the sites as described earlier in Section 2.3.1 that affected modeled NEP to sufficient extents that further improvements are needed (e.g. Fig. 2-4 (c, d, h)).

Although NARR incoming shortwave radiation was well correlated with measurements, underestimation of more than 10% in some sites, (e.g. DL, Table 2-4) could reduce soil heat and water transfers and hence reduce the rate of CO₂ fixation by lowering T_c and T_s. Seasonal patterns of modeled NEP could also be controlled by variations shown in NARR vs. measured precipitation, apparent in variations in total annual precipitation and SD (Table 2-4). These variations control NEP by directly controlling the amount of soil moisture available for plant uptake and indirectly affecting the availability of nutrients. For instance, CA-Soa 2001 / 2003 NARR precipitation had higher summer values than measured (Fig. 2-3 (e, f)) which caused higher SD of NEP from EC values (Table 2-4) than did site precipitation (Fig. 2-7). Similar to the NARR T_a and incoming shortwave radiation, the relative differences of NARR vs. measured precipitation and their effects on modeled NEP varied among sites (Fig. 2-3).

2.4.3. Gridded Soil Attributes that Control NEP Deviations

UNASM soil attributes such as maximum soil depth and SOC, as well as SON which was estimated independently from UNASM SOC, were shown to affect NEP for most of the sites as demonstrated from the deviations of *simulation-p* compared to *simulation-s* shown in the Taylor diagrams (Fig. 2-4). McKenney and Pedlar (2003) reported a decline in modeled productivity of jack pine and black spruce when replacing measured soil properties with coarser scale soil properties and this was attributed to shallower soil depth of the coarser dataset across much of the northern forests of Canada. This result corroborated our findings at CA-Soa, DL, US-Dk3 and Mead in which UNASM had shallower soil depth compared to measured soil (Table 2-5). These effects of shallower soil depth were shown to reduce productivity in some of the sites (e.g. CA-Soa) by reducing soil water storage, hastening soil drying (Fig. 2-8 (a1, b1)), lowering ψ_s and water uptake and hence lowering NEP (Fig. 2-8 (a2, b2); Table 2-6). Soil databases that were used to make UNASM in the higher latitudes such as SLC version 3.2 and Harmonized World Soil Database (HWSD) version 1.1 had much smaller maximum soil depth values than measured. The lack of deeper soil profiles in UNASM could limit responses of modeled rooting depth to climate change, particularly at higher latitudes where rooting depth is determined by deepening permafrost which is explicitly modeled in *ecosys*. There were also significant differences in total SOC between UNASM and measured soil inputs (Table 2-5) and between estimated and measured SON that directly affected the amount of available nutrients hence ecosystem productivity at CA-Qfo (e. g. Fig. 2-10 (a3, b3)). Although this effect of gridded SON was modeled at the site scale, it has important implications as the site represents an ecosystem (boreal black forest) widely distributed across boreal NA.

Although these effects of NARR and UNASM on NEP were shown at a pixel scale of the gridded datasets, it is apparent that the effects could be reflected in model estimates when scaled-up and that would certainly affect the regional and continental carbon budget estimates. These impacts at regional scales could have direct implications when modeling the impacts of climate change on ecosystem productivity. For instance, key model responses to extreme weather events such as drought might not be captured well as demonstrated at CA-Soa 2001 (Fig. 2-8a2). However, it should also be noted that over/underestimations of fluxes among pixels would possibly compensate each other, thereby smoothing out the overall impacts of the gridded model inputs on carbon estimates at regional and continental scales.

2.5. Conclusions

NEP differences attributed to gridded vs. measured model inputs varied among sites when tested against EC-derived values (Fig. 2-4). The degree of agreements between the NARR and site T_a were shown to be generally high enough (Fig. 2-1) that the NEP modeled under contrasting weather could be reproduced with NARR with an accuracy similar to that with measured weather for most of the sites (e.g. Fig. 2-5). Incoming shortwave radiation was slightly underestimated for most of the sites, hence needing further improvements (Fig. 2-2). Deviations in precipitation intensity should also be improved (Fig. 2-3), as accurate temporal distribution of precipitation determined water availability for plant growth and enabled the model to capture the impacts of extreme weather events such as drought.

Lack of detailed and deeper UNASM soil profiles affected modeled NEP at most of the sites, especially by reducing WHC and hence θ during extreme weather events such as drought as demonstrated at CA-Soa 2001 (Fig. 2-8a2). Total SOC content of UNASM was also varied from what was measured at the sites (Table 2-5). Besides, UNASM did not include SON and therefore,

incorporating this attribute in the database is important to better estimate available soil nitrogen, hence NEP.

These differences in modeled NEP associated with the quality of gridded model drivers that we tested for the selected EC sites at grid cell scale would certainly be reflected at regional scale. Therefore, further refinement of these gridded datasets to improve their accuracy, spatial and temporal resolutions and better represent spatial heterogeneity is essential for improving estimates of carbon fluxes at regional and global scales.

List of Tables

Table 2-1. Eddy Covariance flux tower sites and years with contrasting weather used for site and gridded runs

Site name	Ecosystem	Climate	Latitude +N/-S	Longitude +E/-W	Site climate data	Years	Contrast
CA-Ca1	Douglas-fir forest	Cool temperate with dry, warm summer	49.87	-125.33	1999 - 2008	2001/2004	cool/warm
DL	Arctic Tundra	Low arctic	64.87	-111.57	2004 - 2009	2006/2008	warm/cool
Ca-Soa	Old Aspen	Boreal	53.63	-106.20	1994 - 2008	2001/2003	pre-drought vs. drought
US-Dk3	Loblolly pine forest	Warm temperate	35.98	-79.10	1999 - 2005	2001/2002	pre-drought vs. drought
Ca-Qfo	Boreal black spruce forests	Boreal	49.69	-74.34	2004 - 2008	2004/2005	cool/warm
Mead	Maize soybean rotation	Warm temperate with humid hot summer	41.18	-96.44	2001 - 2006	2003	irrigated vs. rainfed

Table 2-2. Model drivers used in the gridded and site simulations

Model Drivers	Simulation	Temporal period	Temporal resolution	Data source
Climate	site	vary with EC sites	half-hourly	Ameriflux sites ¹
	grid	1979-2010	3-hourly	NARR ²
Soil	site	one-time	one-time	Ameriflux sites
	grid	one-time	one-time	UNASM ³ (SSURGO (US) + SLC v3.2 (CA) + HWSD v1.1 (MX))
CO₂	site, grid	1800-2010	monthly	Enhanced GlobalView ²
Nitrogen deposition	site, grid	1800-2010	yearly	Enhanced Dentener ²
Land use change	site, grid	1800-2010	yearly	Hurttt's harmonized with SYNMAP ²

*all gridded model inputs had 0.25⁰ x 0.25⁰ spatial resolutions

site = simulation using measured inputs, grid = simulation using pixel extracted from gridded dataset

¹ http://fluxnet.ornl.gov/site_list/Network/1

² MsTMIP model drivers (Wei et al., 2014)

³ Unified North America Soil Map (Liu et al., 2013)

Table 2-3. Simulation design to partition NEP sensitivity to gridded weather and soil drivers

Simulation name	Climate forcing	Soil	Simulation period	Output
<i>Simulation-s</i>	site	site	1800 – 2010	Site estimate
<i>Simulation-r</i>	grid	grid	1800 – 2010	Gridded estimate
<i>Simulation-n</i>	grid	site	1800 - 2010	Model sensitivity to gridded weather
<i>Simulation-p</i>	site	grid	1800 – 2010	Model sensitivity to gridded soil

site = simulation using measured inputs, grid = simulation using pixel extracted from gridded dataset

Table 2-4. Measured and gridded mean annual T_a , annual total precipitation and radiation for contrasting years

EC - site	Year	Model inputs	Surface air temperature		Precipitation		Incoming shortwave radiation	
			Mean annual ($^{\circ}\text{C}$)	Standard deviation ($^{\circ}\text{C}$)	Annual total (mm)	Standard deviation (mm month^{-1})	Annual total (MJ m^{-2})	Standard deviation ($\text{W m}^{-2} \text{day}^{-1}$)
CA-Ca1	2001	site	8.1	5.8	1115	222	3935	196
		grid	8.0	5.9	1575	297	3943	189
	2004	site	8.8	6.7	1232	152	4109	212
		grid	9.4	6.6	2319	270	3919	188
DL	2006	site	-7.3	15.7	288	40	3608	177
		grid	-5.4	15.4	311	16	2968	148
	2008	site	-10	17.3	277	29	3569	181
		grid	-6.8	17.8	304	22	3003	151
CA-Soa	2001	site	3.0	12.2	235	18	4574	213
		grid	3.7	14.2	313	20	4293	197
	2003	site	1.9	14.5	261	15	4412	206
		grid	2.4	15.4	385	23	4185	192
US-Dk3	2001	site	14.5	8.9	947	48	5241	229
		grid	15.8	9.1	1106	30	4662	206
	2002	site	15.0	9.8	1092	59	4896	221
		grid	16.4	10.2	1118	47	5237	219
CA-Qfo	2004	site	-0.3	13.8	1016	29	3931	196
		grid	0.8	13.6	941	30	4166	190
	2005	site	1.6	14.3	943	50	4144	204
		grid	2.7	14	933	35	4170	191
Mead	2003	site	10.3	12.3	570	35	5616	253
		grid	10.9	12.7	631	36	5248	221

site = measured at EC sites, grid = pixel extracted from gridded dataset

Table 2-5. List of soil variables (maximum depth, initial available soil water and organic carbon) for measured and gridded soil inputs of the six EC flux tower sites

EC - site	Simulation	Maximum Depth(m)	Available Water Content (mm)	Total Organic Carbon (g C m ⁻²)		Total Nitrogen* (g N m ⁻²)	
				0 – 30 cm	Below 30 cm	0 – 30 cm	Below 30 cm
CA-Ca1	site ¹	1.63	279	24062	12395	1197	1913
	grid ³	1	281	5984	14650	624	1606
DL	site ²	2.3	576	23215	8327	1032	580
	grid ³	1.8	494	4080	12239	448	1344
CA-Soa	site ¹	3	323	19176	4794	1259	355
	grid ³	1	100	7600	4463	660	388
US-Dk3	site ¹	3.75	378	7270	3116	586	316
	grid ³	1.65	170	2928	11716	345	1383
CA-Qfo	site ¹	1	140	10077	1115	328	165
	grid ³	1	178	10047	6698	820	546
Mead	site ¹	2	366	7377	6542	561	608
	grid ³	1.5	308	12769	27135	1012	2150

site = measured at EC sites, grid = pixel extracted from gridded dataset

*gridded total soil nitrogen was estimated from gridded total organic carbon

¹ data source: <http://ameriflux.ornl.gov/>; <http://fluxnet.ornl.gov/>

² data source: Lafleur and Humphreys, 2008

³ data source: The Unified North American Soil Map: (Liu et al., 2013)

Table 2-6. Annual carbon budget of measured vs. gridded simulations and EC measurements for contrasting years for six EC flux tower sites

EC site	Year	Model inputs	C balance ^a - modeled						C balance - derived from EC measurements			
			GPP	Ra	NPP	Rh	Re	NEP	GPP	Re	NEP	Source
CA-Ca1	2001	site	1969	1163	806	386	1549	420	2077	1668	409	(Krishnan et al., 2009)
		grid	1923	1211	711	362	1573	349				
	2004	site	1872	1195	677	440	1635	228	2338	2143	195	
		grid	2015	1330	685	469	1799	216				
DL*	2006	site	308	137	170	103	238	68	-	-	61*	(Lafleur and Humphreys, 2008)
		grid	245	106	139	98	204	41				
	2008	site	261	120	141	78	198	63	-	-	73*	
		grid	252	111	141	83	194	58				
CA-Soa	2001	site	1457	779	678	449	1228	229	1217	892	325	(Krishnan et al., 2006)
		grid	730	392	337	249	641	88				
	2003	site	1190	680	509	444	1124	65	917	823	91	
		grid	789	413	376	272	685	104				
US-Dk3	2001	site	2640	1219	1421	712	1931	709	-	-	607	(Oren et al., 2006)
		grid	1669	927	745	437	1364	304				
	2002	site	2316	1228	1088	639	1867	449	2346	2076	270	
		grid	1519	943	575	423	1366	153				
CA-Qfo	2004	site	692	378	314	304	682	10	600	590	9.8	(Bergeron et al., 2008)
		grid	997	569	428	322	891	106				
	2005	site	790	452	338	305	757	34	699	656	42	
		grid	1034	650	384	346	996	39				
Mead	2003	site-i	1895	792	1103	278	1070	825	1793	1221	600	(Verma et al., 2005)
		grid-i	1384	539	845	158	697	687				
		site-r	1593	657	936	296	953	640				
		grid-r	1167	457	710	153	610	557				

site = measured at EC sites, grid = pixel extracted from gridded dataset, site-i = measured and irrigated, site-r = measured and rainfed, grid-i = grid pixel and irrigated, grid-r = grid pixel and rainfed

^a C balance in g C m⁻²yr⁻¹ except for

*DL in g C m⁻² growing season⁻¹ measured during day of the year (DOY): 137 – 240 for 2006 and 121 -246 for 2008

List of Figures

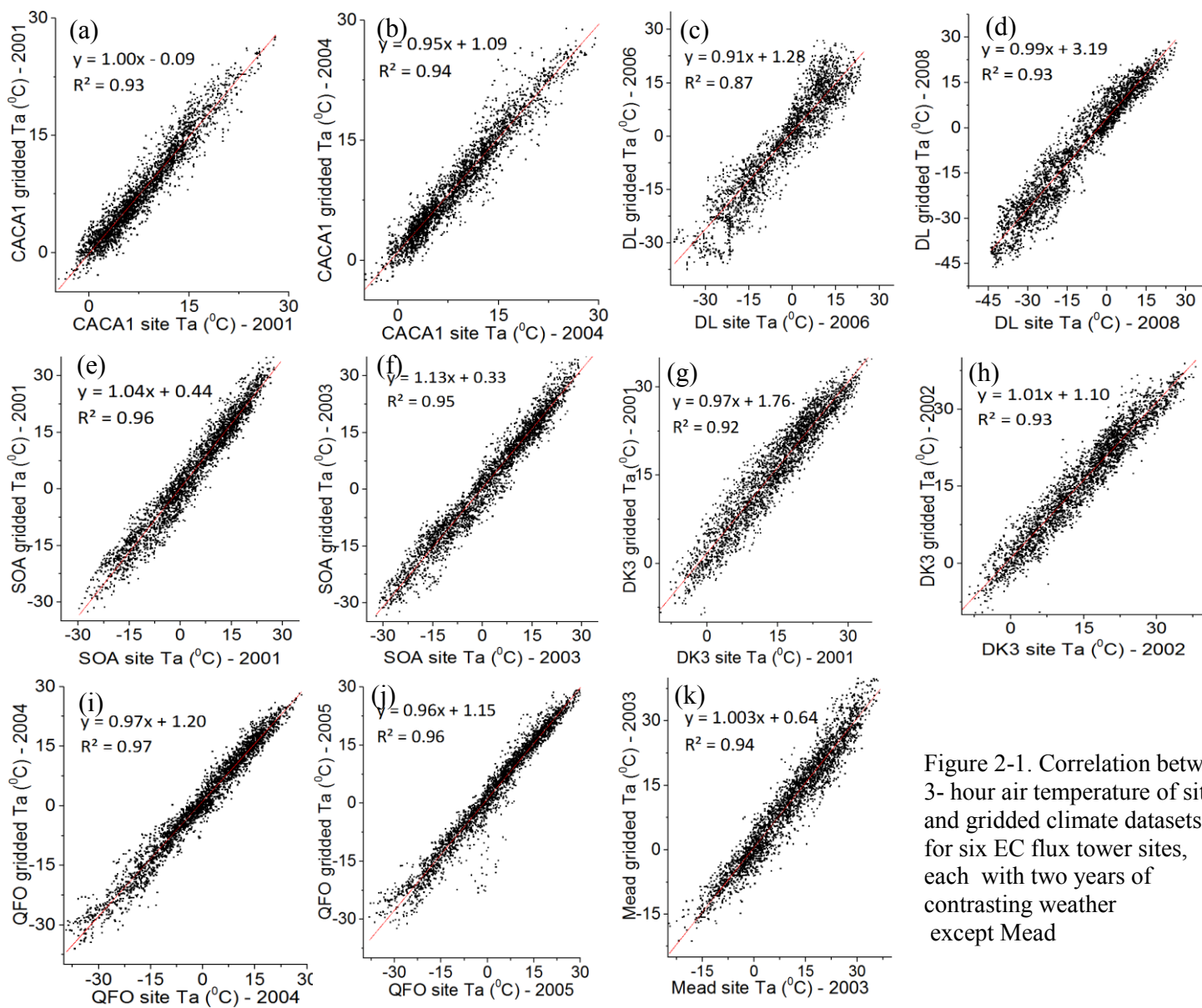


Figure 2-1. Correlation between 3- hour air temperature of site and gridded climate datasets for six EC flux tower sites, each with two years of contrasting weather except Mead

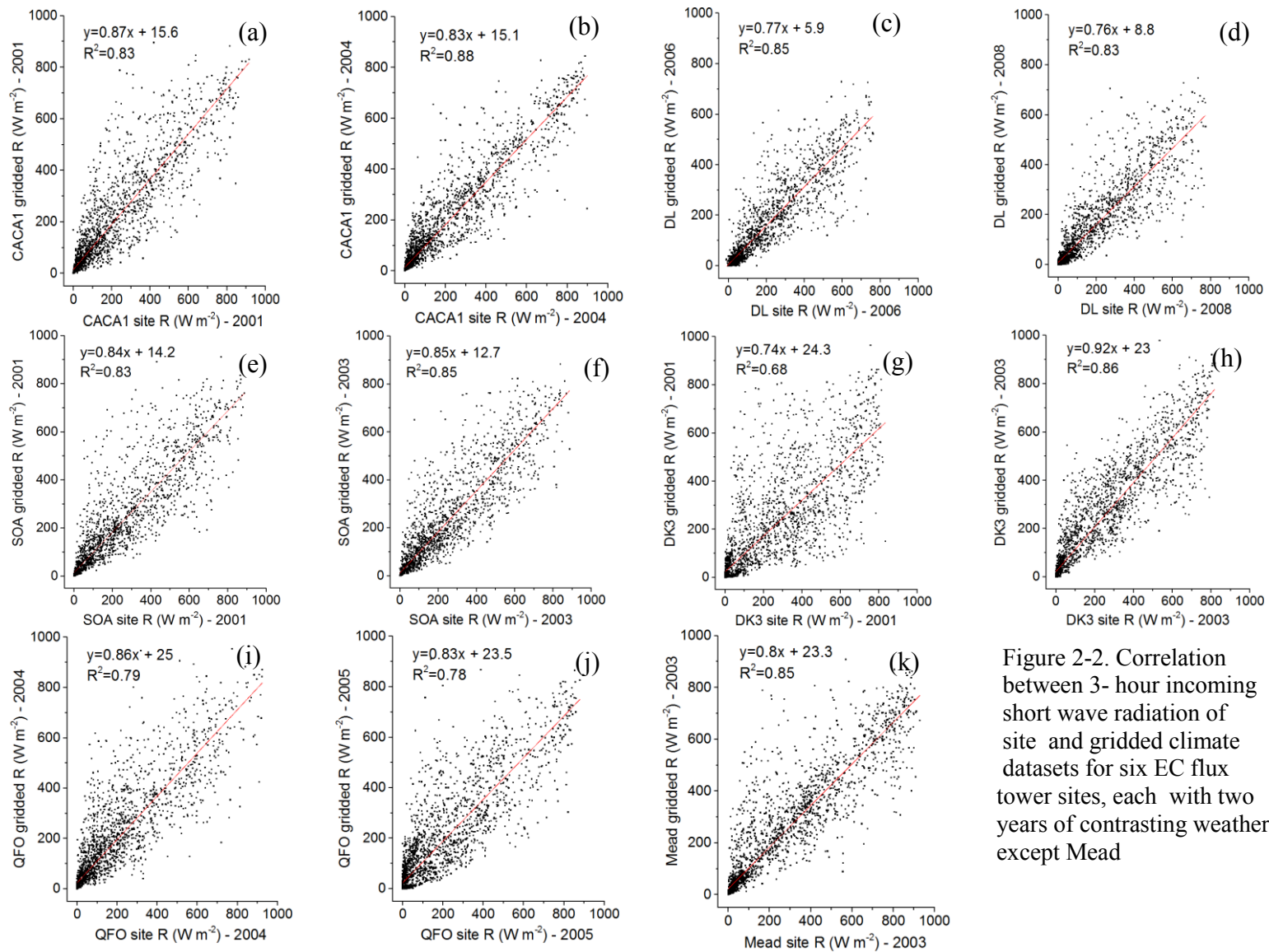


Figure 2-2. Correlation between 3- hour incoming short wave radiation of site and gridded climate datasets for six EC flux tower sites, each with two years of contrasting weather except Mead

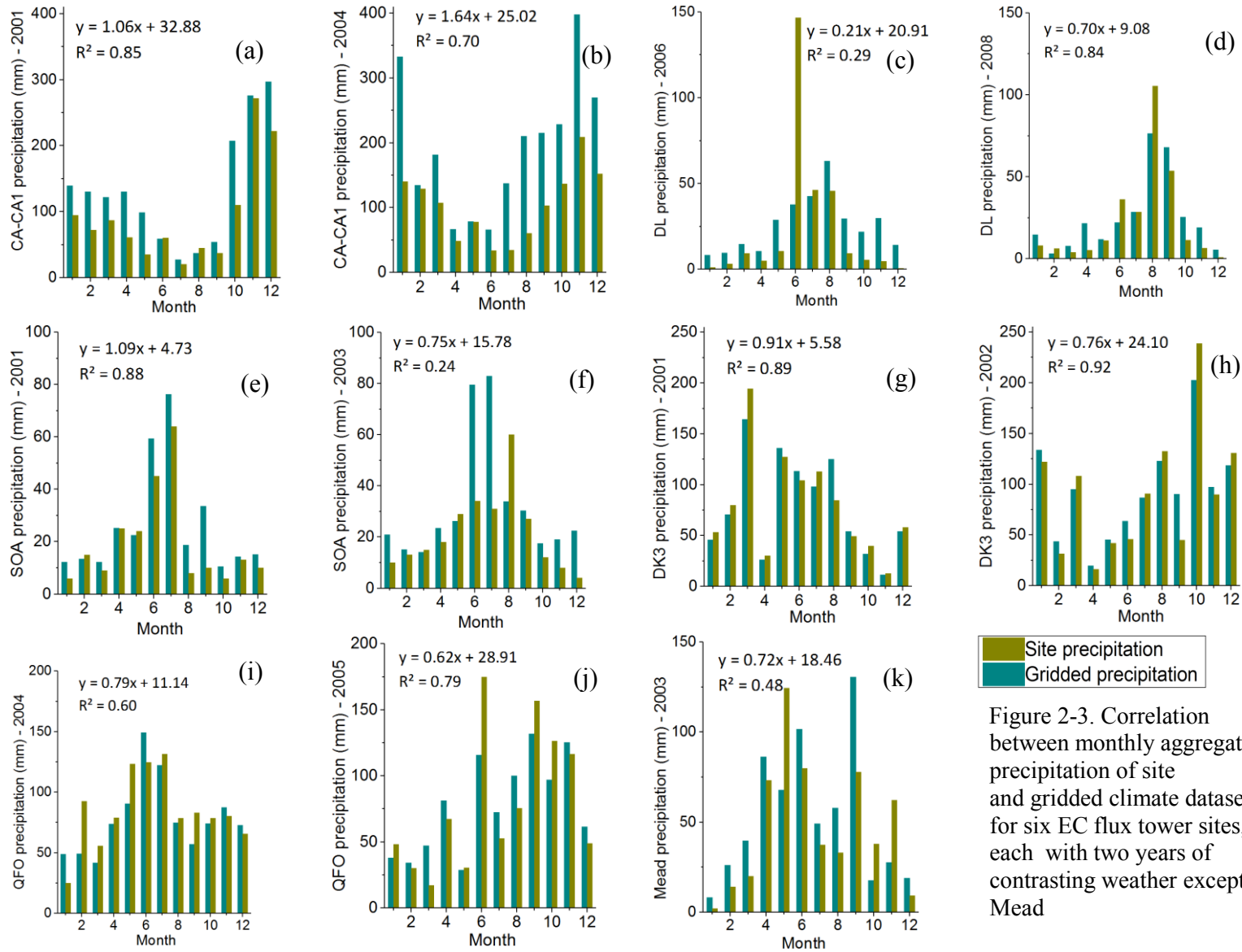


Figure 2-3. Correlation between monthly aggregated precipitation of site and gridded climate datasets for six EC flux tower sites, each with two years of contrasting weather except Mead

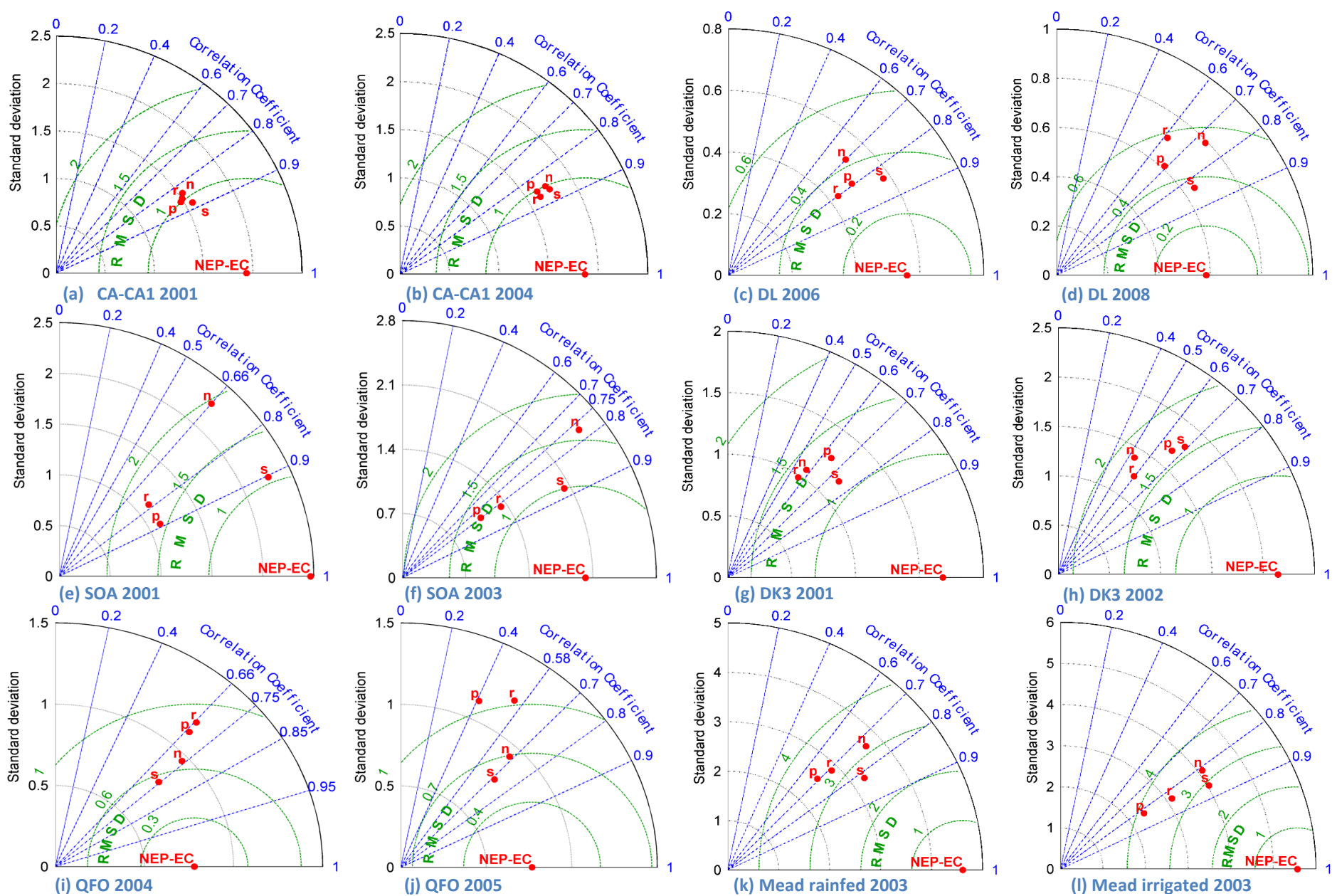


Figure 2-4. Taylor diagrams showing a comparison of four sets of simulated NEPs (g C day^{-1}) (*s*: site weather and soil, *n*: NARR weather and site soil, *p*: site weather and UNASM soil, *r*: NARR weather and UNASM soil) with observed NEP (NEP-EC) of six EC flux tower sites under a contrasting weather (Table 2-1). The RMSD (g C day^{-1}) between the simulated and observed NEP is the distance between a simulated values along the green line to the x-axis at NEP – EC, standard deviation (g C day^{-1}) is the distance from a point to the origin and correlation coefficient of each simulated values is shown in the blue line

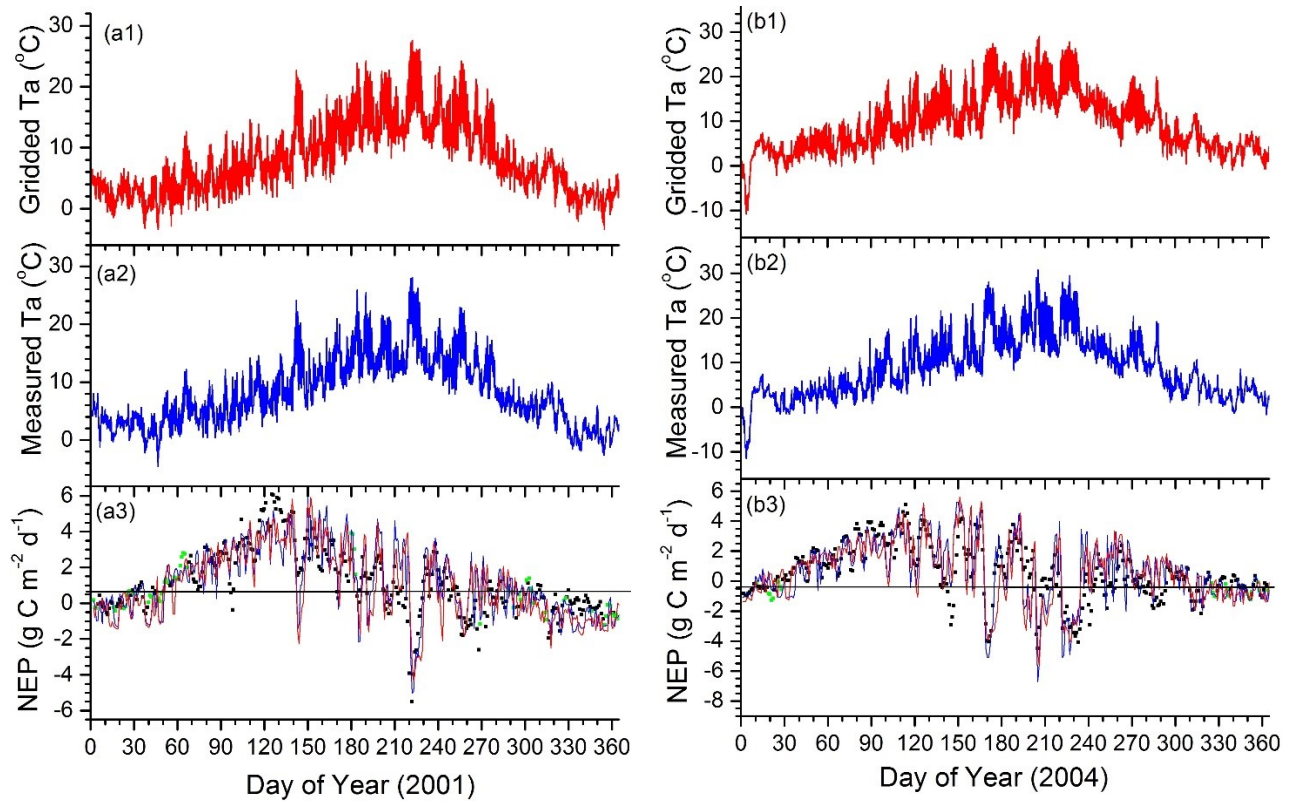


Figure 2-5. Campbell river Douglas-fir forest (CA-CA1): (a1, a2, b1, b2) 3-hourly air temperature, (a3, b3) daily NEP measured at EC (black closed symbols), gap-filled from EC measurements (green closed symbols), modeled NEP using site climate and soil (blue lines) and regional climate and soil (red lines) for a cooler year 2001 and a warmer year 2004.

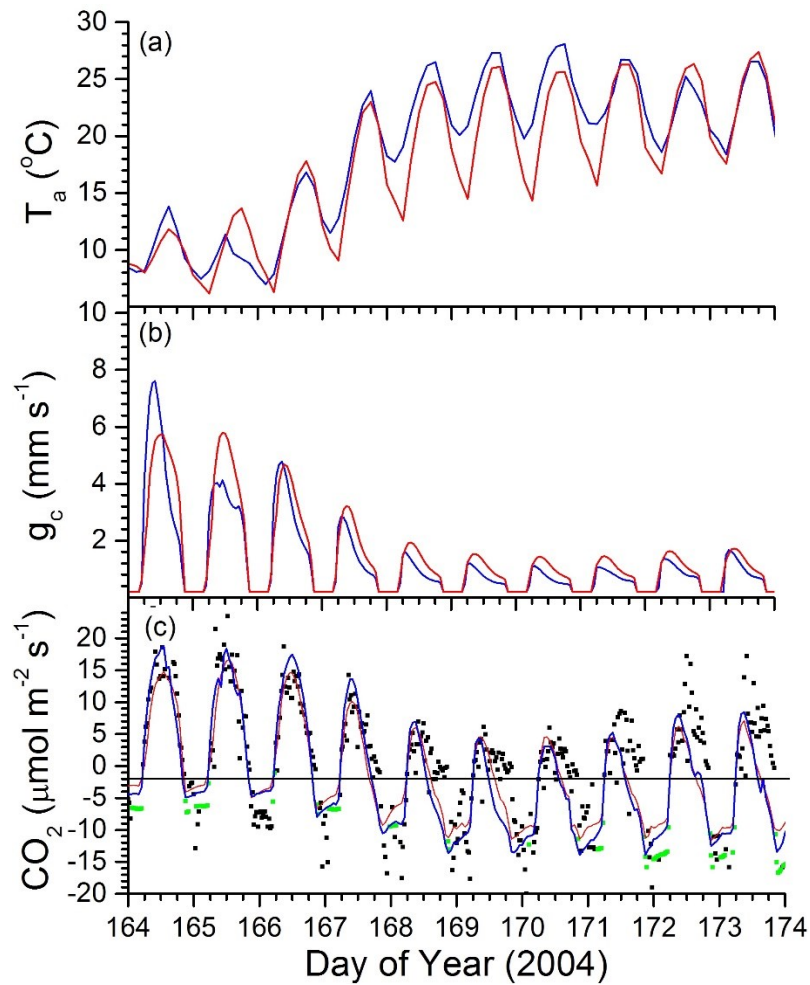


Figure 2-6. Campbell river Douglas-fir forest (CA-CA1): (a) hourly gridded (red line) and site (blue line) air temperature (T_a), (b) hourly modeled canopy stomatal conductance (g_c), modeled with site climate and soil (blue lines) and regional climate and soil (red lines) and (c) hourly modeled CO_2 flux, modeled with site climate and soil (blue lines) and regional climate and soil (red lines) at EC (black closed symbols), gap-filled from EC measurements (green closed symbols), for DOY 164 – 174 of a warmer year (2004)

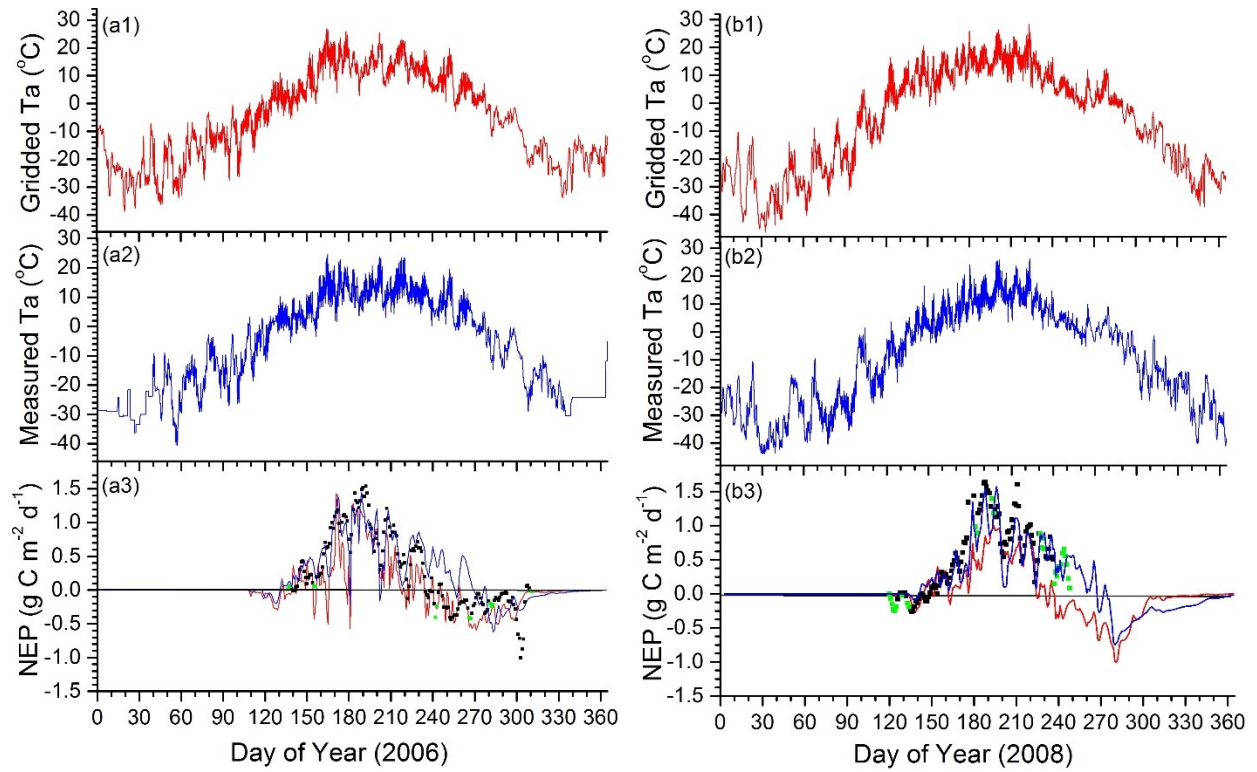


Figure 2-7. Daring lake arctic tundra (DL): (a1, a2, b1, b2) 3-hourly air temperature, (a3, b3) daily NEP measured at EC (black closed symbols), gap-filled from EC measurements (green closed symbols), modeled NEP using site climate and soil (blue lines) and regional climate and soil (red lines) for the years of 2004 and 2005.

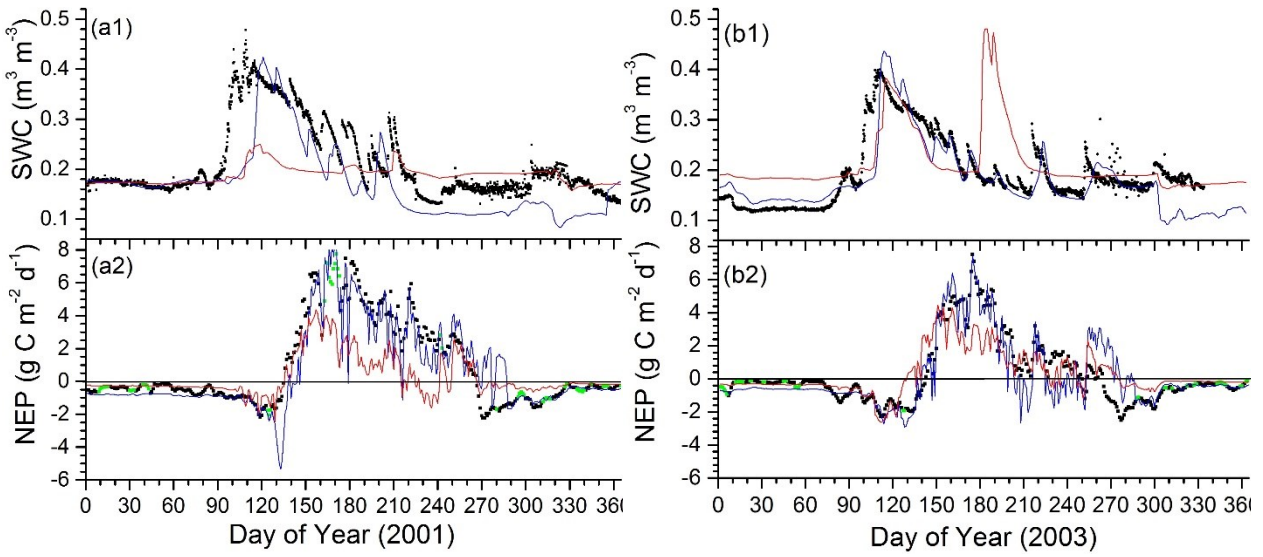


Figure 2-8. Old Aspen forest (SOA): (a1, b1) daily volumetric soil water content at 15cm soil depth, (a2, b2) daily NEP measured at EC (black closed symbols), gap-filled from EC measurements (green closed symbols), modeled NEP using site climate and soil (blue lines) and gridded climate and soil (red lines) for the first (2001) and third (2003) years of a drought

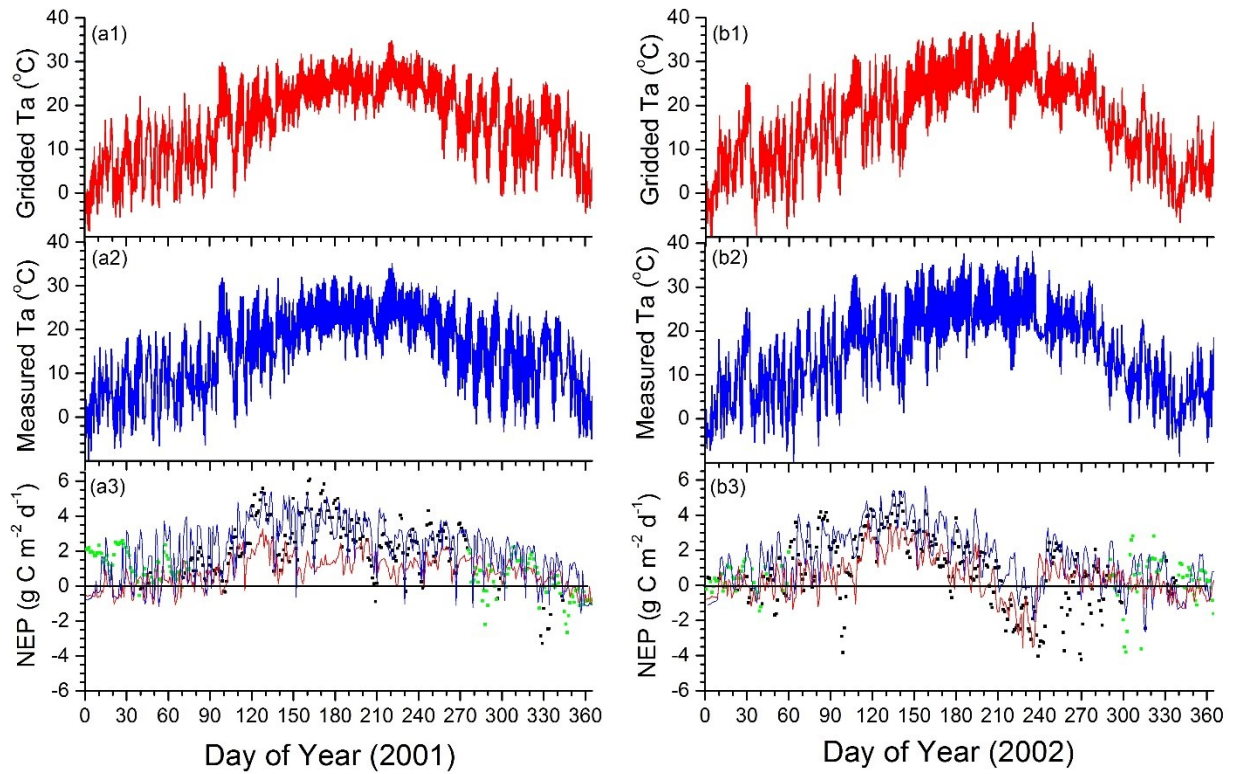


Figure 2-9. Duke forest (DK3): (a1, a2, b1, b2) 3-hourly air temperature, (a3, b3) daily NEP measured at EC (black closed symbols), gap-filled from EC measurements (green closed symbols), modeled NEP using site climate and soil (blue lines) and regional climate and soil (red lines) for a pre-drought year 2001 and a drought year 2002

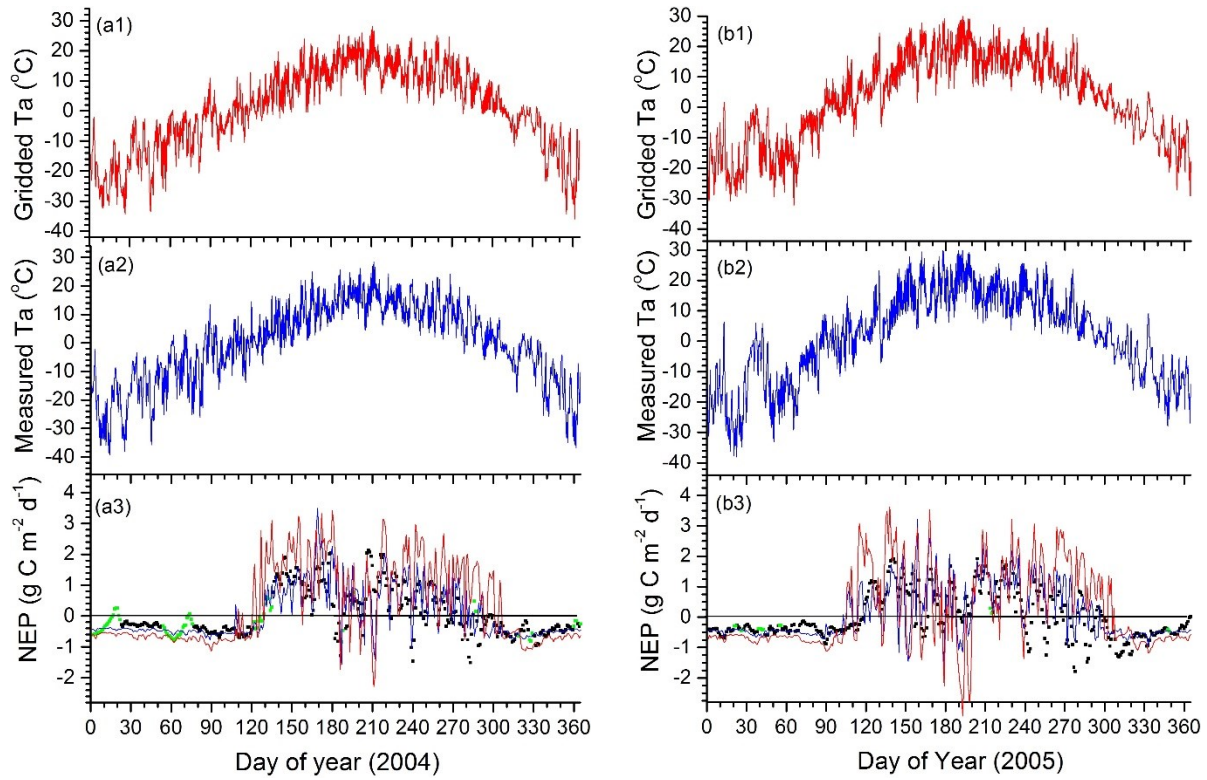


Figure 2-10. Quebec mature boreal black spruce forest (QFO): (a1, a2, b1, b2) 3-hourly air temperature, (a3, b3) daily NEP measured at EC (black closed symbols), gap-filled from EC measurements (green closed symbols), modeled NEP using site climate and soil (blue lines) and regional climate and soil (red lines) for a cooler year 2004 and a warmer year 2005.

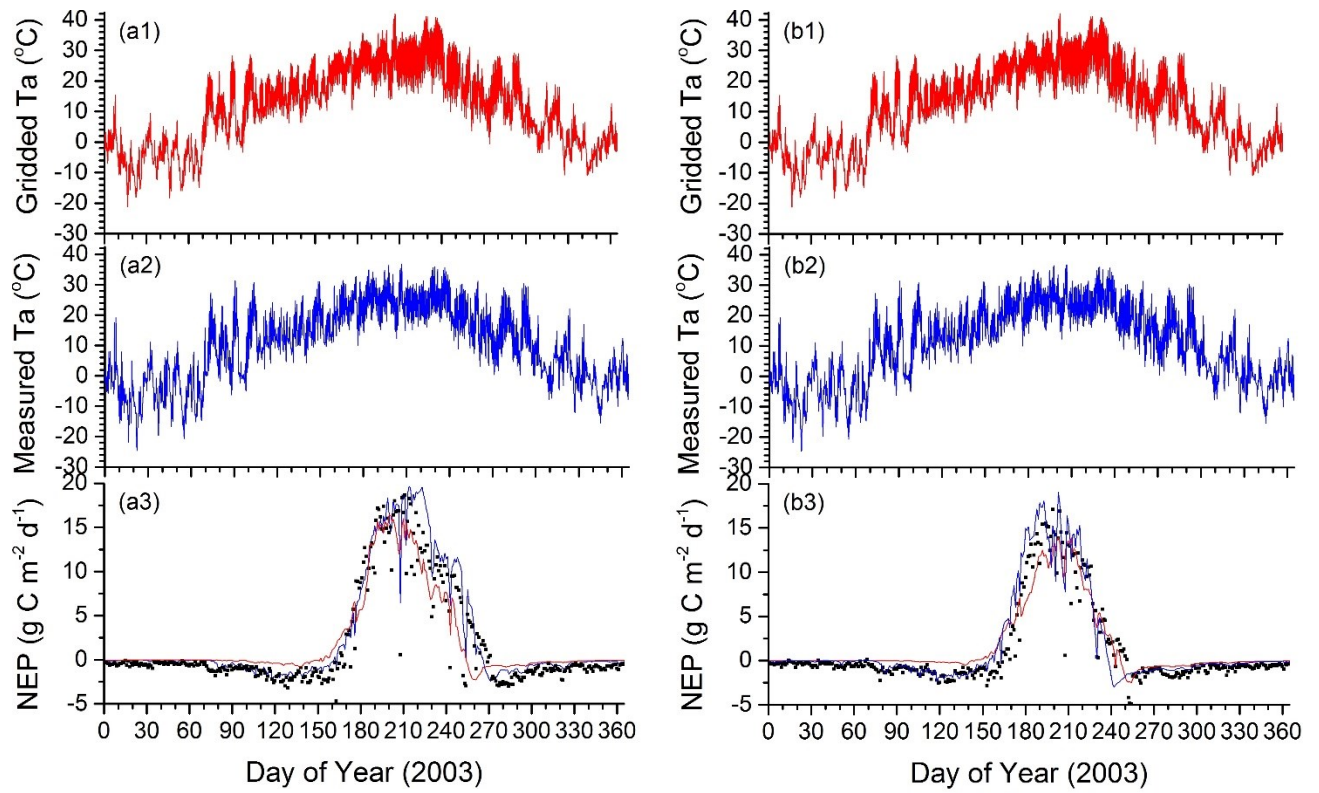


Figure 2-11. Mead crop land site (Mead): (a1, a2, b1, b2) 3-hourly air temperature, daily NEP measured at EC (black closed symbols), modeled NEP using site climate and soil (blue lines) and regional climate and soil (red lines) for (a3) irrigated vs. (b3) rainfed for maize in 2003

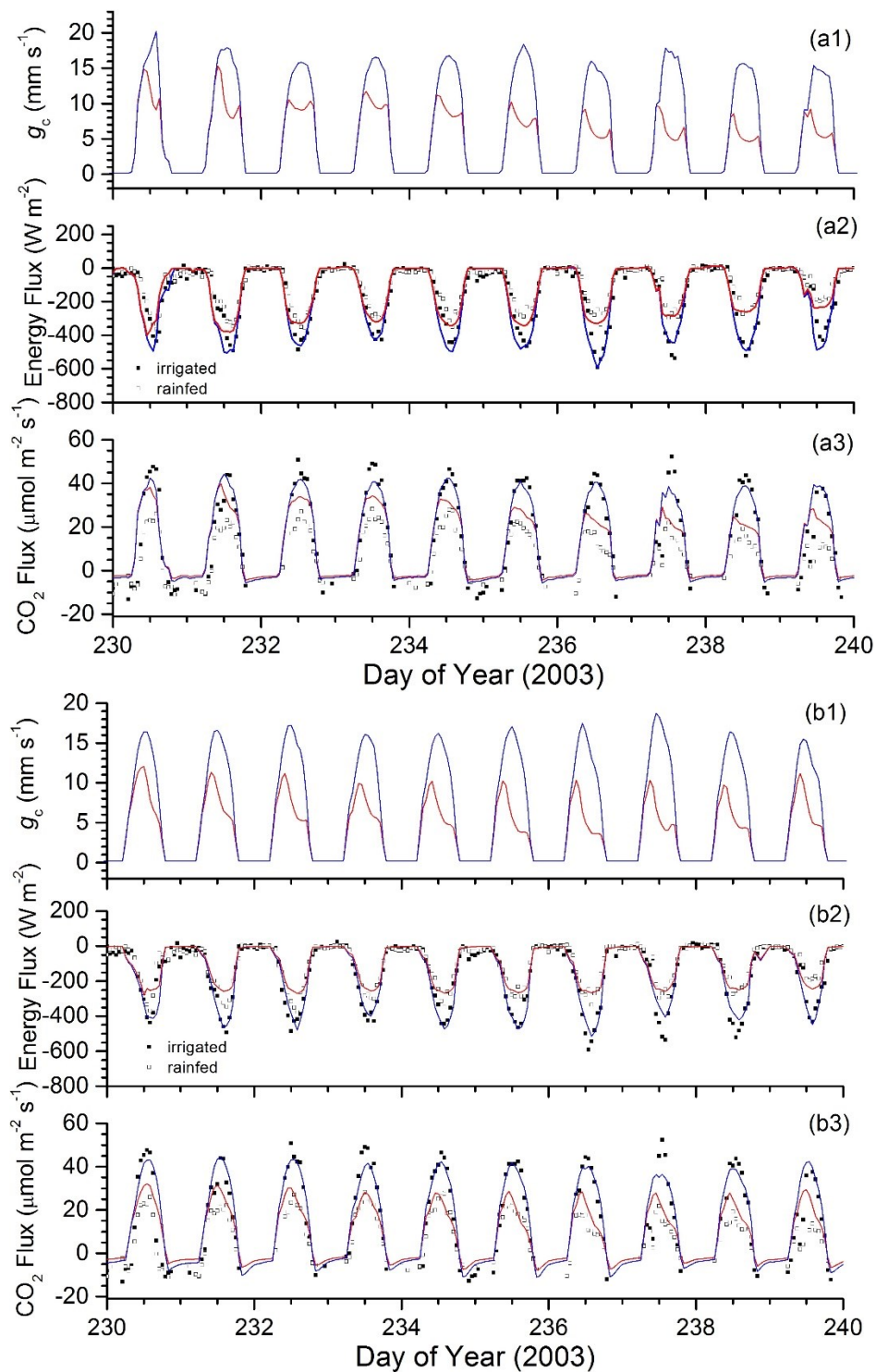


Figure 2-12. Mead crop land site (Mead): comparison of CO₂ fluxes, latent heat fluxes and canopy conductance for irrigated (blue lines) vs. rainfed (red lines) for maize in 2003 modeled for runs with (a1, a2, a3) site and (b1, b2, b) gridded soil and weather inputs

Chapter 3

Contrasting changes in gross primary productivity of different regions of North America as affected by recent warming

3.1. Introduction

There is widespread evidence that ecosystems are responding to warming in recent decades. Increase in the length of growing season has been reported by several studies using normalized difference vegetation index (NDVI) in different regions: northern hemisphere (Kim et al., 2012), North America (NA) (White et al., 2009; Zhu et al., 2012), northern higher latitudes (McManus et al., 2012; Myneni et al., 1997; Olthof et al., 2008; Tucker et al., 2001; Verbyla, 2008; Zhang et al., 2008). In many cases, NDVI values are strongly correlated with photosynthetically active radiation absorbed by vegetation. Increasing NDVI values indicating increasing vegetation density and gross primary productivity (GPP) (Box et al., 1989) over time in northern higher latitudes have been reported in some studies (Myneni et al., 1997; White et al., 2009). Evidence of increases in vegetation cover and northward movement of the tree line in northern higher latitudes has also been reported in several studies (Beck et al., 2011; Swann et al., 2010; Van Bogaert et al., 2011). In contrast, a study in southwest US reported a decline in productivity as a result of warming (Williams et al., 2010).

Warming affects GPP and ecosystem respiration (R_e) which are the major components of carbon exchange between the terrestrial ecosystem and the atmosphere (Albert et al., 2011; Hatfield et al., 2011; Klady et al., 2011). There are direct and indirect effects of elevated air temperature (T_a) on ecosystem productivity. The direct effects depend on current T_a . In areas with lower T_a , as in boreal climates, warming improves kinetics of carboxylation and hence rates of

CO₂ fixation (Bernacchi et al., 2001) due to larger Q_{10} at lower temperatures. However, warming also raises the Michaelis-Menten constant for carboxylation, K_c (Bernacchi et al., 2003; 2001) and lowers aqueous CO₂ concentration in canopy chloroplasts, C_c with respect to gaseous CO₂ concentration in canopy leaves, C_i (Farquhar et al., 1980). Consequently, in areas with higher T_a , as in tropical and subtropical climates, warming with smaller Q_{10} increases photorespiration relatively more than carboxylation (Jordan and Ogren, 1984), and hence causes smaller increases, or even decreases, in rates of CO₂ fixation.

Warming indirectly affects GPP and R_e through alteration of the environment (Shaver et al., 2000). It can have an adverse effect on water relations: warming increases vapor pressure deficits (D), thereby hastening evaporation, transpiration, and soil drying, particularly in warmer climates (Grant et al., 2008). Consequent declines in canopy water potential (ψ_c), induce rises in canopy (r_c) and leaf (r_l) resistances (Grant et al., 1999) and hence declines in rates of CO₂ diffusion and carboxylation, reducing CO₂ fixation. Warming also increases autotrophic maintenance respiration (R_m) which rises exponentially with temperature while CO₂ fixation does not, so that rises in R_m increasingly offset those in GPP on net CO₂ fixation with warming. Other indirect effects of warming on GPP occur through hastened decomposition, hence N mineralization (Hart, 2006; Ineson et al., 1998) and root and mycorrhizal N uptake, thereby raising leaf nitrogen concentrations and so increasing CO₂ fixation rates. Warming may also affect GPP by altering species composition and abundance (Hudson and Henry, 2009; Izaurrealde et al., 2011; Pieper et al., 2011; Shaver et al., 2000) and may thereby change woody carbon stock.

These direct and indirect effects cause ecosystems to increase GPP relatively more with warming in higher latitudes and cooler regions than in lower latitudes and warmer regions (Shaver et al., 2000). This might be due to greater temperature response of CO₂ fixation and nutrient

mineralization when temperature is low and Q_{10} values are larger (Sjögersten and Wookey, 2002). In warmer regions, however, D rises more rapidly with warming, hastening declines in soil water potential (ψ_s), ψ_c and stomatal conductance (g_c), and hence in GPP.

These direct and indirect responses of GPP to warming may also vary with plant functional types and climatic zones. For instance, warming may reduce seasonal carbon fixation of annual plants by hastening phenological advance thereby reducing length of growing season, but may raise seasonal fixation in perennial plants by increasing length of growing season (Grant et al., 2009a; Kim et al., 2012; Myneni et al., 1997; Piao et al., 2007; Tucker et al., 2001; Zhu et al., 2012). The same rise in temperature can have different impacts on ecosystem processes in different biomes (Oberbauer et al., 2007) and the responses over time can be different (Peng et al., 2009; Way and Oren, 2010).

To examine these contrasting responses to warming, in this study we first analyzed the spatial and temporal variability and trends of warming and precipitation over the last three decades (1979 - 2010) in NA using climate data from the North American Regional Reanalysis (NARR) (Wei et al., 2014). We then used a comprehensive mathematical process model, *ecosys* (Grant, 2001; 2011b; 2014) to examine how this variability affected the spatial and temporal changes in GPP and leaf area index (LAI) across different ecological regions (eco-regions) of NA. *Ecosys* was used because the direct and indirect effects of warming on biochemical and physical processes that control CO₂ fixation, as described above, are explicitly modeled. The skill of the model to capture these warming effects on ecosystem productivity at different time steps (hourly, daily, annual and decadal) were shown to be generally high, when rigorously tested against measured fluxes over a wide range of climates across different biomes: e.g. wheat growth under controlled warming (Grant et al., 2011b), natural warming in coastal Arctic tundra in Alaska (Grant et al.,

2003), mesic Arctic tundra in Northwest Territories, Canada (Grant et al., 2011a); diverse temperate and boreal forests (Grant et al., 2009a,b; 2010), dry grassland in Mediterranean climate zones (Grant et al., 2012); semi-arid grassland in Lethbridge, Alberta (Grant and Flanagan, 2007b-a; Li et al., 2004). In a more recent study (Grant, 2014), the effects of experimental soil warming on nutrient cycling, particularly N mineralization, hence ecosystem productivity in the Harvard forest mixed deciduous stand were tested.

3.2. Materials and Methods

3.2.1. Model Description

A detailed description of inputs, parameters and algorithms used in *ecosys* can be found in earlier publications (Grant, 2001; 2014) and (Grant et al., 2011b; 2012). However, the general descriptions of the algorithms and parameters that are most relevant to modeling the direct and indirect impacts of warming on GPP as described in the introduction are given below and details of the equations used are given in Appendices A – D.

3.2.1.1. Direct Effects

CO₂ fixation

Warming affects GPP directly through its effects on carboxylation (Eqs. C6b, C10a), oxygenation (Eqs. C6d, C10b), K_c (Eqs. C6e, C10d, C10e) and modeled by the Arrhenius functions for light and dark reactions, using parameters developed by Bernacchi et al. (2003) for temperatures from 10 to 40 °C and additional parameters for low and high temperatures inactivation by Kolari et al. (2007) as presented in Grant (2014). CO₂ diffusion is controlled by leaf resistance r_l (Eq. C4) which is calculated from a minimum value r_{lmin} (Eq. C5) for each leaf surface at full hydration that allows a set ratio for intercellular to canopy gaseous CO₂ concentration $C_i:C_b$ to be maintained at CO₂ fixation rate V_c under ambient CO₂ concentration

(C_a), irradiance, canopy temperature (T_c), leaf nutrient content and zero ψ_c (Grant et al., 2007a). In areas with lower T_a , warming improves kinetics of carboxylation and hence rates of CO_2 fixation (Bernacchi et al., 2001) due to larger Q_{10} at lower temperatures. However, increasing T_a also raises K_c (Bernacchi *et al.*, 2001; 2003) and lowers C_c with respect to C_i (Farquhar et al., 1980). In areas with lower T_a where Q_{10} is larger, the beneficial effect of warming on carboxylation kinetics is greater than the adverse effects of warming on K_c and C_c . But in areas with higher T_a where Q_{10} is smaller, the beneficial effects of warming may be smaller than the adverse effects, thereby slowing CO_2 fixation by hastening oxygenation more than carboxylation.

3.2.1.2. Indirect Effects

Water relations

Warming affects GPP indirectly by increasing D , hence transpiration demand that lowers ψ_c (Eq. B14) and raises r_c (Eq. B2b), thereby slowing CO_2 diffusion (Eq. C2) (Grant et al., 2008). The impact of D on transpiration is solved through the first-order closure of the energy balance (net radiation R_n , (Eq. B1a) latent heat flux LE (Eqs. B1b, c), sensible heat flux H (Eq. B1d), and change in heat storage G). Total energy and water exchange between the atmosphere and the ecosystem is the sum of the exchanges with vegetation, snow, residue, and ground surfaces. Surface energy and water exchanges are coupled with soil heat and water transfers through the surface residue and soil profile (Eq. D12), including freezing and thawing (Eq. D13), surface runoff *vs.* infiltration (Eq. D1) and subsurface flows through micro- and macropores (Eq. D7), which determine soil temperatures (T_s) and water contents (θ) (Grant, 2004b).

Canopy transpiration (E_c) is coupled with water uptake U (Grant et al., 1999) through a convergence solution for ψ_c at which E_c equals U + change in plant water storage (Eq. B14). During this solution, r_c rises from the minimum value $r_{c\min}$ aggregated by leaf surface area from

r_{\min} (Eq. B2a) at zero ψ_c in Section 3.2.1.1 through an exponential function of canopy turgor potential ψ_t (Eq. B2b) calculated from ψ_c and osmotic water potential ψ_{π} (Eq. B4). The value of U from the soil to the canopy is determined by the potential difference between ψ_c and ψ_s across soil Ω_s (Eq. B9) and root Ω_r (Eqs. B10 – B12) hydraulic resistances in each rooted soil layer (Eq. B6) (Grant et al., 2007c). Root resistances are calculated from root radial resistivities (Eq. B10) and from primary (Eq. B11) and secondary (Eq. B12) axial resistivities using root lengths and surface areas from a root system sub-model (Eqs. B13) driven by exchange of nonstructural C, N and P along concentration gradients generated by uptake vs. consumption of C, N and P in shoots and roots (Grant, 1998). By raising D and hence E_c and U , warming lowers ψ_c and hence ψ_t and increases r_c , depending on current ψ_s . Increases in r_c reduce rates of CO₂ diffusion (Eq. C2), (Grant et al., 1999).

Nutrient uptake

Soil warming enhances N uptake and hence productivity by hastening soil N mineralization (Eq. A26) and root and mycorrhizal active uptake (Eq. C23) through the Arrhenius function of T_s (Eq. A6) (Grant, 2014). Active uptake of N and P U_{NH_4} , U_{NO_3} and U_{PO_4} is calculated from solutions $[\text{NH}_4^+]$, $[\text{NO}_3^-]$ and $[\text{H}_2\text{PO}_4^-]$ at root and mycorrhizal surfaces (Eqs. C23b, d, f) at which uptake equals radial transport by mass flow and diffusion (Eqs. C23a, c, e) from the soil solution (Grant et al., 2007c). Path lengths and surface areas of roots and mycorrhizae used to model uptake are calculated from a root and mycorrhizal growth sub-model driven by exchange of nonstructural C, N and P along concentration gradients generated by uptake vs. consumption of C, N and P in shoots and roots (Grant, 1998). A product inhibition function is included to limit excess uptake (Eq. C23g).

Heterotrophic respiration

Warming hastens oxidation of dissolved organic carbon (DOC) that drives heterotrophic respiration (Eq. A11) (R_m (Eq. A18) + growth respiration (R_g) (Eq. A20)) through the Arrhenius function of T_s . R_m is driven by DOC oxidation through Q_{10} function of T_s (Eq. A19) and R_h remaining from R_m drives R_g (Grant, 2014).

3.2.2. Model Drivers

Model drivers are external variables that influence the state of the ecosystem. In this study, climate, soil, land use/ land cover dynamics, CO_2 concentration, nitrogen deposition and disturbance were used as inputs to drive *ecosys* (Table 3-1). The NARR dataset was produced at the National Oceanic and Land Administration (NOAA) National Center for Environmental Prediction (NCEP) Global Reanalysis (Mesinger et al., 2006). NARR is a combined data and model assimilation product that made use of wide network of observational datasets across the continent (Mesinger et al., 2006). For this study, we used a NARR dataset which was reprojected to $0.25^0 \times 0.25^0$ spatial resolution in geographic latitude/ longitude projection made available through the Multi-Scale Synthesis and Terrestrial Model Inter-comparison Project (MsTMIP) (Huntzinger et al., 2013). This dataset extended from 1979 to 2010 with a temporal resolution of 3-hours, and was interpolated linearly to 1-hour for use in *ecosys*. The NARR variables used to drive *ecosys* were air temperature at 2m, total precipitation at surface, downward shortwave radiation flux at surface, relative humidity at 2m and wind speed at 10m.

The soil dataset used in this study was a Unified North America Soil Map (UNASM) which was a reanalysis product of MsTMIP for NA that was prepared using three different soil databases (Liu et al., 2013). The model was provided with attributes for each soil layer in the dataset, including layer depth, clay/sand fraction, pH, total organic carbon, cation exchange capacity and bulk density. Time-varying land use/land cover was modeled from a dataset for the years 1800 -

2010 developed by merging historical land cover classification (Hurt et al., 2006) and 2000/2003 SYNMAP (Jung et al., 2006) land cover classification products (Wei et al., 2014). The atmospheric CO₂ concentration used in the model from 1800 to 1979 was created from GLOBEVIEW-CO₂. For the period before 1979 a reanalysis product of GLOBEVIEW- CO₂, Mauna Loa (MLO) and South Pole (SPO) annual mean concentrations as described in Wei et al. (2014) was used. However, for years after 1979 the GLOBEVIEW data were directly used. Annual nitrogen deposition used in the model for 1800 - 2010 was derived from Dentener's global atmospheric nitrogen deposition maps in the years of 1860, 1993 and 2050 (Dentener, 2006). The annual variation of nitrogen deposition rate from 1890 to 1990 was controlled by EDGAR-HYDE 1.3 (van Aardenne et al., 2001) nitrogen emission data (Wei et al., 2014). Nitrogen deposition was assumed to increase linearly over the remaining period up to the present (1990 - 2010).

Disturbance due to fire was introduced as external forcing in the model simulation. Four different data sources for Canada, US and Mexico were harmonized to create a continuous historical fire disturbance dataset. The Canadian wildfire information system dataset was available for 1959 – 1999. US Land Fire Product is a product from United States Geological Survey (USGS). This dataset indicates historical fire regimes based on vegetation dynamics, fire spread and effects and it contains mean fire return interval and a severity index in the average period between fires under the presumed historical fire regime. Another data source used was Global Fire Emission Database (GFED) which is a Moderate Resolution Imaging Spectroradiometer (MODIS) global product that combines satellite information on fire activity and vegetation productivity to estimate a burned area and fire emissions. The datasets have a monthly temporal resolution and are available from 1997 to 2012. NACP Forest Age Maps compiled from forest inventories, historical fire data, satellite data, and images from NASA's Landsat Ecosystem Disturbance Adaptive Processing

System (LEDAPS) project at 1km Resolution for Canada and the US were also applied to forested areas (Pan et al., 2011). The Canadian and US maps were produced from data available in 2004 and 2006 respectively. These different products of fire disturbance were not consistent in spatial and temporal resolutions and were in different data models (point and polygon vectors, and raster). Therefore, the products were all geo-rectified, resampled, interpolated and re-gridded to a $0.25^{\circ} \times 0.25^{\circ}$ spatial resolution to make it consistent with the projection and spatial resolution of the other model drivers used in this study.

3.2.3. Model Runs and Testing

The simulation spatial domain covered the NA landmass with $0.25^{\circ} \times 0.25^{\circ}$ resolution consisting of 51,061 independently simulated grid cells. Model runs for each grid cell were prepared with time-varying drivers for a simulation period of 1800 - 2010. To represent historical weather, NARR data from 1979 - 1993 were randomly distributed to form a 100-year spinup sequence that cycled through 1800 - 1978. This spinup enabled the model to attain a steady state prior to 1979. Then the real time NARR data were used for the rest of the period (1979 - 2010) to simulate real time ecosystem productivity as stated in MsTMIP protocol (Huntzinger et al., 2013). The model was initialized with attributes from the soil dataset, and run under dynamic land use/land cover changes, atmospheric CO₂ concentrations, nitrogen deposition and disturbances (Section 3.2.2; Table 3-1).

3.2.3.1. Site Scale Model Testing

Model responses of CO₂ exchange to changes in weather are best tested directly against measurements of CO₂ fluxes. However, these measurements can only be done at a site scale at eddy covariance (EC) flux towers with footprints in order of few km² (Houborg and Soegaard, 2004; Sasai et al., 2007), making it difficult to validate regional scale model outputs. However, we

compared annual modeled GPP aggregated from hourly values for 2005 in pixels corresponding to the locations of 20 EC flux towers, with annual GPP derived from EC measurements (Table 3-2) over a broad range of eco-regions (Fig. 3-1) with different climates and biomes across NA. Key responses of modeled vs. EC derived GPP to mean annual T_a (MAT) and precipitation were also compared for 2005. The year 2005 was selected due to data availability for a broader range of EC sites.

3.2.3.2. Continental Scale Model Testing

At a continental scale, modeled annual GPP was also compared with annual averages of MODIS GPP to assess similarities in spatial patterns in 2002 (drought year) vs. 2005 (normal year). Spatial patterns of average annual (2000 - 2010) modeled vs. MODIS GPP for NA were tested using geographically weighted regression (GWR). This regression generated separate equations for every spatial cluster in the datasets as a method of analyzing spatially varying relationships. The interannual variability of spatially averaged modeled GPP aggregated to annual totals for NA was compared with that of the MODIS annual GPP product for 2000 - 2010. Modeled GPP anomalies from the long-term (2000 - 2010) mean were also compared with those from MODIS.

3.2.4. Analysis of Outputs from Continental Scale Model Runs

Three-hourly T_a from NARR and hourly GPP from model outputs for the years 1979 - 2010 were aggregated to annual averages and totals respectively to create continuous gridded data across NA for each year of the study. Model output for mid-August LAI was also extracted. To analyze the long-term temporal trends in T_a and model outputs, the spatially averaged values were computed considering area of grid cells as a weighing factor. Long-term trends in GPP were done across level I eco-regions of NA with 15 broad eco-region categories (Fig. 3-1). Long-term spatial

and temporal changes in T_a and GPP were computed by subtracting averages of the initial five years of gridded annual values (1980 - 1984) from those of the final five years (2006 - 2010). Averaging the initial and final five years was important to smooth out inter-annual variability and detect the long-term spatial and temporal changes of the last three decades. Temporal trends for T_a were also conducted along latitudes and longitudes taking areas of each grid cell as a weighting factor. Disturbances affect productivity in a forest chronosequence (Grant et al., 2007d; Grant et al., 2010; Grant et al., 2007c). Thus, pixels with forest stand age less than 60 years from the last stand replacing fire were excluded from spatial and temporal trend analysis to avoid forest age effects on GPP. Moreover, pixels with forest stands in Mexico were excluded from the trend analysis due to lack of historical disturbance data for the region.

3.3. Results

3.3.1. Model Testing

3.3.1.1. Site scale

Annual GPP derived from 20 selected EC site measurements agreed well with modeled GPP from the corresponding pixels where the EC sites were located ($R^2 = 0.76$) demonstrating the ability of the model to simulate CO_2 exchange in a wide range of climates and ecosystems across NA (Fig. 3-2a). Key modeled responses of carbon fixation to differences in MAT and annual precipitation under wider ranges of climates apparent in EC derived GPP were captured in modeled GPP (Fig. 3-3). Annual GPP was shown to rise with MAT for EC sites with lower MAT (e.g. CA-NS1, CA-SJ3 and CA-Ojp), with an increasing rate of $\sim 100 \text{ g C m}^{-2}$ per $1 \text{ }^\circ\text{C}$ rise in MAT until the MAT of e.g. $-10 - 12 \text{ }^\circ\text{C}$ (e.g. CA-Ca3, US-Ne2, CA-TP4) (Table 3-2; Fig. 3-3a), above which GPP declined with further rises in MAT (declined $\sim 200 \text{ g C m}^{-2}$ per $1 \text{ }^\circ\text{C}$ rise in MAT), particularly

at sites with relatively low precipitation (e.g. $>15^{\circ}\text{C}$ in US-Var and US-Ton). Annual GPP also rose with annual precipitation (Fig. 3-3b), particularly at sites with higher MAT (Fig. 3-3).

3.3.1.2. Continental scale

MODIS GPP tested against EC-derived GPP from 20 EC towers (Fig. 3-2b) had a good correlation ($R^2 = 0.64$), providing greater confidence to compare the spatial and temporal trends of MODIS against the modeled GPP at continental scale. Long-term (2000 - 2010) annual modeled vs. MODIS GPP were shown to have similar spatial patterns: higher GPP in south east, Midwest, west coast and southern Mexico (Fig. 3-4) and lower GPP in the south, southwest and high latitudes. These spatial patterns of modeled vs. MODIS GPP were tested with GWR ($R^2 = 0.8$) which demonstrated close similarities in spatial patterns (Fig. 3-4). Interannual anomalies in modeled vs. MODIS GPP for NA agreed well showing adverse effects of mid-continental droughts in 2002 and 2009 (Fig. 3-5). Spatial patterns indicated smaller modeled GPP in 2002 for most parts of the southwest and the Great Plains, attributed to the drought compared to a normal year in 2005 (Fig. 3-6 (a, b)). The spatial patterns of reductions in modeled GPP in the drought-affected regions were corroborated by the similar patterns of reduced MODIS GPP in 2002 vs. 2005 (Fig. 3-6 (c, d)), with GWR of $R^2 = 0.85$ for 2002 and 0.86 for 2005.

3.3.2. Continental Scale: Changes in T_a 1979 – 2010

Changes in T_a derived from the NARR over the last three decades had contrasting regional trends across NA, with some areas at higher latitudes experiencing the most rapid warming while other areas in the western part of the continent were experiencing a slight cooling (Fig. 3-7a). Average T_a for the entire NA landmass increased by $+0.38^{\circ}\text{C decade}^{-1}$ from 1979 - 2010, indicating an amplified warming in recent decades (Table 3-3). Average T_a rose by $+0.72^{\circ}\text{C decade}^{-1}$ in the northeast including the Canadian Arctic, indicating the most rapid warming at

higher latitudes. The western parts of the continent had the slowest warming ($+0.08\text{ }^{\circ}\text{C decade}^{-1}$); with some areas mainly in the northwestern coastal regions experiencing a slight cooling. There were contrasting patterns of warming along latitudinal and longitudinal gradients (Fig. 3-7 (c, d)). Warming slowed from east to west along spatially averaged longitudes. Regions north of 45° N had more rapid warming of $+0.46\text{ }^{\circ}\text{C decade}^{-1}$, than did regions south of 45° N with $+0.19\text{ }^{\circ}\text{C decade}^{-1}$. Regions between 60° N and 83° N had the most rapid warming, compared to the southern regions except for the small land mass of southern Mexico between 10° N and 15° N .

Seasonal trends in spatially averaged T_a for the entire NA landmass (Table 3-3) indicated warming in all seasons, however a more pronounced warming of $+0.59\text{ }^{\circ}\text{C decade}^{-1}$ was observed in autumn. A slower warming of $+0.25\text{ }^{\circ}\text{C decade}^{-1}$ was observed in spring. This result indicated a greater possible increase in length of growing season during late autumn than during early spring in recent decades.

Changes in long-term precipitation were more variable than those in T_a across NA (Fig. 3-7b). Despite the lack of clear spatial trends in precipitation change, most areas at higher latitudes were shown to gain in annual precipitation over the last three decades. Mid and lower latitudes had more spatially variable changes in precipitation. Western coastlines, south western and south eastern US and southern Mexico had declines in annual precipitation in recent decades.

3.3.3. Continental Scale: Changes in GPP 1980 - 2010

Model results indicated that the different eco-regions of NA varied in their contribution to the total GPP of the continent (Table 3-4). Productivity was high along the coastlines of northwest and southeast US, south and southeast Mexico (Fig. 3-8a). Eastern temperate forest, Great Plains and Northern forests contributed most ($>60\%$), accounting for 25%, 18% and 17% of total NA long-term (1980 – 2010) mean annual GPP, respectively. GPP of tropical forests in parts of

southeast Mexico was as much as $3000 \text{ g C m}^{-2} \text{ yr}^{-1}$. However, ecosystems constrained by temperature such as Arctic cordillera, tundra and those constrained by water such as the deserts in the southwest had the smallest GPP. The GPP contribution of Arctic cordillera and Mediterranean California was less than 1% of the total NA. Spatial variation in productivity was better indicated by the ratios of total productivity to area of each eco-region (Table 3-4) which varied from $3 \text{ g C m}^{-2} \text{ yr}^{-1}$ for Arctic cordillera to $1802 \text{ g C m}^{-2} \text{ yr}^{-1}$ for tropical wet forests. Spatial variability in LAI was apparent among eco-regions with generally higher values in areas with higher productivity (Fig. 3-8c).

Percentage changes in GPP over the last three decades varied among different eco-regions (Table 3-4). Higher latitude and cooler eco-regions such as Arctic cordillera, tundra, taiga, Hudson plain, northern forests and eastern temperate forest had greater percentage increases in modeled GPP due to early spring and late autumn warming observed in NARR (Table 3-3). However, declines in GPP were modeled in eco-regions which were already warmer and drier such as North America deserts, temperate Sierras, tropical dry forests and Mediterranean California. These eco-regions were mainly in the mid and lower latitudes with higher MAT. Of the total NA landmass about 61% had long-term gains in GPP compared to 23% with long-term losses. The relative contributions of eco-regions to increases in continental GPP vary. Eastern temperate forests, northern forests and Taiga contributed 92% of the increases in NA GPP over the last three decades (Table 3-3). However, modeled GPP declined in most southwestern regions of NA (accounting >50% of ecosystems with declining GPP) implying that projected dryness in this region (IPCC, 2013) could further reduce NA carbon uptake. Overall, modeled GPP across NA increased by 5.8 % in the last 30 years, with a positive trend of $+0.012 \text{ Pg C yr}^{-1}$ and a range of -1.16 to $+0.87 \text{ Pg C yr}^{-1}$ caused by interannual variability of GPP from the long-term (1980 – 2010) mean.

The effects of 30-year changes in T_a and precipitation (Fig. 3-7) on modeled GPP differed among regions of NA (Fig. 3-9). In most northern regions, GPP increased with T_a and less so with precipitation (Fig. 3-9a). However, in some regions, mainly in Alaska, declines in GPP were caused by slight declines in T_a , (Fig. 3-4a). In most regions of the south and southwest, GPP declined, particularly in regions with rises in T_a and declines in precipitation (Fig. 3-9b). In a small fraction of the region, GPP rose with increases in precipitation and small changes in T_a . The southeast GPP rose in regions with increased precipitation and declined in those with decreased precipitation, particularly when accompanied by increasing T_a (Fig. 3-9c). These modeled responses to changes in T_a and precipitation were corroborated by similar responses observed from EC-derived GPP (Fig. 3-3).

3.3.4. Continental Scale: Interannual Variability in T_a , Precipitation and GPP

Although we could observe long-term trends in continental T_a and precipitation, interannual variation was apparent (Fig. 3-10 (a, b)) which caused an anomaly range of -1.16 to +0.87 Pg C yr⁻¹ in GPP from the long-term mean (Fig. 3-10c). Despite the apparent long-term positive trend in continental GPP (Fig. 3-10c), its interannual variability was controlled by that in T_a and precipitation. This variability was indicated by the standard deviation (SD) of modeled annual GPP and LAI from the long-term means which varied spatially across the continent (Fig. 3-11). Parts of the Great Plains, southwest US and northern Mexico had large relative standard deviation ($RSD = (SD / \text{absolute value long-term mean}) \times 100$) for GPP and LAI, indicating that these parts of the continent had greater interannual variability in productivity. The Great Plains which contributed 18% of the NA GPP had large SD (Table 3-4) demonstrating that this region contributed much of continental scale interannual variability of ecosystem productivity compared to NA deserts and southern semi-arid highlands which had also large RSD but contributed only

3.33% and 1.15% of the total NA GPP, respectively. The coastlines of western Canada and southern Alaska had also large RSD.

3.4. Discussion

3.4.1. 30-year Spatial and Temporal Changes in T_a

Our result from analysis of NARR temporal and spatial trends of T_a suggested that most parts of NA have experienced warming in recent decades (Fig. 3-7a). A particularly amplified warming trend in higher latitudes of the northern hemisphere has also been reported in several other studies, although the range of reported warming varied, mainly from different gridded climate datasets. Global increases of $+0.04\text{ }^{\circ}\text{C decade}^{-1}$ (1861 – 1997) and $+0.06\text{ }^{\circ}\text{C decade}^{-1}$ (1901 – 1997) were reported in a study by Jones et al. (1999a). Another study covering areas of the Arctic (Polyakov et al., 2002) indicated an increase of $+0.17\text{ }^{\circ}\text{C decade}^{-1}$ (1875 – 2001). An increase of $+0.19\text{ }^{\circ}\text{C decade}^{-1}$ in the Arctic was reported for the years 1961 – 1990 by Chapman and Walsh (1993). A more recent time range (1981 – 2001) of satellite thermal infrared data was shown to have a greater increase of $+1.06\text{ }^{\circ}\text{C decade}^{-1}$ in the NA Arctic (Comiso, 2003). The rates of warming were not the same for all seasons although increasing trends of warming were observed in all seasons (Table 3-3). A winter warming of $+1.00\text{ }^{\circ}\text{C decade}^{-1}$ and a cooling of $-1.00\text{ }^{\circ}\text{C decade}^{-1}$, were reported in the eastern and western Arctic Ocean respectively from 1979 - 1997 (Rigor et al., 2000). However, spring warming occurred both in the east and the west Arctic and this was partly associated to the Arctic Oscillation mainly in the east (Rigor et al., 2000). A similar longitudinal influence was observed in the NARR with the eastern, particularly the northeast part of NA landmass experiencing a greater warming trend compared to the west (Fig. 3-7d) which could be attributed to changes in patterns of North Atlantic Oscillation (NAO) (Belkin, 2009). Comiso (2003), reported a positive trend in spring, summer and autumn suggesting recent warming

in the Arctic that may be related to changes in phases of Arctic Oscillation and increase in atmospheric greenhouse gases. Similar increases in early spring and late autumn warming (Table 3-3) observed in NARR had increased modeled GPP (Fig. 3-8b) in most areas with lower mean annual T_a , such as those in boreal climate zones.

3.4.2. Uncertainties in Continental Modeled GPP

In a model-data inter-comparison of 26 models from NACP site synthesis project, modeled vs. EC derived GPP from 39 flux towers across NA demonstrated that *ecosys* performed very well in simulating GPP across a wide range of biomes (correlation coefficient > 0.9) as shown in Fig. 3-4 of Schaefer et al. (2012). Similarly, we have shown high correlation ($R^2 = 0.76$) of modeled GPP in 20 selected EC sites (Section 3.3.1; Fig. 3-2). However, in this study our simulation used model drivers from coarser resolution gridded inputs for weather and soil that may have affected the accuracy of the estimated GPP.

In Chapter 2 a detailed analysis was conducted of uncertainties in the model estimates associated with model drivers such as NARR and UNASM for six EC sites. CO_2 flux measurements from each site were compared with CO_2 fluxes from the model using gridded vs. measured inputs under contrasting weather (cool vs. warm and wet vs. dry) to analyze differences in modeled NEP. The comparisons indicated that NEP modeled with gridded inputs had less accurate diurnal and seasonal patterns than NEP modeled with inputs from site measurements at some sites, when tested against NEP derived from EC flux measurements. Although differences in NEP were apparent at some sites (e.g. due to shallower soil depth, lack of SON, inaccurate precipitation pattern), key modeled responses of net CO_2 exchange under contrasting weather were nonetheless maintained for most of the sites, supporting their use in the present study. Gridded weather and soil inputs that caused such differences in NEP would certainly affect regional and

global carbon budget estimates from models using these inputs, and uncertainties observed in out model outputs are partly attributed to these model inputs.

3.4.3. Impacts of Warming in Recent Decades on Ecosystem Productivity

Most parts of NA warmed over the last three decades, although changes in precipitation varied, and the combined effects of changes in T_a and precipitation determined changes in ecosystem GPP in the different climate zones and biomes (Fig. 3-10). Increases in modeled GPP and LAI in boreal and Arctic ecosystems (Fig. 3-8 (b, d); Table 3-4) supported the hypothesis that higher latitude and cooler regions tend to have greater relative gains in GPP attributed to warming in recent decades. This is mainly due to temperature responses which are relatively larger in cooler regions where Q_{10} values are larger, but which decline with increasing temperature and declining Q_{10} (Sjögersten and Wookey, 2002), as described in the direct effects of warming modeled in *ecosys* (Section 3.2.1.1). In these climates warming was mostly coupled with an increase in precipitation (Fig. 3-7) which increased rates of CO_2 fixation through enhancing kinetics of carboxylation (Bernacchi et al., 2001; Grant et al., 2009a), while largely avoiding the indirect effects on CO_2 fixation through declining ψ_s . Furthermore, spring and autumn warming in higher latitude regions observed in NARR (Table 3-3) increased the length of growing season thereby increasing duration of CO_2 fixation (Grant et al., 2011a). Studies using NDVI have indicated similar increases in length of growing season in higher latitudes of NA (White et al., 2009; Zhu et al., 2012). These direct and indirect effects of warming drove the rise in GPP measured and modeled with increases in MAT in cooler climates across NA (Fig. 3-3). Spatial average modeled GPP were shown to increase by 102, 141 and 87 g C m⁻² per 1 °C increase in spatial average MAT of eastern temperate forests, northern forests and Taiga respectively (Table 3-4). This modeled

result was corroborated with similar responses of increases in MAT of ecosystems in cooler climates observed from EC-derived GPP (Section 3.3.1.1 in Fig. 3-3a).

The modeled responses of productivity to warming in boreal and Arctic ecosystems in this study were also corroborated by ecosystem responses observed in numerous studies using artificial warming experiments (Elmendorf et al., 2012b; Walker et al., 2006). Some of these experiments reported increases in biomass attributed to warming in the higher latitudes (Hill and Henry, 2011; Klady et al., 2011; Oberbauer et al., 2007). In another test of *ecosys* against experimental warming on wheat growth, Grant et al. (2011b) reported that warming increased wheat yield in cooler weather due to an increase in CO₂ fixation, whereas the same warming decreased wheat yield in warmer weather due to adverse impacts on water status, increases in respiration and shortening of the growing period. In a further test of *ecosys* against an artificial soil warming experiment (Grant, 2014; Melillo et al., 2011) modeled increased forest productivity was caused by more rapid N mineralization, hence uptake. Findings from a long-term (1981 – 2008) plot study (Hudson and Henry, 2009) were also consistent with the modeled increases in productivity in Canadian high Arctic (Fig. 3-8b) mainly attributed to warming over the past 30 – 50 years that resulted in an increase in the length of growing season. Another study (Pouliot et al., 2009) revealed changes in Landsat and AVHRR NDVI from 1985 – 2006 over Canada that showed an increasing trend in the northern regions, demonstrating increases in GPP with warming.

The declines in GPP modeled mainly in areas with high MAT as in NA deserts, Mediterranean California, temperate Sierras and tropical dry forests (Table 3-4) were caused by adverse impacts of warming at high T_a on CO₂ fixation (Grant et al., 2008), as described in the direct effects of warming modeled in *ecosys* (Section 3.2.1.1) and apparent in the declines of GPP with increasing MAT modeled and measured in warmer climates (Fig. 3-3, Table 3-4). These

results support the hypothesis that warming in areas of high T_a , as noted in the introduction would result in a decline in productivity. For instance, spatial average modeled GPP declined by 248 g C m^{-2} per $1 \text{ }^\circ\text{C}$ increase in spatial average MAT of Mediterranean California (Table 3-4), similar to GPP declines with increases in MAT of ecosystems in warm climates observed from EC-derived GPP (Section 3.3.1.1 in Fig. 3-3a). Moreover, a decline in precipitation in these warmer and drier regions coupled with an increase in T_a , caused further declines in CO_2 fixation (Table 3-4), through an indirect effect by hastening transpiration and soil drying as demonstrated in Grant and Flanagan (2007) and described in Section 3.2.1.2. For instance, modeled GPP declined by 85 g C m^{-2} with 21 % decline in precipitation and $0.03 \text{ }^\circ\text{C}$ increase in and T_a in NA deserts (Table 3-4). A study (Williams et al., 2010) that compared tree-ring width data in the southwest forest for the 20th century with long-term climate data reported that 18% of the forest area experienced mortality from 1984 to 2008 as a result of increasing warming and aridity in the southwest. Breshears et al. (2005) reported mortality of over-story trees in southwestern NA woodlands during in 2002 - 2003 as a result of drought and associated bark beetle infestation that may drive rapid changes in vegetation. Declines in forest density and basal area suggesting increases in tree mortality forests in 76 long-term forest plots in western US, which may be attributed to warming and water deficit in recent decades (Van Mantgem et al., 2009). Changes in forest structure and composition as a result of tree mortality could affect ecosystem functioning, hence ecosystem carbon exchange (Van Mantgem et al., 2009). Drought-induced tree mortality has also been reported in Canadian boreal forests from a study (Peng et al., 2011) that used long-term forest plots and demonstrated an increase in rate of tree mortality over recent decades, suggesting that recent warming and subsequent drought may alter vegetation composition of ecosystems in higher latitudes of NA as in southwestern part of the continent.

Declines in GPP were also modeled in southern Alaska and northwestern Canada (Fig. 3-8b) from localized declines in precipitation (Fig. 3-7b) and T_a (Fig. 3-7a). These declines in GPP were similar to one reported by Beck et al. (2011) in which satellite and tree ring data were used to attribute a decline in productivity in the interior Alaska to water stress as a result of warming. Diverse responses of Arctic GPP to warming were inferred in a meta-analysis by Elmendorf et al. (2012a) of 61 tundra sites experimentally warmed for up to 20 years in which strong regional variations of plant responses to warming varied with ambient summer temperature, soil moisture and plant functional type.

Despite various contrasting regional responses to warming, it is apparent that projected further warming, can have negative feedbacks to productivity, particularly in warmer regions that have already shown such declines. Climate model projections (Seager et al., 2007; Williams et al., 2013) have shown that the southwestern NA will be drier and more arid in the 21st century, indicating further declines in GPP from those already modeled (Fig. 3-8b) and observed. Similarly, increasing productivity attributed to recent warming, particularly in higher latitudes may not continue indefinitely as further warming may eventually change the general trends of increased continental GPP with warming (Grant et al., 2011a). Warming in higher latitudes could result in deepening of the active layer and consequently expose the huge volume of carbon in the permafrost (Koven et al., 2011; Lawrence et al., 2008). Although, the deepening of the active layer could increase nutrient cycling, thus carbon uptake, it may alter the carbon cycle by increasing ecosystem respiration (Nowinski et al., 2010).

3.4.4. Interannual Variability in Ecosystem Productivity

The greater interannual variability in modeled GPP and LAI observed in south and southwest US, northern Mexico and the Great Plains (Fig. 3-11) could mainly be attributed to

frequent occurrences of El Niño–Southern Oscillation' (ENSO) events that led to major droughts (Herweijer et al., 2007) as in 2002 (Fig. 3-10a). This variability in modeled GPP was corroborated with that in MODIS GPP (Fig. 3-6 (a, b) vs. Fig. 3-6 (c, d)). Ropelewski and Halpert (1986) reported that declines in NA precipitation from normal patterns were associated with ENSO for western NA and northern Mexico. Greater interannual variability in the south and the prairies could also be attributed to a fast moving low pressure system called ‘Alberta Clipper’ that moves from southwestern Canada through the Great Plains (Baker et al., 2010). Large interannual variability of sea surface temperature observed in the west of NA in the last century could be associated with changes in coastal ecosystem productivity leading to greater interannual variability (McGowan et al., 1998). Overall continental interannual variability in modeled GPP was most sensitive to interannual variability in the Great Plains, as it contributed 18% of the total GPP of NA, compared to other regions of NA with higher interannual variability in GPP such as the deserts, southern semiarid highlands and temperate Sierras that contribute small fractions to NA GPP. This indicated that impacts of future warming on the Great Plains will most likely have a greater impact on the interannual variability of NA carbon budget.

3.5. Conclusions

Productivity of ecosystems modeled across NA has shown spatial variability and contrasting responses to warming in recent decades. Modeled GPP increased with warming in ecosystems with cooler climates due to an increase in the rate of carboxylation, whereas GPP declined with warming in ecosystems with warmer and drier climates due to adverse impacts on carboxylation and water status associated with higher T_a . Interannual variability was shown to vary spatially across the continent, with greater variability in the southwest US, northern Mexico and

the Great Plains that may be attributed to frequent occurrences of ENSO events that led to major droughts.

Climate projections are showing that global warming is expected to continue as a result of increasing atmospheric CO₂ concentration. Impacts of future warming, under different climate change scenarios, on ecosystem productivity are partly uncertain and need to be carefully examined. Gains in GPP modeled and observed as a result of recent warming may not be sustained indefinitely under further warming. In this regard, process-based modeling approach may provide the predictive capability needed to estimate gains and losses of GPP under future climate change scenarios. To this end, model results for changes in CO₂ exchange with those in T_a and precipitation should be tested rigorously against measurements such as those from EC flux towers and plot-based studies. It is only through such testing that we can build confidence in projections of ecosystem productivity under future climates.

List of Tables

Table 3-1. Model drivers and their temporal resolution used to drive *ecosys*

Model Drivers	Temporal period	Temporal resolution	Data source
Climate	1979-2010	3-hourly	NARR ¹
Soil	One-time	One-time	UNASM ² (SSURGO (US) + SLC v3.2 (CA) + HWSD v1.1 (MX))
CO₂	1800-2010	Monthly	Enhanced GlobalView ¹
Nitrogen deposition	1800-2010	Yearly	Enhanced Dentener ¹
Land use change	1800-2010	Yearly	Hurtt's harmonized with SYNMAP ¹

*all gridded model inputs had 0.25 x 0.25 spatial resolutions

¹ MsTMIP model drivers (Wei et al., 2014)

² Unified North America Soil Map (Liu et al., 2013)

Table 3-2. Location of 20 EC sites and mean annual air temperature (MAT) and annual precipitation (P) extracted from corresponding pixels of NARR for 2005

Site	Ecosystem	Latitude	Longitude	MAT (°C)	Annual P (mm)	EC data Reference
CA-Ca3	Young Plantation Site-Douglas Fir	49.5	-124.9	10.2	1999	(Krishnan et al., 2009)
CA-Gro	Mature Boreal Mixed Wood	48.2	-82.2	4.4	726	(McCaughey et al., 2006)
CA-NS1	Boreal black spruce -burn site	55.9	-98.5	0.0	799	(Goulden et al., 2006)
CA-Obs	Old Black Spruce	54.0	-105.1	2.6	614	(Krishnan et al., 2008)
CA-Ojp	Old Jack Pine	53.9	-104.7	2.5	536	(Kljun et al., 2006)
CA-Qfo	Mature Boreal Forest Site	49.7	-74.3	2.7	933	(Bergeron et al., 2008)
CA-SJ3	1975 Harv. Yng Jack Pine	53.9	-104.7	2.5	536	(Zha et al., 2009)
CA-TP4	Mature White Pine	42.7	-80.4	10.1	951	(Arain and Restrepo-Coupe, 2005)
CA-WP1	Black Spruce/Larch Fen	55.0	-112.5	3.6	507	(Flanagan and Syed, 2011)
US-Ha1	Deciduous broadleaf forest	42.5	-72.2	8.6	1740	(Urbanski et al., 2007)
US-Los	Shrub wetland	46.1	-90.0	6.4	937	(Sulman et al., 2009)
US-Me2	Mid-aged ponderosa pine forest	44.5	-121.6	7.4	983	(Thomas et al., 2009)
US-MMS	Deciduous Broad-leaf Forest	39.3	-86.4	9.5	1245	(Schmid et al., 2000)
US-MOz	Transitional zone-hardwood and grassland	38.7	-92.2	14.0	1162	(Gu et al., 2006)
US-NR1	Subalpine forest	40.0	-105.6	3.4	506	(Monson et al., 2005)
US-Ne2	Mead - irrigated maize-soybean rotation site	41.2	-96.5	11.9	819	(Verma et al., 2005)
US-Ton	Oak savanna woodland	38.4	-121.0	16.0	815	(Ma et al., 2007)
US-UMB	Arboreal composition of the forest	45.6	-84.7	8.3	800	(Gough et al., 2008)
US-Var	Grassland	38.4	-121.0	16.0	815	(Ma et al., 2007)
US-WCr	Deciduous broadleaf forest	45.8	-90.1	6.4	839	(Cook et al., 2004a)

Table 3-3. Trends in annual and seasonal T_a ($^{\circ}\text{C decade}^{-1}$) across sub-regions of North America

Spatial annual average trends in T_a across sub-regions of NA				
Region	Trend ($^{\circ}\text{C decade}^{-1}$)	Latitude	Longitude	Time
North America	0.38	$10^{\circ}\text{N} - 84^{\circ}\text{N}$	$50^{\circ}\text{W} - 170^{\circ}\text{W}$	1979 - 2010
Northern	0.46	$45^{\circ}\text{N} - 84^{\circ}\text{N}$	$110^{\circ}\text{W} - 170^{\circ}\text{W}$	1979 - 2010
North east	0.72	$51^{\circ}\text{N} - 84^{\circ}\text{N}$	$50^{\circ}\text{W} - 170^{\circ}\text{W}$	1979 - 2010
Southern	0.19	$10^{\circ}\text{N} - 45^{\circ}\text{N}$	$110^{\circ}\text{W} - 170^{\circ}\text{W}$	1979 - 2010
West	0.08	$24^{\circ}\text{N} - 68^{\circ}\text{N}$	$110^{\circ}\text{W} - 170^{\circ}\text{W}$	1979 - 2010
Spatial seasonal average trends in T_a across NA				
Winter	0.44	$10^{\circ}\text{N} - 84^{\circ}\text{N}$	$50^{\circ}\text{W} - 170^{\circ}\text{W}$	1979 - 2010
Spring	0.25	$10^{\circ}\text{N} - 84^{\circ}\text{N}$	$50^{\circ}\text{W} - 170^{\circ}\text{W}$	1979 - 2010
Summer	0.25	$10^{\circ}\text{N} - 84^{\circ}\text{N}$	$50^{\circ}\text{W} - 170^{\circ}\text{W}$	1979 - 2010
Autumn	0.59	$10^{\circ}\text{N} - 84^{\circ}\text{N}$	$50^{\circ}\text{W} - 170^{\circ}\text{W}$	1979 - 2010

Table 3-4. Long-term (1980-2010) spatial average and changes in modeled GPP, T_a and precipitation across level I eco-regions of North America

Level I Eco-regions of NA ^a	% GPP ^b	% Area ^c	(GPP/Area) ^d	GPP % change/ 31 yrs ^e	Changes in T _a /31yrs ^f	Precipitation % change/31 yrs ^g	NA GPP % change ^h
Arctic cordillera	0.01	1.75	3.2	24.2	1.80	14	0.002
North American deserts	3.33	9.04	239	-35.8	-0.03	-21	-1.19
Mediterranean California	0.71	0.79	584	-18.7	0.44	-36	-0.13
Southern semi-arid highlands	1.15	1.27	586	-5.2	0.47	0.3	-0.06
Temperate Sierras	3.82	2.63	944	-5.7	0.75	-19	-0.22
Tropical dry forests	1.91	1.59	779	-1.8	0.65	-11	-0.034
Tropical wet forests	4.14	1.49	1803	-0.4	0.83	-22	-0.02
Tundra	3.10	15.97	126	11.0	2.12	20	0.34
Taiga	9.03	13.72	426	21.9	1.07	15	1.98
Hudson plain	1.59	1.69	610	13.3	1.68	0.3	0.21
Northern forests	17.13	13.51	823	21.7	1.26	0.3	3.72
Northwestern forested mountains	8.33	9.52	567	-5.9	-0.08	-4	-0.49
Marine west coast forest	2.68	2.52	688	2.9	-0.69	-7	0.08
Eastern temperate forests	25.16	11.91	1369	6.9	0.92	-12	1.74
Great plains	17.90	12.59	922	-0.5	0.52	-1	-0.09

^a North America level I eco-regions had 15 broad ecological regions with distinct biological, physical and human characteristics that can be used at regional and continental scale

^b Percentage GPP for eco-regions calculated from a long-term (1980–2010) mean GPP map of North America

^c Area percentage (area of eco-region / total area of North America)

^d The ratio of total GPP to the area of eco-regions (g C m⁻² yr⁻¹)

^e Percentage of GPP change (long-term (1980-2010) change in GPP / long-term mean GPP), positive values indicated an increase in GPP, whereas negative values indicated a decline in GPP

^f Change in air temperature (°C 31 yrs⁻¹)

^g Change in precipitation (mm 31 yrs⁻¹)

^h Percentage of North America GPP contributed by eco-regions (% GPP^b x GPP % change/ 31 yrs^e)

List of Figures

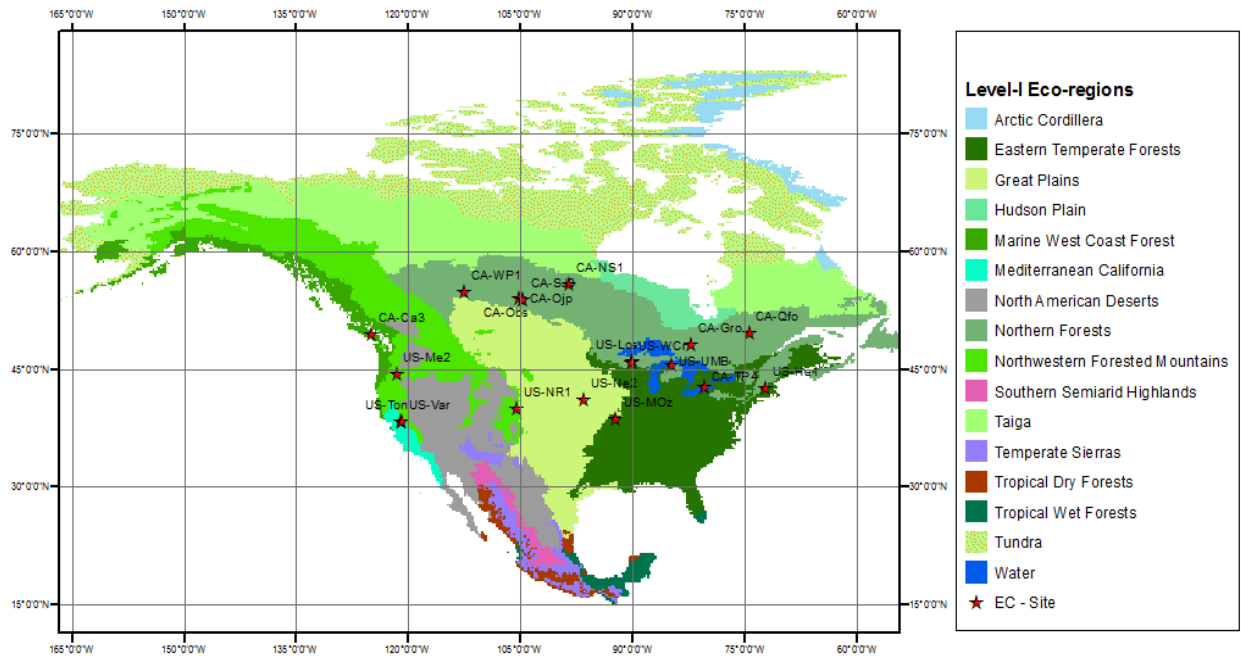


Figure 3-1. Level-I eco-regions of North America and selected eddy covariance sites for model validation

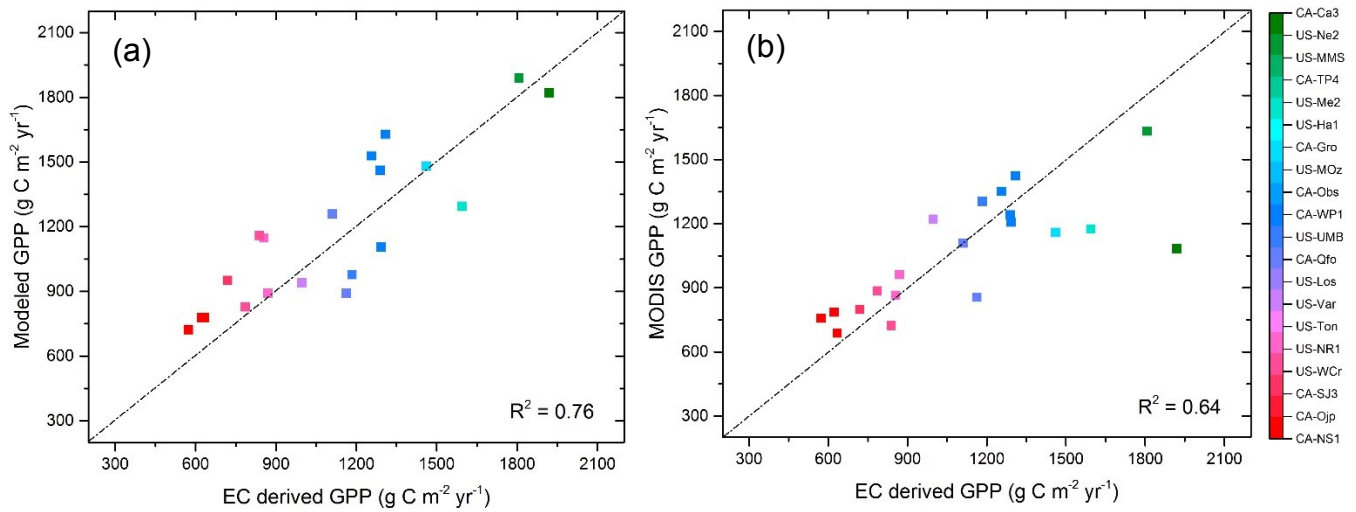


Figure 3-2. Correlation between annual GPP for 2005 (a) derived from measurements at 20 selected EC flux tower sites (Table 3-2) vs. modeled GPP from the corresponding pixels where the EC flux towers were located (b) EC-derived vs. MODIS GPP averaged for corresponding pixels within 0.25° x 0.25° where the EC flux towers were located

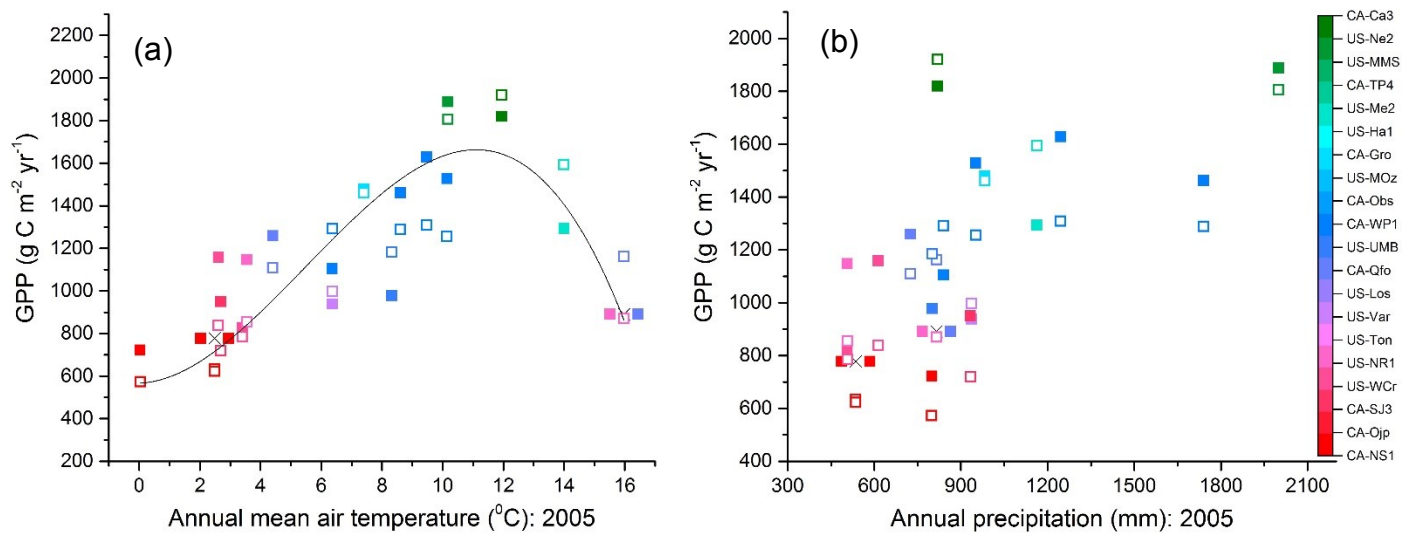


Figure 3-3. Relationship between 2005 (a) mean annual air temperature (MAT) and (b) annual precipitation extracted from NARR vs. modeled annual GPP (closed squares) and EC derived annual GPP (open squares) for 20 EC sites across North America. The x symbols represent overlapping points.

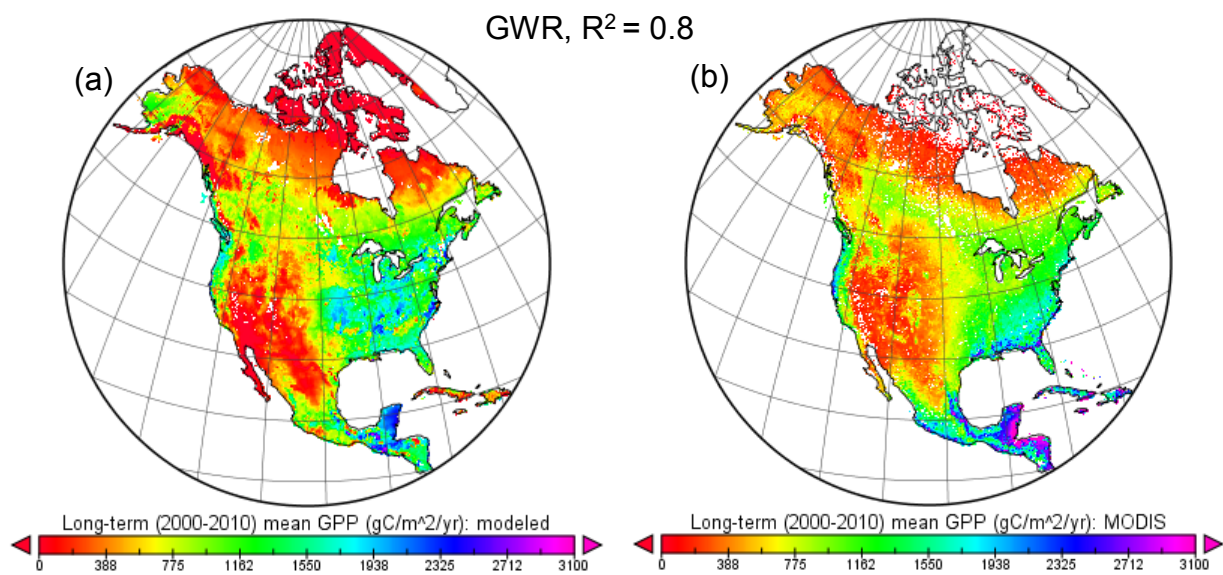


Figure 3-4. Long-term (2000 – 2010) annual average (a) modeled GPP and (b) MODIS GPP for North America

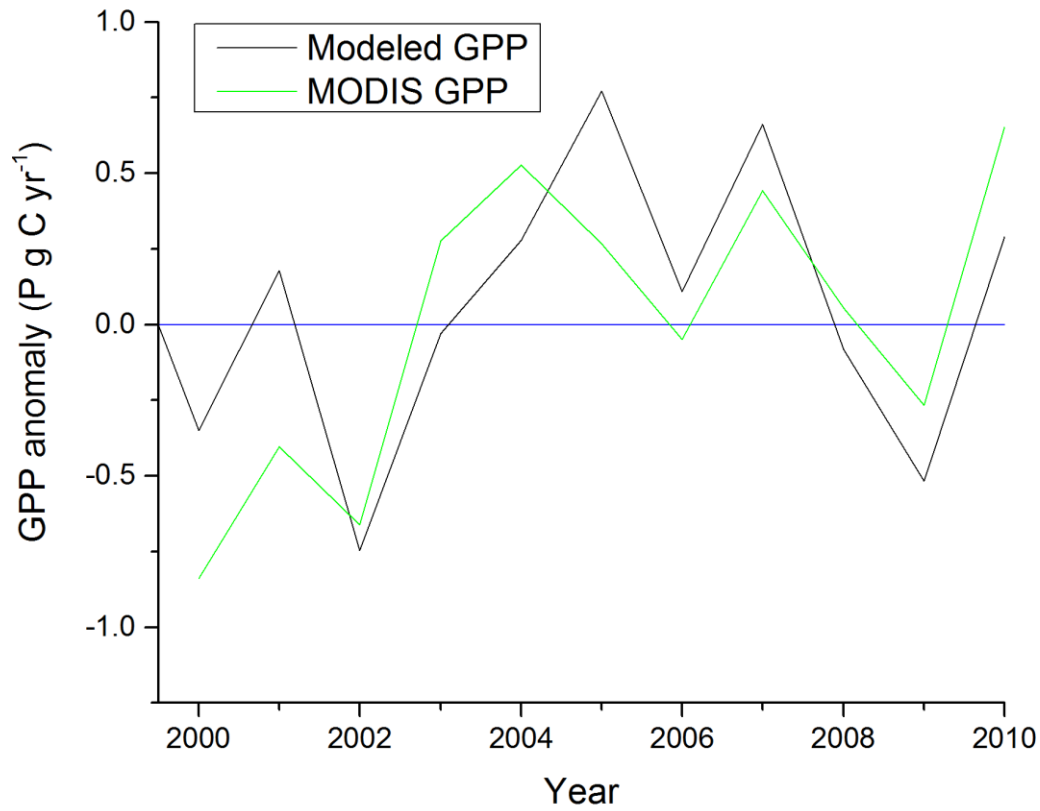


Figure 3-5. GPP anomaly for spatial average modeled vs. MODIS GPP from 2000-2010 for North America

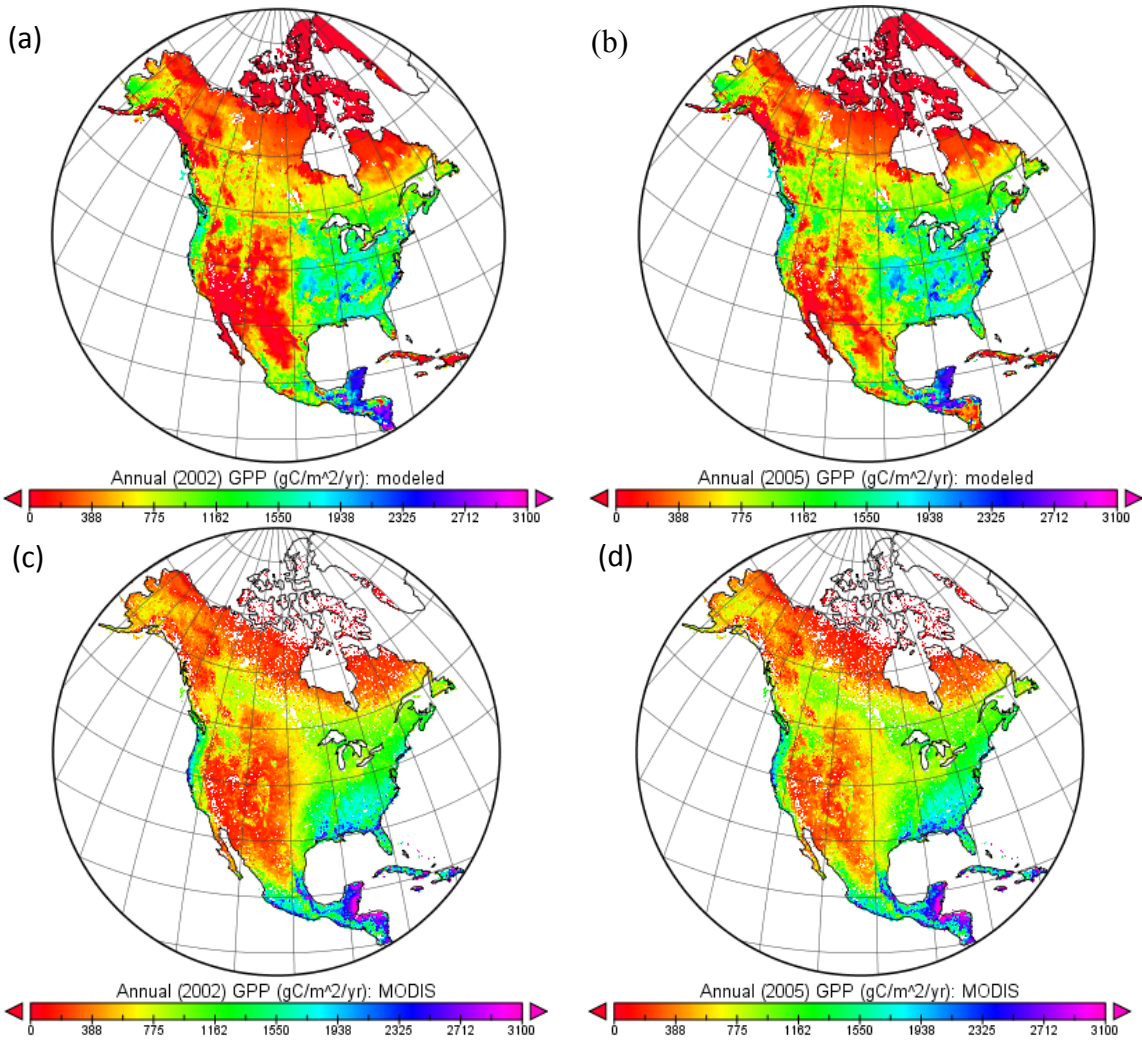


Figure 3-6. Comparison of spatial patterns in modeled annual GPP (a, b) vs. MODIS GPP (c, d) for 2002 (drought) vs. 2005 (non-drought) years for North America: GWR for modeled vs. MODIS GPP $R^2 = 0.85$ for 2002 and 0.86 for 2005

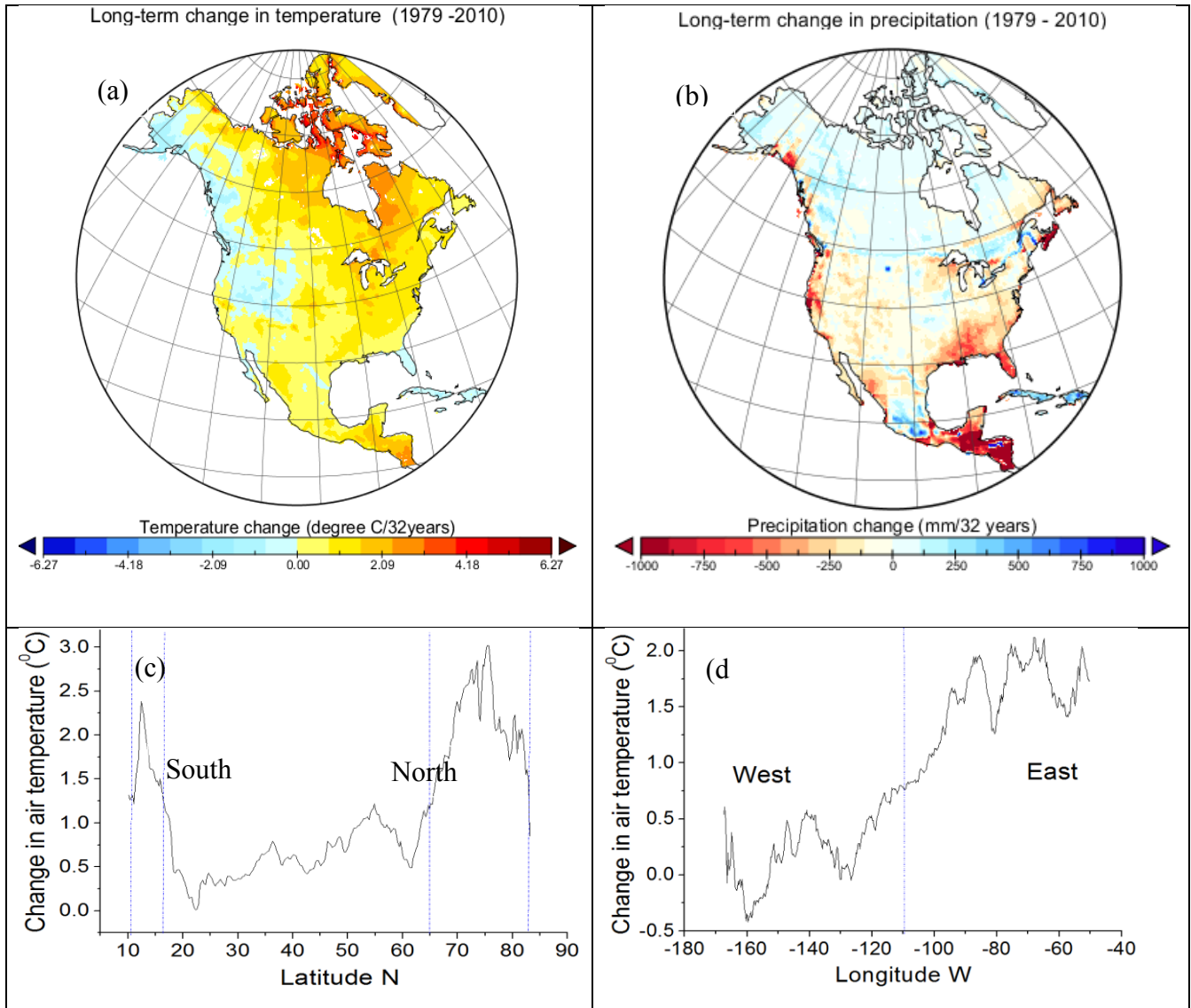


Figure 3-7. Long-term (1979 – 2010) changes in (a) mean annual air temperature (b) annual precipitation across North America landmass (c) average air temperature across latitudes, and (d) average air temperature across longitudes.

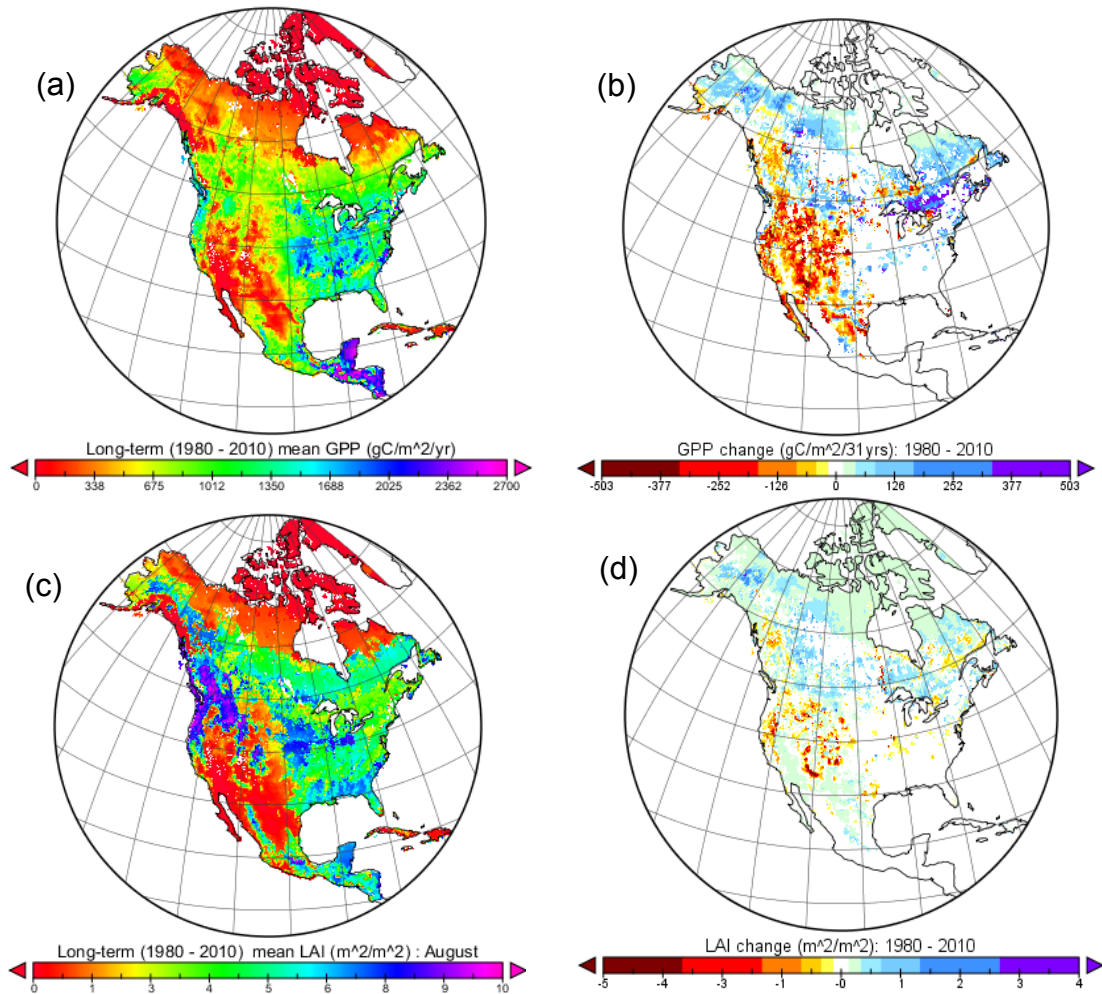


Figure 3-8. Long-term mean (a) annual GPP (c) mid-August LAI and spatially averaged changes (average of the first 5 years (1980 – 1984) subtracted from average of the last 5 years (2006 – 2010) for (b) annual GPP and (d) mid-August LAI over the last three decades in North America. Pixels with no value in b and d represents forested stands with less than 60 years from the last stand replacing fire and pixels with forest stands in Mexico with no historical disturbance data

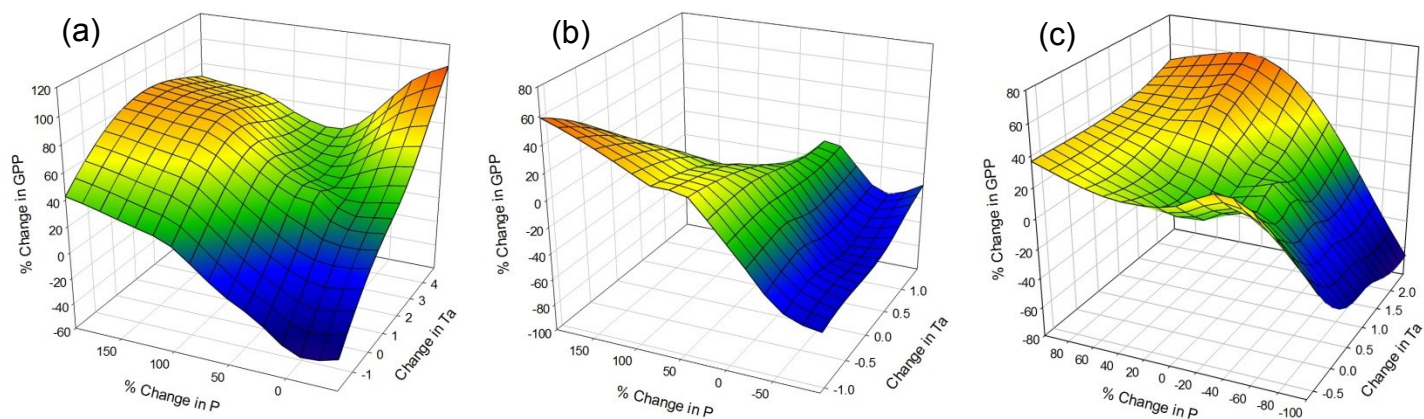


Figure 3-9. 3D Mesh graph showing the relationship among long-term (1980 – 2010) % change in modeled GPP and NARR precipitation (P) and changes in T_a for (a) northern (above 50° N), (b) south and southwest and (c) southeast parts of North America

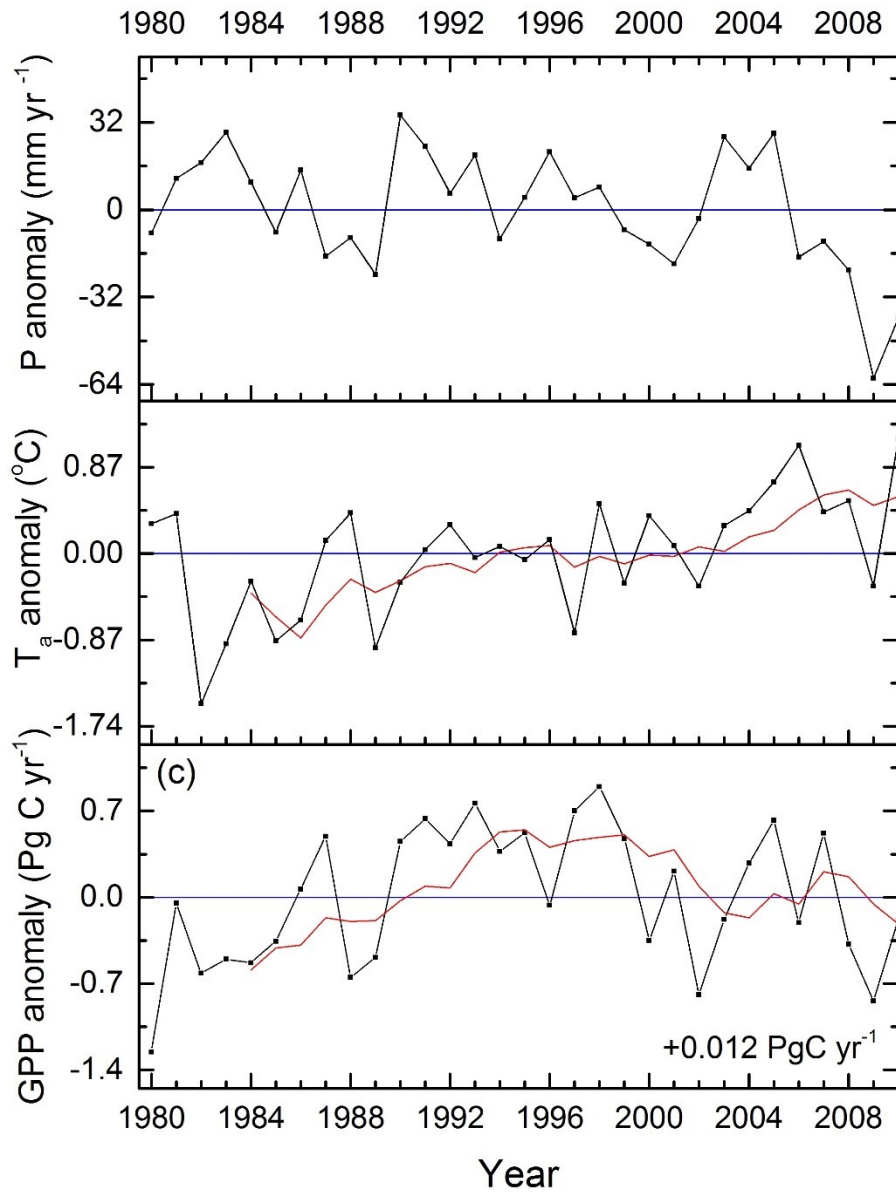


Figure 3-10. Anomalies of annual average (a) precipitation, and (b) T_a derived from NARR, and (c) modeled GPP from the long-term mean for North America over the last three decades

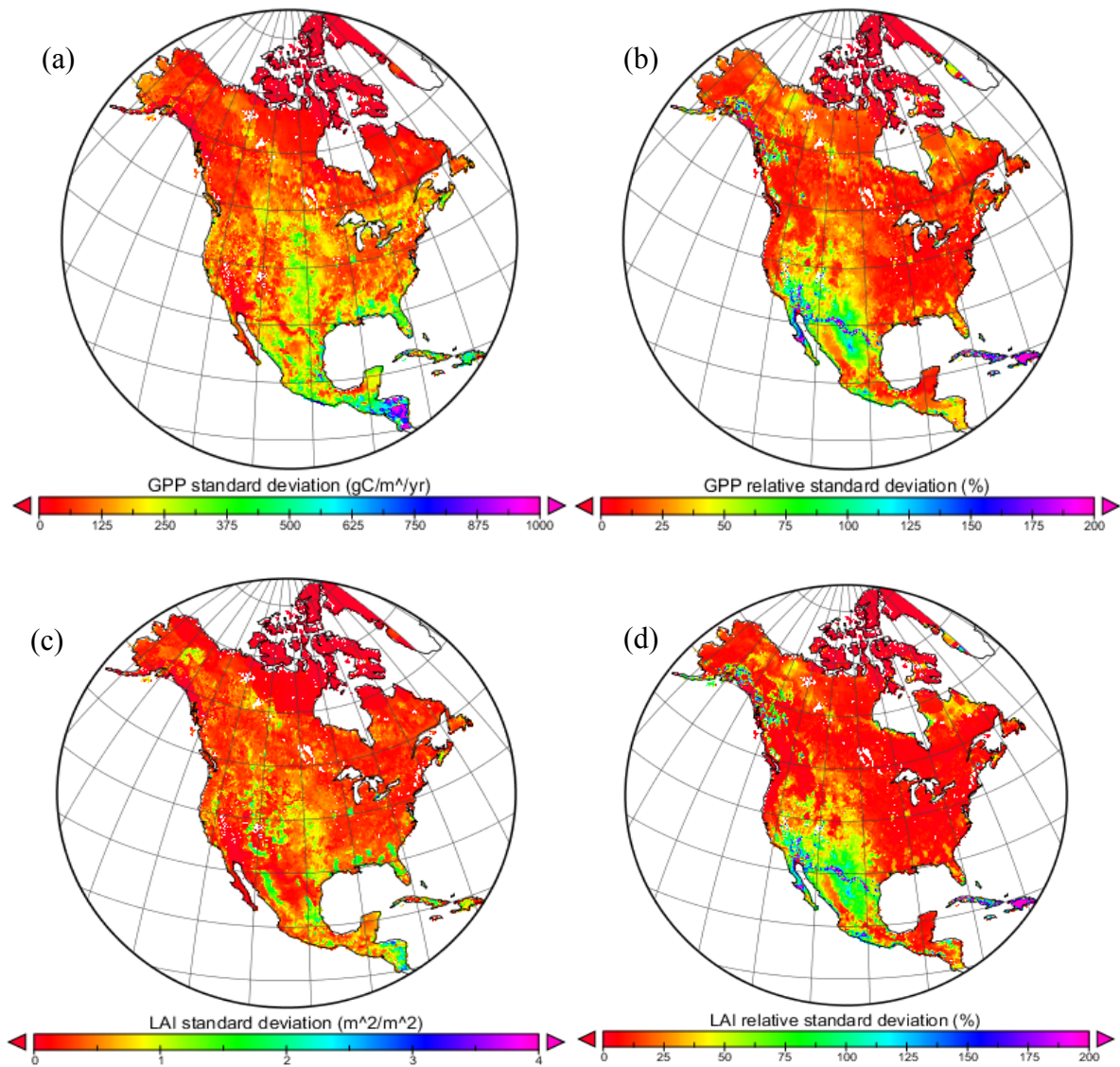


Figure 3-11. Long-term (1980 – 2010) North America (a) GPP standard deviation, (b) GPP relative standard deviation (standard deviation / long-term mean), (c) mid-August LAI standard deviation and (d) mid-August LAI relative standard deviation

Appendices: A - D

Appendix A: Soil C, N and P transformations

<i>Decomposition</i>			
$f_{igl} = T_{sl} \{ e^{(B - H_a / (R T_{sl}))} \} / \{ 1 + e^{(H_{dl} - ST_{sl}) / (R T_{sl})} + e^{(ST_{sl} - H_{dh}) / (R T_{sl})} \}$	Arrhenius function for D and R_h		[A6]
<i>Microbial Growth: respiration</i>			
$R_h = \sum_i \sum_n \sum_l R_{hi,n,l}$	total heterotrophic respiration		[A11]
$R_{mi,n,j,l} = R_m M_{i,n,j,l,N} f_{tml}$	maintenance respiration		[A18]
$f_{tml} = e^{[v(T_{sl} - 298.16)]}$	temperature sensitivity of R_m		[A19]
$R_{gi,n,l} = R_{hi,n,l} - \sum_j R_{mi,n,j,l}$	growth respiration		[A20]
<i>Microbial Nutrient Exchange</i>			
$U_{NH_4i,n,j,l} = (M_{i,n,j,l,C} C_{Nj} - M_{i,n,j,l,N})$	$U_{NH_4} < 0$	net mineralization	[A26a]
$U_{NH_4i,n,j,l} = \min \{ (M_{i,n,j,l,C} C_{Nj} - M_{i,n,j,l,N}),$ $U'_{NH_4} a_{i,n,j,l} ([NH_4^+_{i,n,j,l}] - [NH_4^+_{mn}]) / ([NH_4^+_{i,n,j,l}] - [NH_4^+_{mn}] + K_{NH_4}) \}$	$U_{NH_4} > 0$	net immobilization	[A26b]
$U_{NO_3i,n,j,l} = \min \{ (M_{i,n,j,l,C} C_{Nj} - (M_{i,n,j,l,N} + U_{NH_4i,n,j,l})),$ $U'_{NO_3} a_{i,n,j,l} ([NO_3^-_{i,n,j,l}] - [NO_3^-_{mn}]) / ([NO_3^-_{i,n,j,l}] - [NO_3^-_{mn}] + K_{NO_3}) \}$	$U_{NO_3} > 0$	net immobilization	[A26c]
$U_{PO_4i,n,j,l} = (M_{i,n,j,l,C} C_{Pj} - M_{i,n,j,l,P})$	$U_{PO_4} < 0$	Net mineralization	[A26d]
$U_{PO_4i,n,j,l} = \min \{ (M_{i,n,j,l,C} C_{Pj} - M_{i,n,j,l,P}),$ $U'_{PO_4} A_{i,n,j,l} ([H_2PO_4^-_{i,n,j,l}] - [H_2PO_4^-_{mn}]) / ([H_2PO_4^-_{i,n,j,l}] - [H_2PO_4^-_{mn}] + K_{PO_4}) \}$	$U_{PO_4} > 0$	Net immobilization	[A26e]

Appendix B: Soil-plant water relations

<i>Canopy Transpiration</i>			
$Rn_{ci} + LE_{ci} + H_{ci} + G_{ci} = 0$	canopy energy balance		[B1a]
$LE_{ci} = L (e_a - e_{ci(T_{ci}, \psi_{ci})}) / r_{ai}$	LE from canopy evaporation		[B1b]
$LE_{ci} = L (e_a - e_{ci(T_{ci}, \psi_{ci})}) / (r_{ai} + r_{ci}) - LE_{ci}$ from [B1b]	LE from canopy transpiration		[B1c]
$H_{ci} = \rho C_p (T_a - T_{ci}) / r_{ai}$	H from canopy energy balance		[B1d]
$r_{cmini} = 0.64 (C_b - C'_i) / V_{c'i}$	r_c driven by rates of carboxylation vs.		[B2a]
$r_{ci} = r_{cmini} + (r_{cmaxi} - r_{cmini}) e^{(-\beta \psi_{ci})}$	diffusion		[B2b]
	r_c constrained by water status		
$\psi_{ci} = \psi_{ci} - \psi_{\pi i}$			[B4]
<i>Root and Mycorrhizal Water Uptake</i>			
$U_{wi,r,l} = (\psi_{c'i} - \psi_{s'l}) / (\Omega_{si,r,l} + \Omega_{ti,r,l} + \sum_x \Omega_{ai,r,l,x})$	U_w along hydraulic gradient		[B6]
$\Omega_{si,r,l} = \ln \{ (d_{i,r,l} / r_{i,r,l}) / (2\pi L_{i,r,l} \kappa_{i,r,l}) \} \theta_{wl} / \theta_{pl}$			[B9]

$\Omega_{ai,r} = \Omega_{ai,r} / L_{i,r,l}$			[B10]
$\Omega_{ai,r,l,x=1} = \Omega_{ai,r} z_l / \{n_{i,r,l,1} (r_{i,r,l,1} / r'_{i,r})^4\} + \gamma \Omega_{ai,r} z_{bi} / \{n_{i,r,l,1} (r_{bi} / r'_{bi})^4\}$ $\Sigma_{i,r,l} (M_{i,r,l}) / M_{i,r,l}$			[B11]
$\Omega_{ai,r,l,x=2} = \Omega_{ai,r} (L_{i,r,l,2} / n_{i,r,l,2}) / \{n_{i,r,l,2} (r_{i,r,l,2} / r'_{i,r})^4\}$			[B12]
<i>Canopy Water Potential</i>			
$(e_a - e_{i(T_{ci})}) / (r_{ai} + r_{ci}) [B1] = \Sigma_l \Sigma_r (\psi_{ci}' - \psi_{s'}') / (\Omega_{si,r,l} + \Omega_{ti,r,l} + \Sigma_x \Omega_{ai,r,l,x}) + X_{ci} \delta \psi_{ci} / \delta t$		ψ_{ci} solved when transpiration from [B1-B4] (LHS) equals uptake from [B5-B13] + change in storage (RHS)	[B14]
<i>Canopy Water Potential</i>			
$(e_a - e_{i(T_{ci})}) / (r_{ai} + r_{ci}) [B1] = \Sigma_l \Sigma_r (\psi_{ci}' - \psi_{s'}') / (\Omega_{si,r,l} + \Omega_{ti,r,l} + \Sigma_x \Omega_{ai,r,l,x}) + X_{ci} \delta \psi_{ci} / \delta t$		ψ_{ci} solved when transpiration from [B1-B4] (LHS) equals uptake from [B5-B13] + change in storage (RHS)	[B14]

Appendix C: Gross primary productivity, Autotrophic respiration, Growth and Litterfall

<i>C₃ Gross Primary Productivity</i>			
$GPP = \Sigma_{i,j,k,l,m,n,o} (V_{ci,j,k,l,m,n,o} = V_{gi,j,k,l,m,n,o}) A_{i,j,k,l,m,n,o}$		solve for $C_{ii,j,k,l,m,n,o}$ at which $V_{ci,j,k,l,m,n,o} = V_{gi,j,k,l,m,n,o}$	[C1]
$V_{gi,j,k,l,m,n,o} = (C_b - C_{ii,j,k,l,m,n,o}) / r_{ii,j,k,l,m,n,o}$		diffusion	[C2]
$V_{ci,j,k,l,m,n,o} = \min\{V_{bi,j,k,l,m,n,o}, V_{ii,j,k,l,m,n,o}\}$		carboxylation	[C3]
$r_{ii,j,k,l,m,n,o} = r_{i\text{mini},j,k,l,m,n,o} + (r_{i\text{maxi}} - r_{i\text{mini},j,k,l,m,n,o}) e^{(-\beta \psi_{ti})}$		r_1 is leaf-level equivalent of r_c	[C4]
$r_{i\text{mini},j,k,l,m,n,o} = (C_b - C_i') / V_{ci,j,k,l,m,n,o}$		minimum r_1 is driven by carboxylation	[C5]
$V_{bi,j,k,l,m,n,o} = V_{b\text{maxi},j,k} (C_{ci,j,k,l,m,n,o} - \Gamma_{ij,k}) / (C_{ci,j,k,l,m,n,o} + K_{ci}) f_{\psi ij,k,l,m,n,o}$ $V_{b\text{maxi},j,k} = V_b' F_{rubisco} M_{ij,k,prot} / A_{ij,k} f_{tb} f_{ci}$ $\Gamma_{ij,k} = 0.5 O_c V_{o\text{maxi},j,k} K_{ci} / (V_{b\text{maxi},j,k} K_{oi})$ $V_{o\text{maxi},j,k} = V_o' F_{rubisco} M_{ij,k,prot} / A_{ij,k} f_{toi}$ $K_{ci} = K_{ci} f_{tkci} (1 + O_c / (K_{oi} f_{tkoi}))$		CO ₂ and water f_{ψ} constraints on V_b temperature f_{tb} and nutrient f_{ci} constraints on $V_{b\text{max}}$ CO ₂ compensation point oxygenation M-M constant for V_b	[C6a] [C6b] [C6c] [C6d] [C6e]
$V_{ji,j,k,l,m,n,o} = J_{ij,k,l,m,n,o} Y_{ij,k,l,m,n,o} f_{\psi ij,k,l,m,n,o}$ $Y_{ij,k,l,m,n,o} = (C_{ci,j,k,l,m,n,o} - \Gamma_{ij,k}) / (4.5 C_{ci,j,k,l,m,n,o} + 10.5 \Gamma_{ij,k})$		water constraints on V_j carboxylation efficiency of V_j	[C7a] [C7b]
$J_{ij,k,l,m,n,o} = (\varepsilon I_{i,l,m,n,o} + J_{\text{maxi},j,k} - ((\varepsilon I_{i,l,m,n,o} + J_{\text{maxi},j,k})^2 - 4\alpha\varepsilon I_{i,l,m,n,o} J_{\text{maxi},j,k})^{0.5}) / (2\alpha)$ $J_{\text{maxi},j,k} = V_j' F_{chlorophyll} M_{ij,k,prot} / A_{ij,k} f_{yi} f_{ci}$		irradiance constraints on J temperature and nutrient constraints on J_{max}	[C8a] [C8b]
$f_{\psi ij,k,l,m,n,o} = (r_{i\text{min},j,k,l,m,n,o} / r_{ii,j,k,l,m,n,o})^{0.5}$		non-stomatal effect related to stomatal effect	[C9]
$f_{tb} = \exp[B_v - H_{av} / (RT_{ci})] / \{1 + \exp[(H_{al} - ST_{ci}) / (RT_{ci})] + \exp[(ST_{ci} - H_{ah}) / (RT_{ci})]\}$ $f_{toi} = \exp[B_o - H_{ao} / (RT_{ci})] / \{1 + \exp[(H_{al} - ST_{ci}) / (RT_{ci})] + \exp[(ST_{ci} - H_{ah}) / (RT_{ci})]\}$ $f_{yi} = \exp[B_j - H_{aj} / (RT_{ci})] / \{1 + \exp[(H_{al} - ST_{ci}) / (RT_{ci})] + \exp[(ST_{ci} - H_{ah}) / (RT_{ci})]\}$ $f_{tkci} = \exp[B_{kc} - H_{ake} / (RT_{ci})]$ $f_{tkoi} = \exp[B_{ko} - H_{ako} / (RT_{ci})]$		Arrhenius functions for carboxylation, oxygenation and electron transport temperature sensitivity of K_{ci}, K_{oi}	[C10a] [C10b] [C10c] [C10d] [C10e]

$f_{Ci} = \min \{ \sigma_{Ni,j} / (\sigma_{Ni,j} + \sigma_{Ci,j} / K_{iC_N}), \sigma_{Pi,j} / (\sigma_{Pi,j} + \sigma_{Ci,j} / K_{iC_P}) \}$	control of σ_N and σ_P vs. σ_C in shoots on V_b, V_j through product inhibition and on leaf protein growth through leaf structural C:N:P ratios	[C11]
$\delta M_{L_{Rij,k}} / \delta t = \delta M_{L_{ij,k}} / \delta t \min \{ [N'_{leaf} + (N_{leaf} - N'_{leaf}) f_{Ci}] / N_{prot}, [P'_{leaf} + (P_{leaf} - P'_{leaf}) f_{Ci}] / P_{prot} \}$	growth of remobilizable leaf protein C	[C12]
<i>Root and Mycorrhizal Nutrient Uptake</i>		
$U_{NH4i,r,l} = \{ U_{wi,r,l} [NH_4^+{}_i] + 2\pi L_{i,r,l} D_{eNH4l} ([NH_4^+{}_i] - [NH_4^+{}_{i,r,l}]) / \ln(d_{i,r,l} / r_{i,r,l}) \}$ $= U'_{NH4} (U_{O2i,r,l} / U'_{O2i,r,l}) A_{i,r,l} ([NH_4^+{}_{i,r,l}] - [NH_4^+{}_{mn}]) / ([NH_4^+{}_{i,r,l}] - [NH_4^+{}_{mn}] + K_{NH4})$	root N and P uptake from mass flow + diffusion coupled with active uptake of NH_4^+ , NO_3^- and $H_2PO_4^-$ constrained by O_2 uptake, as modelled for microbial N and P uptake in [A26]	[C23a]
$f_{tai,l} f_{iNi,r,l}$ $U_{NO3i,r,l} = \{ U_{wi,r,l} [NO_3^-{}_i] + 2\pi L_{i,r,l} D_{eNO3l} ([NO_3^-{}_i] - [NO_3^-{}_{i,r,l}]) / \ln(d_{i,r,l} / r_{i,r,l}) \}$ $= U'_{NO3} (U_{O2i,r,l} / U'_{O2i,r,l}) A_{i,r,l} ([NO_3^-{}_{i,r,l}] - [NO_3^-{}_{mn}]) / ([NO_3^-{}_{i,r,l}] - [NO_3^-{}_{mn}] + K_{NO3})$		[C23b]
$f_{tai,l} f_{iNi,r,l}$ $U_{PO4i,r,l} = \{ U_{wi,r,l} [H_2PO_4^-{}_i] + 2\pi L_{i,r,l} D_{ePO4l} ([H_2PO_4^-{}_i] - [H_2PO_4^-{}_{i,r,l}]) / \ln(d_{i,r,l} / r_{i,r,l}) \}$ $= U'_{PO4} (U_{O2i,r,l} / U'_{O2i,r,l}) A_{i,r,l} ([H_2PO_4^-{}_{i,r,l}] - [H_2PO_4^-{}_{mn}]) / ([H_2PO_4^-{}_{i,r,l}] - [H_2PO_4^-{}_{mn}] + K_{PO4}) f_{tai,l} f_{iPi,r,l}$		[C23c]
$f_{iNi,r,l} = \sigma_{Ci,r,l} / (\sigma_{Ci,r,l} + \sigma_{Ni,r,l} / K_{iNC})$ $f_{iPi,r,l} = \sigma_{Ci,r,l} / (\sigma_{Ci,r,l} + \sigma_{Pi,r,l} / K_{iPC})$		[C23d]
	product inhibition of U_{NH4} , U_{NO3} and U_{PO4} determined by σ_N and σ_P vs. σ_C in roots	[C23e]
		[C23f]
		[C23g]
		[C23h]

Appendix D: Soil water, heat, gas and solute fluxes

<i>Surface Water Flux</i>		
$Q_{rx(x,y)} = v_{x(x,y)} d_{mx,y} L_{y(x,y)}$	2D Manning equation in x (EW) and y (NS) directions	[D1]
<i>Subsurface Water Flux</i>		
$Q_{wx(x,y,z)} = K'_x (\psi_{sx,y,z} - \psi_{sx+1,y,z})$	3D Richard's or Green-Ampt equation depending on saturation of source or target cell in x (EW), y (NS) and z (vertical) directions	[D7]
$Q_{wy(x,y,z)} = K'_y (\psi_{sx,y,z} - \psi_{sx,y+1,z})$		
<i>Heat Flux</i>		
$R_n + LE + H + G = 0$	for each canopy, snow, residue and soil surface, depending on exposure	[D11]
$G_{x(x,y,z)} = 2 K_{(x,y,z),(x+1,y,z)} (T_{(x,y,z)} - T_{(x+1,y,z)}) / (L_x(x,y,z) + L_x(x+1,y,z)) + c_w T_{(x,y,z)} Q_{wx(x,y,z)}$	3D conductive – convective heat flux among snowpack, surface residue and soil layers in x (EW), y (NS) and z (vertical) directions	[D12]
$G_{y(x,y,z)} = 2 K_{(x,y,z),(x,y+1,z)} (T_{(x,y,z)} - T_{(x,y+1,z)}) / (L_y(x,y,z) + L_y(x,y+1,z)) + c_w T_{(x,y,z)} Q_{wy(x,y,z)}$		
$G_{z(x,y,z)} = 2 K_{(x,y,z),(x,y,z+1)} (T_{(x,y,z)} - T_{(x,y,z+1)}) / (L_z(x,y,z) + L_z(x,y,z+1)) + c_w T_{(x,y,z)} Q_{wz(x,y,z)}$		
$G_{x(x-1,y,z)} - G_{x(x,y,z)} + G_{y(x,y-1,z)} - G_{y(x,y,z)} + G_{z(x,y,z-1)} - G_{z(x,y,z)} + LQ_{f(x,y,z)} + c_{(x,y,z)} (T_{(x,y,z)} - T'_{(x,y,z)}) / \Delta t = 0$	3D general heat flux equation in snowpack, surface residue and soil layers	[D13]

Definition of Variables in the Appendices

Variable	Definition	Unit	Value	Reference
<i>subscripts</i>				
<i>i</i>	(b,c)plant species or functional type: coniferous, deciduous, annual, perennial, C ₃ , C ₄ etc.; (a) substrate-microbe complex: coarse woody litter, fine non-woody litter, POC, humus;			
<i>j</i>	(b)branch or tiller; (a)kinetic component			
<i>k</i>	node			
<i>l</i>	soil or canopy layer			
<i>m</i>	leaf azimuth			
<i>n</i>	leaf inclination			
<i>o</i>	leaf exposure (sunlit vs. shaded)			
<i>r</i>	root or mycorrhizae; (a) microbial functional type: heterotrophic (bacteria, fungi), autotrophic (nitrifiers, methanotrophs), diazotrophic, obligate aerobe, facultative anaerobes (denitrifiers), obligate anaerobes (methanogens)			
<i>x</i>	grid cell position in west to east direction			
<i>y</i>	grid cell position in north to south direction			
<i>z</i>	organ including leaf, stem, root <i>r</i> , mycorrhizae <i>m</i> ; (d) grid cell position in vertical direction		<i>z</i> = 0: surface residue, <i>z</i> = 1 to <i>n</i> : soil layers	
<i>variables</i>				
<i>A</i>	leaf, root or mycorrhizal surface area	m ² m ⁻²		
<i>B</i>	parameter such that $f_{lg} = 1.0$ at $T_l = 298.15$ K		26.235	
<i>a</i>	microbial surface area	m ² m ⁻²		
<i>β</i>	shape parameter for stomatal effects on CO ₂ diffusion and non-stomatal effects on carboxylation	MPa ⁻¹	-5.0	Grant and Flanagan (2007)
<i>B_j</i>	parameter such that $f_{ij} = 1.0$ at $T_c = 298.15$ K		17.354	
<i>B_{kc}</i>	parameter such that $f_{kci} = 1.0$ at $T_c = 298.15$ K		22.187	
<i>B_{ko}</i>	parameter such that $f_{koi} = 1.0$ at $T_c = 298.15$ K		8.067	
<i>B_o</i>	parameter such that $f_{oi} = 1.0$ at $T_c = 298.15$ K		24.212	
<i>B_v</i>	parameter such that $f_{vi} = 1.0$ at $T_c = 298.15$ K		26.229	
<i>C_b</i>	[CO ₂] in canopy air	μmol mol ⁻¹		
<i>C_c</i>	[CO ₂] in canopy chloroplasts in equilibrium with $C_{i,j,k,l,m,n,o}$	μM		
<i>C_i'</i>	[CO ₂] in canopy leaves when $\psi_{ci} = 0$	μmol mol ⁻¹	0.70 x <i>C_b</i>	Larcher (2001)

C_{N,P_j}	maximum ratio of $M_{i,n,j,N,P}$ to $M_{i,n,j,C}$ maintained by $M_{i,n,j,C}$	g N or P g C ⁻¹	0.22 and 0.13 (N), 0.022 and 0.013 (P) for j = labile and resistant, respectively	Grant et al. (1993a, b)
C_i	[CO ₂] in canopy leaves	μmol mol ⁻¹		
$D_{e\text{ NH}_4I}$	effective dispersivity-diffusivity of NH ₄ ⁺ during root uptake	m ² h ⁻¹		
$D_{e\text{ NO}_3I}$	effective dispersivity-diffusivity of NO ₃ ⁻ during root uptake	m ² h ⁻¹		
$D_{e\text{ PO}_4I}$	effective dispersivity-diffusivity of H ₂ PO ₄ ⁻ during root uptake	m ² h ⁻¹		
$d_{i,r,l}$	half distance between adjacent roots assumed equal to uptake path length	m	$(\pi L_{s,z} / \Delta Z)^{-1/2}$	Grant (1998)
d_m	depth of mobile surface water	m		
d_w	depth of surface water	m		
E_{ci}	canopy transpiration	m ³ m ⁻² h ⁻¹		
F_{chl}	fraction of leaf protein in chlorophyll	-	0.025	
f_{iC}	N,P inhibition on carboxylation, leaf structural N,P growth	-		
f_{iN}	N inhibition on root N uptake	-		
f_{iP}	P inhibition on root P uptake	-		
$F_{rubisco}$	fraction of leaf protein in rubisco	-	0.125	
f_{ta}	temperature effect on $R_{ai,j}$ and U	-		
f_{tb}	temperature effect on carboxylation	-		
f_{ij}	temperature effect on electron transport			
f_{tkc}	temperature effect on K_{c_i}			Bernacchi et al. (2001,2003)
f_{tgl}	temperature function for microbial growth respiration	dimensionless		
f_{tml}	temperature function for maintenance respiration	dimensionless		
f_{tko}	temperature effect on K_{o_i}			Bernacchi et al. (2001,2003)
f_{to}	temperature effect on oxygenation			
f_{wi}	non-stomatal water effect on carboxylation	-		Medrano et al. (2002)
H_a	energy of activation	J mol ⁻¹	65 x 10 ³	Addiscott (1983)
H_{aj}	energy of activation for electron transport	J mol ⁻¹	43 x 10 ³	Bernacchi et al. (2001,2003)
H_{akc}	parameter for temperature sensitivity of K_{c_i}	J mol ⁻¹	55 x 10 ³	Bernacchi et al. (2001,2003)
H_{ako}	parameter for temperature sensitivity of K_{o_i}	J mol ⁻¹	20 x 10 ³	Bernacchi et al. (2001,2003)

H_{ao}	energy of activation for oxygenation	$J mol^{-1}$	60×10^3	Bernacchi et al. (2001,2003)
H_{av}	energy of activation for carboxylation	$J mol^{-1}$	65×10^3	Bernacchi et al. (2001,2003)
H_{dh}	energy of high temperature deactivation	$J mol^{-1}$	222.5×10^3	
H_{dl}	energy of low temperature deactivation	$J mol^{-1}$	197.5×10^3	
$[H_2PO_4^-]$	concentration of $H_2PO_4^-$ in soil solution	$g P m^{-3}$		
$[H_2PO_4^-]_{i,r,l}$	concentration of $H_2PO_4^-$ root or mycorrhizal surfaces	$g N m^{-3}$		
$[H_2PO_4^-]_{mn}$	concentration of $H_2PO_4^-$ at root or mycorrhizal surfaces below which $U_{PO_4} = 0$	$g N m^{-3}$	0.002	Barber and Silberbush, 1984
I	irradiance	$\mu mol m^{-2} s^{-1}$		
J	electron transport rate in C_3 mesophyll	$\mu mol m^{-2} s^{-1}$		
J_{max}	electron transport rate at non-limiting I , ψ_{ci} , temperature and N,P	$\mu mol m^{-2} s^{-1}$		
K_c	Michaelis-Menten constant for carboxylation at zero O_2	μM	12.5 at 25 °C	Farquhar et al. (1980)
K_c	Michaelis-Menten constant for carboxylation at ambient O_2	μM		
K_{iNC}	inhibition constant for N uptake in roots from $\sigma_{C_{i,j}}$ vs. σ_{N_j}	$g N g C^{-1}$	0.1	Grant (1998)
K_{iPC}	inhibition constant for P uptake in roots from $\sigma_{C_{i,j}}$ vs. $\sigma_{P_{i,j}}$ roots	$g P g C^{-1}$	0.01	Grant (1998)
K_{NH_4}	M-M constant for NH_4^+ uptake at root or mycorrhizal surfaces; microbial surfaces	$g N m^{-3}$	0.40	Barber and Silberbush, 1984
K_{NO_3}	M-M constant for NO_3^- uptake at root or mycorrhizal surfaces; microbial surfaces	$g N m^{-3}$	0.35	Barber and Silberbush, 1984
K_{PO_4}	M-M constant for $H_2PO_4^-$ uptake root or mycorrhizal surfaces; microbial surfaces	$g P m^{-3}$	0.125	Barber and Silberbush, 1984
K_o	inhibition constant for O_2 in carboxylation	μM	500 at 25 °C	Farquhar et al. (1980)
$\kappa_{i,r,l}$	hydraulic conductivity between soil and root surface	$m^2 MPa^{-1} h^{-1}$		
K'_x, K'_y, K'_z	hydraulic conductance in x , y or z directions	$m MPa^{-1} h^{-1}$		
γ	scaling factor for bole axial resistance from primary root axial resistance	-	1.6×10^4	Grant et al. (2007)
L	root length	$m m^{-2}$		
$L_{i,r,l}$	length of roots or mycorrhizae	$m m^{-2}$		
L_x, L_y, L_z	length of landscape element in x , y or z directions	m		
$M_{i,n,j,l,C}$	microbial C	$g C m^{-2}$		
$M_{i,n,j,l,N}$	microbial N	$g N m^{-2}$		
$M_{i,n,j,l,P}$	microbial P	$g P m^{-2}$		
M_{iprot}	leaf protein phytomass calculated from leaf N, P contents	$g N m^{-2}$		
$M_{i,r,l}$	mass of roots or mycorrhizae	$g m^{-2}$		
$n_{i,r,l,x}$	number of primary ($x = 1$) or secondary ($x = 2$) axes	m^2		

$[\text{NH}_4^+_{i,r,l}]$	concentration of NH_4^+ at root or mycorrhizal surfaces	g N m^{-3}		
$[\text{NH}_4^+_{mn}]$	concentration of NH_4^+ at root or mycorrhizal surfaces below which $U_{\text{NH}_4} = 0$	g N m^{-3}	0.0125	Barber and Silberbush, 1984
$[\text{NH}_4^+_{i,n,j,l}]$	concentration of NH_4^+ at microbial surfaces	g N m^{-3}		
$[\text{NH}_4^+_{mn}]$	concentration of NH_4^+ at microbial surfaces below which $U_{\text{NH}_4} = 0$	g N m^{-3}	0.0125	
$[\text{NO}_3^-_{i,r,l}]$	concentration of NO_3^- at root or mycorrhizal surfaces	g N m^{-3}		
$[\text{NO}_3^-_{mn}]$	concentration of NO_3^- at root or mycorrhizal surfaces below which $U_{\text{NO}_3} = 0$	g N m^{-3}	0.03	Barber and Silberbush, 1984
$[\text{NO}_3^-_{i,n,j,l}]$	concentration of NO_3^- at microbial surfaces	g N m^{-3}		
$[\text{NO}_3^-_{mn}]$	concentration of NO_3^- at microbial surfaces below which $U_{\text{NO}_3} = 0$	g N m^{-3}	0.03	
$[\text{H}_2\text{PO}_4^-_{i,n,j,l}]$	concentration of H_2PO_4^- at microbial surfaces	g N m^{-3}		
$[\text{H}_2\text{PO}_4^-_{mn}]$	concentration of H_2PO_4^- at microbial surfaces below which $U_{\text{PO}_4} = 0$	g N m^{-3}	0.002	
O_c	$[\text{O}_2]$ in canopy chloroplasts in equilibrium with O_2 in atm.	μM		
Q_{rx}, Q_{ry}	surface water flow in x or y directions	$\text{m}^3 \text{m}^{-2} \text{h}^{-1}$		
Q_{wx}, Q_{wy}, Q_{wz}	subsurface water flow in x, y or z directions	$\text{m}^3 \text{m}^{-2} \text{h}^{-1}$		
$\mathcal{R}_{ai,r}$	axial resistivity to water transport along root or mycorrhizal axes	MPa h m^{-4}	4.0×10^9 deciduous 1.0×10^{10} coniferous	Larcher (2001)
$\mathcal{R}_{ai,r,l,x}$	axial resistance to water transport along axes of primary ($x = 1$) or secondary ($x = 2$) roots or mycorrhizae	MPa h m^{-1}		
$\mathcal{R}_{ri,r}$	radial resistivity to water transport from surface to axis of roots or mycorrhizae	MPa h m^{-2}	1.0×10^4	Doussan et al. (1998)
$\mathcal{R}_{ri,r,l}$	radial resistance to water transport from surface to axis of roots or mycorrhizae	MPa h m^{-1}		
$\mathcal{R}_{si,r,l}$	radial resistance to water transport from soil to surface of roots or mycorrhizae	MPa h m^{-1}		
θ_{wl}	soil water content	$\text{m}^3 \text{m}^{-3}$		
θ_{bl}	soil porosity	$\text{m}^3 \text{m}^{-3}$		
R	gas constant	$\text{J mol}^{-1} \text{K}^{-1}$	8.3143	
r_{bi}	radius of bole at ambient ψ_{ci}	m		
r'_{bi}	radius of bole at $\psi_{ci} = 0$ MPa	m		
r_{ci}	canopy stomatal resistance to vapor flux	s m^{-1}		
r_{cmaxi}	canopy cuticular resistance to vapor flux	s m^{-1}	5.0×10^3	Larcher (2001)
r_{cmini}	minimum r_{ci} at $\psi_{ci} = 0$ MPa	s m^{-1}		
$R_{gi,n,l}$	growth respiration of $M_{i,n,a,l}$ on $Q_{i,l,C}$ under nonlimiting O_2 and nutrients	$\text{g C g C}^{-1} \text{h}^{-1}$		

R_h	total heterotrophic respiration of all $M_{i,n,a,l}$ under ambient DOC, O ₂ , nutrients, θ and temperature	$\text{g C m}^{-2} \text{h}^{-1}$		
$R_{hi,n,l}$	heterotrophic respiration of $M_{i,n,a,l}$ under ambient DOC, O ₂ , nutrients, θ and temperature	$\text{g C m}^{-2} \text{h}^{-1}$		
$r_{i,r,l,x}$	radius of primary ($x=1$) or secondary ($x=2$) roots or mycorrhizae at ambient $\psi_{r_i l,z}$	m		
$r'_{i,r}$	radius of secondary roots or mycorrhizae at $\psi_{r_i l,z} = 0$ MPa	m	2.0 x 10 ⁻⁴ tree 1.0 x 10 ⁻⁴ bush 0.05 x 10 ⁻⁴ mycorrhizae	
$r_{i,j,k,l,m,n,o}$	leaf stomatal resistance	s m^{-1}		
r_{lmaxi}	leaf cuticular resistance	s m^{-1}		
$r_{lmini,j,k,l,m,n,o}$	leaf stomatal resistance when $\psi_{ci} = 0$	s m^{-1}		
R_m	specific maintenance respiration at 25°C	$\text{g C g N}^{-1} \text{h}^{-1}$	0.0115	Barnes et al. (1998)
$R_{mi,n,j,l}$	maintenance respiration by $M_{i,n,j,l}$	$\text{g C m}^{-2} \text{h}^{-1}$		
$r_{i,r,l}$	root or mycorrhizal radius	m	1.0 x 10 ⁻⁴ or 5.0 x 10 ⁻⁶	
S	change in entropy	$\text{J mol}^{-1} \text{K}^{-1}$	710	Sharpe and DeMichelle (1977)
σ_C	nonstructural C product of CO ₂ fixation	g C g C^{-1}		
σ_N	nonstructural N product of root uptake	g N g C^{-1}		
σ_P	nonstructural P product of root uptake	g P g C^{-1}		
T_c	canopy temperature	K		
T_{sl}	soil temperature	K		
$U_{\text{NH}_4i,n,j,l}$	NH ₄ ⁺ uptake by microbes	$\text{g N m}^{-2} \text{h}^{-1}$		
$U_{\text{NH}_4i,r,l}$	NH ₄ ⁺ uptake by roots or mycorrhizae	$\text{g N m}^{-2} \text{h}^{-1}$		
U'_{NH_4}	maximum U_{NH_4} at 25 °C and non-limiting NH ₄ ⁺	$\text{g N m}^{-2} \text{h}^{-1}$	5.0 x 10 ⁻³	Barber and Silberbush, 1984
$U_{\text{NO}_3i,r,l}$	NO ₃ ⁻ uptake by roots or mycorrhizae	$\text{g N m}^{-2} \text{h}^{-1}$		
$U_{\text{NO}_3i,n,j,l}$	NO ₃ ⁻ uptake by microbes	$\text{g N m}^{-2} \text{h}^{-1}$		
U'_{NO_3}	maximum U_{NO_3} at 25 °C and non-limiting NO ₃ ⁻	$\text{g N m}^{-2} \text{h}^{-1}$	5.0 x 10 ⁻³	Barber and Silberbush, 1984
$U_{\text{PO}_4i,r,l}$	H ₂ PO ₄ ⁻ uptake by roots or mycorrhizae	$\text{g N m}^{-2} \text{h}^{-1}$		
$U_{\text{PO}_4i,n,j,l}$	H ₂ PO ₄ ⁻ uptake by microbes	$\text{g N m}^{-2} \text{h}^{-1}$		
U'_{PO_4}	maximum U_{PO_4} at 25 °C and non-limiting H ₂ PO ₄ ⁻	$\text{g N m}^{-2} \text{h}^{-1}$	5.0 x 10 ⁻³	Barber and Silberbush, 1984
$U_{\text{O}_2i,r,l}$	O ₂ uptake by roots and mycorrhizae under ambient O ₂	$\text{g O m}^{-2} \text{h}^{-1}$		
$U'_{\text{O}_2i,l,r}$	O ₂ uptake by roots and mycorrhizae under nonlimiting O ₂	$\text{g O m}^{-2} \text{h}^{-1}$		

U_{wi}	total water uptake from all rooted soil layers	$m^3 m^{-2} h^{-1}$		
$U_{w_{i,r,l}}$	water uptake by root and mycorrhizal surfaces in each soil layer	$m^3 m^{-2} h^{-1}$		
V_b'	specific rubisco carboxylation at 25 °C	$\mu mol g^{-1} rubisco s^{-1}$	45	Farquhar et al. (1980)
$V_{b_{i,j,k,l,m,n,o}}$	CO ₂ -limited leaf carboxylation rate	$\mu mol m^{-2} s^{-1}$		
$V_{b_{max_{i,j,k}}}$	leaf carboxylation rate at non-limiting CO ₂ , ψ_{ci} , T_c and N,P	$\mu mol m^{-2} s^{-1}$		
$V_{c_{i,j,k,l,m,n,o}}$	leaf CO ₂ fixation rate	$\mu mol m^{-2} s^{-1}$		
$V_{c'_{i,j,k,l,m,n,o}}$	leaf CO ₂ fixation rate when $\psi_{ci} = 0$	$\mu mol m^{-2} s^{-1}$		
$V_{g_{i,j,k,l,m,n,o}}$	leaf CO ₂ diffusion rate	$\mu mol m^{-2} s^{-1}$		
V_j'	specific chlorophyll e^- transfer at 25 °C	$\mu mol g^{-1} chlorophyll s^{-1}$	450	Farquhar et al. (1980)
$V_{j_{i,j,k,l,m,n,o}}$	irradiance-limited leaf carboxylation rate	$\mu mol m^{-2} s^{-1}$		
V_o'	specific rubisco oxygenation at 25 °C	$\mu mol g^{-1} rubisco s^{-1}$	9.5	Farquhar et al. (1980)
$V_{o_{max_{i,j,k}}}$	leaf oxygenation rate at non-limiting O ₂ , ψ_{ci} , T_c and N,P	$\mu mol m^{-2} s^{-1}$		
v_x, v_y	velocity of surface flow in x or y directions	$m h^{-1}$		
X_{ci}	canopy capacitance	$m^3 m^{-2} MPa^{-1}$		
ψ_{ci}	canopy water potential	MPa		
$\psi_{c'i}$	ψ_{ci} + canopy gravitational potential	MPa		
$\psi_{\pi i}$	canopy osmotic potential	MPa		
$\psi_{s'l}$	ψ_{sl} + soil gravitational potential	MPa		
ψ_s	soil water potential	MPa		
ψ_{ti}	canopy turgor potential	MPa	1.25 at $\psi_c = 0$	
Y	carboxylation yield from electron transport in C ₃ mesophyll	$\mu mol CO_2 \mu mol e^{-1}$		
y	selected to give a Q_{10} for f_{tm} of 2.25		0.081	
Γ	CO ₂ compensation point in C ₃ mesophyll	μM		
α	shape parameter for response of J to I	-	0.7	
ϵ	quantum yield	$\mu mol e^- \mu mol quanta^{-1}$	0.45	Farquhar et al. (1980)
ψ_t	canopy turgor potential	MPa	1.25 at $\psi_c = 0$	
β	stomatal resistance shape parameter	MPa^{-1}	-5.0	Grant and Flanagan (2007)
z_{bi}	length of bole from soil surface to top of canopy	m		
z_l	depth of soil layer below surface	m		

Chapter 4

Carbon sources and sinks of North America as affected by major drought events during the past 30 years

4.1. Introduction

Current estimates of CO₂ exchange across North America (NA) have shown that on an annual time scale the continental biosphere has been long-term carbon sink (Huntzinger et al., 2012; King et al., 2007; Peters et al., 2007) that has partly offset fossil fuel emissions. King et al. (2007) estimated that the NA biosphere was a sink for 30% of the continental fossil fuel emissions of 1.85 Pg C yr⁻¹ in 2003. However, there have been spatial and temporal variability in carbon sources and sinks attributed to changes in climate (Baldocchi et al., 2001; Goulden et al., 1996), particularly during extreme climate events such as drought (Jentsch et al., 2007) and disturbances (Lindroth et al., 2009).

Studies have shown that areas affected by drought have increased in the last four decades (Dai et al., 2004). The frequency and intensity of drought occurrences have also increased (Huntington, 2006) and are projected to increase under future climate change scenarios (IPCC, 2013). Climate change such as warming and changes in precipitation over recent decades have been observed in most regions of NA and the past decade has included the warmest years within the instrumental record of global surface temperature (IPCC, 2007). Warming could increase specific humidity by increasing evaporation and consequently increase precipitation and accelerate the water cycle (Held and Soden, 2000; Huntington, 2006). Intensifying the water cycle may increase the intensity and frequency of floods and droughts (Huntington, 2006). As drought is a disturbance of the water cycle (van der Molen et al., 2011), it can have direct effects on ecosystem carbon cycling and may have carry-over effects (Reichstein et al., 2013) in subsequent years.

Drought directly affects net ecosystem productivity (NEP) through its effects on component fluxes ($NEP = \text{gross primary productivity (GPP)} - \text{ecosystem respiration (}R_e\text{)}$) (Gaumont-Guay et al., 2006), and contributes to most of the interannual variability in carbon exchange (Ciais et al., 2005; Jentsch et al., 2007; Pereira et al., 2007). These effects of drought on ecosystem productivity at continental scale can be assessed using indices (e.g. normalized difference vegetation index (NDVI), enhanced vegetation index (EVI)) derived from remote sensing products such as Moderate Resolution Imaging Spectroradiometer (MODIS), Advanced Very High Resolution Radiometer (AVHRR) and Landsat (Caccamo et al., 2011; Karnieli et al., 2010; Wan et al., 2004). However, these large scale satellite products have some limitations: their accuracy varies with land cover and soil types (Gu et al., 2008); they may be unable to detect short-term water stress in areas with deep-rooted trees that may sustain water availability (Caccamo et al., 2011); they do not estimate changes in NEP and they lack predictive capability under future climate. Drought can also be assessed using a top-down atmospheric inversion approach with atmospheric transport models (Knorr and Heimann, 1995; Peters et al., 2007) that estimate net ecosystem exchange (NEE) but do not provide estimates of the component fluxes. Although drought indices such as Palmer Drought Severity Index (PDSI) (Alley, 1984) and Standard Precipitation Index (SPI) (Hayes et al., 1999) can be used to examine drought status at continental scale, the actual amount of carbon fluxes cannot be assessed using these indices. Earlier efforts to model regional drought effects included different approaches that use statistical nonlinear regression models (Reichstein et al., 2003) and diagnostic models such as radiation-use efficiency models (Jamieson et al., 1995).

In a more comprehensive approach, here we used a mathematical process model, *ecosys* (Grant, 2001; 2011b; 2014) to simulate the effects of drought on carbon fluxes based on the

fundamental theory of how water moves through the soil-plant-atmosphere and how this movement affects GPP and R_e , explicitly formulated in the model (Grant et al., 2012; 2006a; Grant and Flanagan, 2007b-a). This water transfer scheme of the model was used to examine the underlying biophysical processes during drought and the subsequent effects of soil water deficit on NEP and component fluxes. Soil water deficit during drought reduces GPP by increasing soil hydraulic resistance that lowers canopy water potential (ψ_c) and stomatal conductance (g_c), hence a decline in CO₂ diffusion and carboxylation (Grant et al., 1999). Concurrently, a reduction in the supply of labile carbon due to a decline in GPP and less soil moisture availability for microbial activity causes a decline in R_e (van der Molen et al., 2011).

The skill of the model to capture impacts of climate variability and extreme climate events such as soil water stress on NEP at different time steps (hourly to decadal) has been shown to be generally high. The coupled schemes for soil-plant-atmosphere water transfer and CO₂ exchange of the model have been rigorously tested at site scale against EC-measured CO₂ and energy fluxes over a wide range of climates across different biomes: seasonally dry grassland in Mediterranean climate zones under 2001 - 2008 variable rainy seasons (Grant et al., 2012); semi-arid grassland in Lethbridge, Alberta under 2001 – 2003 drought vs. good rainfall (Grant and Flanagan, 2007b-a; Li et al., 2004), cropland in Nebraska with irrigated vs. rainfed maize-soybean rotation (Grant et al., 2007a); boreal aspen forest in Saskatchewan under the three years drought 2001 - 2003 (Grant et al., 2006a), temperate and boreal deciduous forests (Grant et al., 2006b). While these modeled impacts of drought on ecosystem productivity were captured well when tested at the various EC sites, the model responses of the carbon cycle to major drought events at continental scale in the last 30 years has not been assessed prior to this study. In this study, the long-term

(1980 – 2010) spatial and temporal trends in carbon sources and sinks as affected by these drought events across NA has been examined.

4.2. Methods

4.2.1. Model Description

A detailed description of inputs, parameters and algorithms used in *ecosys* can be found in Grant (2001, 2014) and Grant et al. (2011b, 2012). However, the general descriptions of the algorithms and parameters that are most relevant to modeling the impacts of soil water stress during drought on ecosystem productivity are given below and details of the equations used are given in Appendices A and B.

Effects of water stress on CO₂ fixation (GPP)

The soil-plant-atmosphere water transfer scheme is implemented by calculating ψ_c from a two-stage convergence solution. The first stage is the convergence to canopy temperature (T_c) at which the first-order closure of the canopy energy balance (net radiation R_n (Eq. B1a), latent heat flux LE (Eqs. B1b, c), sensible heat flux H (Eq. B1d), and change in heat storage G is achieved (Grant et al., 2011a). After convergence for T_c , canopy transpiration (E_c) is coupled with total water uptake from all rooted soil layers U (Grant et al., 1999), through a convergence solution for ψ_c at which E_c equals $U +$ change in plant water storage (Eq. B14). The U from the soil to the canopy is determined by the potential difference between ψ_c and soil water potential (ψ_s) across hydraulic resistances in soil Ω_s (Eq. B9) and roots Ω_r (Eqs. B10 – B12) in each rooted soil layer (Eq. B6) (Grant et al., 2007c). The E_c from the canopy to the atmosphere is governed by r_c which rises from a minimum value, r_{cmin} , aggregated by leaf surface area from r_{lmin} (Eq. B2a) at zero ψ_c through an exponential function of canopy turgor potential ψ_t (Eq. B2b) calculated from ψ_c and osmotic water potential ψ_π (Eq. B4). After convergence for T_c and ψ_c , CO₂ fixation V_c is calculated

under ambient ψ_c and r_c from stomatal and non-stomatal effects of canopy water status (Grant and Flanagan, 2007b-a), through the convergence solution for intercellular (C_i) and canopy (C_c) gaseous CO_2 concentration at which rates of diffusion and CO_2 fixation are equal as described in Grant and Flanagan (2007b). Soil drying during drought raises soil hydraulic resistance and lowers ψ_s , thereby lowering ψ_c required to keep U in equilibrium with E_c , inducing rises in canopy (r_c) and leaf (r_l) resistances (Grant et al., 1999) and hence a decline in CO_2 diffusion and carboxylation as demonstrated in Grant and Flanagan (2007).

Effect of water stress on heterotrophic respiration (R_h)

Decomposition rate of each organic matter-microbe complex (coarse woody litter, fine non-woody litter, manure, particulate organic matter and humus) represented in *ecosys* is determined by the active biomass M of heterotrophic microbial populations (Eq. A1) and the substrate concentration (Eq. A3) (Grant et al., 2006a). Decomposition rate is controlled by T_s through an Arrhenius function (Eq. A6) and by θ through its effect on aqueous microbial concentrations $[M]$ (Eq. A3). T_s and θ are calculated from surface energy and water exchanges coupled with soil heat and water transfers through atmosphere-canopy-snow-surface residue-soil profiles (Grant et al., 2012). Decomposition generates dissolved organic carbon (DOC) that drives microbial growth through R_h . Rate of R_h is also controlled by microbial N and P concentrations, DOC, T_s , O_2 , ψ_s . Total R_h drives CO_2 emission from soil through diffusion and volatilization in aqueous and gaseous phases (Grant et al., 2012). Lower θ from soil drying during drought raises $[M]$, slowing decomposition through a competitive inhibition effect, hence lowering DOC and reducing R_h and growth of M that further slows decomposition.

4.2.2. Model Drivers

Gridded datasets for climate, soil, land use/ land cover dynamics, CO₂ concentration, nitrogen deposition and disturbance across North America were used as inputs to drive *ecosys*. The climate dataset used in this study was the North American Regional Reanalysis (NARR) produced at the National Oceanic and Land Administration (NOAA) National Center for Environmental Prediction (NCEP) Global Reanalysis (Mesinger et al., 2004; Wei et al., 2014). NARR is an extension of NCEP, which is a combined data and model assimilation product that made use of a wide network of observational datasets across the continent (Mesinger et al., 2004). For this study, we used a NARR dataset which was resampled and reprojected to 0.25° x 0.25° spatial resolution in Geographic latitude/ longitude projection made available through the Multi-Scale Synthesis and Terrestrial Model Inter-comparison Project (MsTMIP) (Wei et al., 2014). This dataset extended from 1979 to 2010 with a temporal resolution of 3-hours, and was interpolated linearly to 1-hour for use in *ecosys*. The NARR climate variables used to drive *ecosys* were air temperature at 2m, total precipitation at surface, downward shortwave radiation flux at surface, relative humidity and wind speed.

The soil dataset used in this study was a Unified North America Soil Map (UNASM) which was a reanalysis product of MsTMIP for North America that was prepared using three different soil databases (Liu et al., 2013). The model was provided with attributes for each soil layer in the dataset, including layer depth, clay/sand fraction, pH, total organic carbon, cation exchange capacity and bulk density. Time-varying land use/land cover was modeled from a dataset for the years 1800 - 2010 developed by merging Hurtt historical land cover classification (Hurtt et al., 2006) and 2000/2003 SYNMAP land cover classification (Jung et al., 2006) products (Wei et al., 2014). The atmospheric CO₂ concentration used in the model from 1800 to 1979 was created from

GLOBEVIEW-CO₂. For the period before 1979 global CO₂ concentration was a reanalysis product of GLOBEVIEW-CO₂, Mauna Loa (MLO) and South Pole (SPO) annual mean concentrations as described in Wei et al. (2014). However, for years after 1979 the GLOBEVIEW data was directly used. The North America CO₂ concentration was resampled to 0.25° x 0.25° spatial resolution using linear average interpolation in MsTMIP (Wei et al., 2014). Annual nitrogen deposition used in the model for 1800 - 2010 was derived from Dentener's global atmospheric nitrogen deposition maps in the years of 1860, 1993 and 2050 (Dentener, 2006). The annual variation of nitrogen deposition rate from 1890 to 1990 was controlled by EDGAR-HYDE 1.3 (van Aardenne et al., 2001) nitrogen emission data (Wei et al., 2014). Nitrogen deposition was assumed to increase linearly over the remaining period up to the present (1990 - 2010).

Disturbance due to fire was introduced as external forcing in the model simulation. Four different data sources for Canada, US and Mexico were harmonized to create a continuous historical fire disturbance dataset. Canadian wildfire information system dataset was a product of the Canadian fire management agencies and provinces, territories and parks Canada and the data was available for 1959 – 1999. US Land Fire Product is a product from United States Geological Survey (USGS). The dataset indicates a historical fire regimes based on vegetation dynamics, fire spread and effects. The dataset contains mean fire return interval and a severity index in the average period between fires under the presumed historical fire regime. Another data source used was Global Fire Emission Database (GFED) which is a MODIS global product that combines satellite information on fire activity and vegetation productivity to estimate a burned area and fire emissions. The datasets have a monthly temporal resolution and are available from 1997 to 2012. NACP Forest Age Maps compiled from forest inventories, historical fire data, satellite data, and images from National Aeronautics and Space Administration, NASA's Landsat Ecosystem

Disturbance Adaptive Processing System (LEDAPS) project at 1km Resolution for Canada and the US were also applied to forested areas (Pan et al., 2011). The Canadian and US maps were produced from data available in 2004 and 2006 respectively. These different products of fire disturbance were not consistent in spatial and temporal resolutions and were in different data models (point and polygon vectors, and raster). Therefore, the products were all geo-rectified, resampled, interpolated and re-gridded to a $0.25^{\circ} \times 0.25^{\circ}$ spatial resolution to make it consistent with the projection and spatial resolution of the other model drivers used in this study. The carbon transformations and emissions during fire disturbance and the effect on NEP is explicitly modeled in *ecosys* (Grant et al., 2010; Wang et al., 2011).

4.2.3. Simulation Design

The simulation spatial domain covered the NA landmass with $0.25^{\circ} \times 0.25^{\circ}$ resolution consisting of 51,061 independently simulated grid cells. Model runs for each grid cell were prepared with time-varying drivers for a simulation period of 1800 - 2010. To represent historical weather, NARR data from 1979 - 1993 were randomly distributed to form a 100 years sequence that cycled through 1800 - 1978. This enabled the model to attain a steady state prior to 1979. Then the real time NARR data were used for the rest of the period (1979 - 2010) to simulate real time ecosystem productivity as described in MsTMIP protocol (Huntzinger et al., 2013). The model was initialized with attributes from the UNASM soil dataset, and run under dynamic land use/ land cover changes, atmospheric CO₂ concentrations, nitrogen deposition and disturbances.

4.2.4. Model Testing

4.2.4.1. Site Scale

Fluxes measured at eddy covariance (EC) towers offer the best constrained test of modeled drought effects, although this can only be conducted at a site scale. Thus, the effects of water stress

on CO₂ and energy exchanges during drought were tested by comparing hourly-averaged fluxes of CO₂, latent heat (LE) and sensible heat (H) measured at an EC flux tower site during a drought (2001) vs. non-drought (2002) year at a mixed grass prairie in Lethbridge (CA-Let) with those extracted from the corresponding pixel in the NA run in which the CA-Let EC tower was located. Differences in NARR vs. measured annual precipitation of 194 vs. 216 mm during 2001 and 492 vs. 582 mm during 2002 allowed the comparison of effects of water stress on carbon exchange at CA-Let. Besides, 2000 was also dry with lower NARR vs. measured precipitation of 207 vs. 275 mm resulting in carry-over effects to the drought in 2001.

4.2.4.2. Continental Scale

Although direct measurements of carbon fluxes are not available at continental scale, remote sensing products such as MODIS GPP and AVHRR NDVI can be used to test modeled drought effects. Thus, modeled GPP was compared with MODIS GPP for 2002 (drought year) vs. 2005 (non-drought year). We could not compare the GPP for 1988 as MODIS product was not available for that year. Changes in spatial patterns of LAI during drought years 1988 and 2002 from long-term averages were compared with those in NDVI from AVHRR. LAI in *ecosys* is fully prognostic and so represents drought effects on leaf expansion and primary productivity. The declines in modeled LAI could be correlated to a similar reduction in NDVI through its effect on the fraction of absorbed photosynthetically active radiation (fAPAR). Satellite fAPAR products are derived from surface reflectances that indicate canopy energy absorption capacity (Myneni et al., 2002) thus affected by LAI, while NDVI values are strongly correlated to fAPAR in which increasing NDVI values indicate increasing vegetation density (Box et al., 1989; Carlson and Ripley, 1997). Geographically weighted regression (GWR) was used to test the relationships between changes in the spatial patterns of the modeled LAI and AVHRR NDVI. This regression

generated separate equations for every spatial cluster in the gridded datasets (e.g. modeled LAI vs. NDVI) as a method of analyzing spatially varying relationships. Modeled NEP was also compared with other estimates such as atmospheric inversion modeling from CarbonTracker.

4.2.5. Analysis of Data and Model Outputs

Drought indices derived from long-term precipitation data can be used to test the extent of precipitation deviations from the long-term normal prior to using the dataset to model the effects of drought on carbon fluxes. Thus, standardized precipitation index (SPI) was used to assess drought conditions, independent of the model, based on the long-term (1979 - 2010) precipitation data from NARR. SPI was computed at monthly time scale and the growing season (June, July and August) SPI was used to corroborate the model responses during drought. SPI measured drought status based on a probability index calculated from monthly precipitation aggregated from NARR data for a particular time scale (moving average for 3, 6, 12 etc. months), by fitting to a Gamma function to determine relationship between probability and precipitation and then transforming to normal distribution (McKee et al., 1993). Mean values were set to zero and negative values indicate dry periods (< -2, extremely dry; -1 to -1.99, moderate to severely dry; 0.99 to -0.99, near normal) whereas positive values represented wet periods (> 2, extremely wet; 1 to 1.99, moderate to very wet).

To examine the effects of drought on continental scale land-atmosphere carbon exchange, hourly modeled GPP, R_e and NEP for the years 1980 - 2010 were aggregated to annual totals for each grid cell to create continuous gridded data across NA for each year of the study. Annual outputs of modeled mid-August LAI were extracted from each grid cell across NA. To analyze the long-term (1980 – 2010) temporal trends of carbon fluxes for NA the spatially averaged values were computed considering area of grid cells as a weighting factor. The spatial pattern of

reductions in modeled annual GPP and mid-August LAI, and mid-August NDVI from AHVRR caused by droughts in 1988 and 2002 were computed by subtracting gridded long-term values from those for the drought years. Spatial patterns of interannual variability in NARR precipitation, modeled mid-August LAI and NDVI, as affected by drought, were assessed using relative standard deviation ($RSD = (SD / \text{absolute value of long-term mean}) \times 100$).

4.3. Results

4.3.1. Model Testing

4.3.1.1. Site Scale

Both modeled and EC CO₂ and energy fluxes were strongly affected by water stress during drought vs. non-drought years at the CA-Let site (Fig. 4-1). Both the measured and modeled hourly fluxes for selected summer days (days 178 – 188) under NARR weather, indicated greater declines in LE effluxes (Fig. 4-1c1) and CO₂ influxes (Fig. 4-1d1) in drier year of 2001 than in wetter 2002 (Fig. 4-1 (c2, d2)). Smaller declines in CO₂ effluxes than in influxes were modeled in 2001 compared to 2002, causing sharp declines in NEP that changed the grassland from a sink to a source of carbon during drought. These greater declines were due in the model to soil drying, which forced greater midafternoon declines in ψ_c , and g_c (Fig. 4-1a1) to balance U with E_c and consequently lower LE effluxes as described in Section 4.2.1. Lower g_c induced a decline in rate of CO₂ diffusion, hence lower CO₂ fixation in 2001 compared to 2002 (Fig. 4-1a1). These key modeled responses of net CO₂ exchange under contrasting weather in 2001 and 2002 were well captured at CA-Let. In 2001 modeled GPP and NEP declined by 73% and 95% respectively compared to 2002, resulting in a much smaller sink during the 2001 drought year (Table 4-1). These results indicate a realistic response of modeled GPP and NEP to interannual variability in precipitation (Section 4.2.4.1). Modeled mid-August LAI was 70% lower in 2001 than in 2002.

The modeled result was corroborated with the 69%, 94% and 89% declines in EC-derived annual GPP, NEP and mid-August LAI respectively in 2001 compared to 2002 (Table 4-1).

Uncertainty associated with gridded model drivers such as NARR and UNASM could have affected the accuracy of the model. For instance, incoming shortwave radiation from NARR was underestimated in both 2001 and 2002 (Fig. 4-1 (b1, b2)), resulting in lower H and LE (Fig. 4-1 (c1, c2)). This underestimation of radiation was noted in a detailed analysis of uncertainties in the model estimates associated with model drivers such as NARR and UNASM for six EC sites was assessed in an earlier study (Chapter 2) indicating that NEP modeled with these gridded inputs had less accurate diurnal and seasonal patterns than NEP modeled with inputs from site measurements for some sites, when tested against NEP derived from EC flux measurements.

4.3.1.2. Continental Scale

A reduction in modeled annual GPP demonstrated during 2001 drought at CA-Let site (Table 4-1) was similarly shown at continental scale, in which spatial patterns of reductions in modeled annual GPP were shown in regions affected by the 2002 drought across NA (Fig. 3-6a of Chapter 3). The spatial patterns indicated smaller modeled GPP in 2002 for most parts of the southwest and the Great Plains (excluding the Lethbridge region where the drought was ended in 2002 by rainfall), attributed to the drought compared to a normal year in 2005 (Fig. 3-6b) in which relatively higher annual GPP was modeled. The spatial patterns of reductions in modeled GPP in the drought affected regions were corroborated by the similar patterns of reduced MODIS GPP in 2002 vs. 2005 (Fig. 3-6c vs. 3-6d), with GWR for modeled vs. MODIS GPP $R^2 = 0.85$ for 2002 and 0.86 for 2005.

4.3.2. Major Drought Events and Their Impacts on Productivity

4.3.2.1. Regional Impacts on GPP and LAI

Spatial patterns of SPI for NA in June, July and August of 1988 and 2002 indicated declines of precipitation from long-term (1979-2010) monthly normals, well captured by NARR, in regions affected by two of the major drought events of NA in recent decades (Fig. 4-2). Growing season SPI values for most parts of the Great Plains and Midwest were extremely low ($SPI < -2$) indicating severely dry condition in 1988 compared to the long-term normal (Fig. 4-2 (a1, a2, a3)). Similarly, in 2002 SPI remained low ($SPI < -2$) for most parts of the southwest and the great plains, demonstrating a drought condition more pronounced in this region than in the rest of NA (Fig. 4-2 (b1, b2, b3)).

The spatial patterns of declines in the growing season SPI (Fig. 4-2) had patterns similar to reductions in annual modeled GPP from the long-term normal in 1988 (Fig. 4-3a) and 2002 (Fig. 4-3b). Reductions in modeled mid-August LAI from the long-term mean, driven by lower GPP which reduced carbon allocation to foliage and hastened senescence, and by reduced ψ_t which slowed leaf expansion, were shown in the drought affected regions compared to regions that were not affected by the drought (Fig. 4-4 (a1, a2)). The spatial patterns of these reductions in modeled LAI was corroborated by similar patterns of reductions in mid-August AVHRR NDVI of the corresponding years (Fig. 4-4a1 vs. 4-4b1; 4-4a2 vs. 4-4b2) resulting in a good agreement and close similarity in spatial patterns (GWR $R^2 = 0.84$ for 1988 and 0.71 for 2002), and demonstrating the skill of the model to capture drought effects on continental plant growth. In 1988 declines in LAI and NDVI were observed mainly in the southeast US and Great plains (Fig. 4-4 (a1, b1)). Similar declines were observed in 2002 (Fig. 4-4 (a2, b2)) in the west and southwest US, the Great Plains including parts of Alberta (excluding Lethbridge), Manitoba and Saskatchewan.

4.3.2.2. Continental Impacts on NEP

The impacts of these major drought events on modeled carbon exchange, at continental scale, were apparent from anomalies of spatially averaged GPP, net ecosystem productivity ($NPP = GPP - \text{autotrophic respiration } (R_a)$), R_h and NEP from the long-term means (equals zero) with more negative values in 1988 and 2002 (Fig. 4-5 (a1 - d1)). The spatial average of the entire continent annual GPP in the model declined by 4.9% and 5.9% from the long-term mean in 1988 and 2002 respectively (Table 4-2). The drought in 1988 caused NPP to decline to 0.46 Pg C below the long-term annual average NPP (Fig. 4-5c1) for NA demonstrating a substantial loss in productivity. Similarly, the drought in 2002 caused annual NPP to decline to 0.63 Pg C below the long-term average. The decline in R_e was less than that in GPP (1.5% in 1988 and 2.7% in 2002), indicating that carbon fixation and assimilation was more adversely affected by drought than was respiration. Consequently, NEP declined by 0.50 Pg C (92%) in 1988 and by 0.49 Pg C (90%) in 2002 from the long-term mean resulting in much smaller carbon sinks of $+0.04 \text{ Pg C yr}^{-1}$ and $+0.05 \text{ Pg C yr}^{-1}$ in 1988 and 2002 respectively (Table 4-2), similar to the modeled effects of drought on NEP demonstrated at site scale (Fig. 4-1; Table 4-1) and corroborated by EC-derived NEP as described in Section 4.3.1.1. Although significant effects of drought on the carbon balance were apparent at continental scale, there were spatial variations in the carbon sources and sinks along a latitudinal gradient particularly in 2002, in which regions north of 45° N had greater declines in spatially averaged annual GPP (6.5%) than R_e (2.3%) resulting in a $-0.02 \text{ Pg C yr}^{-1}$ net source compared to parts of the continent south of 45° N with $+0.074 \text{ Pg C yr}^{-1}$ net carbon sink (Table 4-2). Overall, spatially averaged annual GPP and R_e declined in all the three spatial domains (NA, NA region north of 45° N and south of 45° N) during the drought years (Table 4-2).

4.3.3. Interannual Variability in Precipitation and Productivity 1980 – 2010

Much of the long-term interannual variability in modeled mid-August LAI was controlled by variations in climate variables, mainly precipitation as shown by similarities in spatial patterns of the RSD (Fig. 4-6 (a, b)). The RSDs of LAI and precipitation were shown to vary spatially across the continent (Fig. 4-6 (a, b)). Parts of the Great Plains, southwest US and northern Mexico were shown to have larger RSD for both modeled LAI and NARR precipitation, indicating that this sub-region of the continent had greater interannual variability in productivity controlled by the interannual variability in precipitation (Fig. 4-6a). This modeled result was corroborated by the higher interannual variability apparent in the mid-August NDVI from AVHRR (Fig. 4-6c). Spatially averaged SPI values for this sub-region of NA became increasingly negative from shorter time scale (1 month) to longer time scale (24 months) during 1988 and 2002, indicating longer, more severe drought conditions during those years (Fig. 4-7 (a1 - d1)). The impacts of these droughts were shown to cause a decline in spatially averaged productivity modeled during the drought years, shown by the lowest GPP, NPP and R_h over the last three decades (Fig. 4-7 (b2, c2, d2)). Consequently, NEP values were lower than the long-term mean such that ecosystems in these regions lost more carbon during those drought years (Fig. 4-7a2).

4.3.4. North American Terrestrial Carbon Budget

4.3.4.1. Sources and Sinks

Continental scale long-term annually averaged GPP, R_e and NEP in the model exhibited large spatial variability (Fig. 4-8). The southeast and Pacific northwest coasts, the Midwest and southern Mexico had higher average annual GPP and NEP (Fig. 4-8 (a, c)) and these regions were dominated by forests and croplands. The south and the southwest US and northern Mexico had lower modeled GPP and NEP due to less vegetation cover as a result of drier climates. Higher

latitude regions had lower productivity as a result of cooler climates with shorter growing seasons. Modeled R_e (Fig. 4-8b) generally varied with GPP (Fig. 4-8a) because GPP drove biomass growth and hence R_a , and NPP that drove litterfall and hence R_h .

Regional differences in GPP vs. R_e caused most boreal, eastern temperate and Pacific northwest ecosystems to be modeled as carbon sinks, apparent in higher NEP, except for localized areas with recent fire which were modeled as carbon sources following the disturbances (Fig. 4-8c). Moreover, some parts of Mediterranean California, southwest US, northern Mexico and parts of western coastlines of Alaska were also modeled as carbon sources. Overall the entire NA continent was modeled as a carbon sink over the last three decades (Table 4-3). We estimated an average annual (2000 - 2005) GPP of 14.4 Pg C yr⁻¹ for NA (Table 4-3). Ecosystem respiration was estimated 13.8 Pg C yr⁻¹ resulting in 0.6 Pg C yr⁻¹ NEP. The carbon emission as a result of fire disturbance resulted in net biome productivity (NBP = GPP - R_e - emission from disturbance) of 0.54. (Table 4-3; Fig. 4-8c). Average annual (2000 - 2005) fossil fuel carbon emission of NA was 1.8 Pg C yr⁻¹ resulting in net emission of 1.26 Pg C yr⁻¹ (Table 4-3), offsetting ~30% of the fossil fuel emissions of NA, excluding the net amount of carbon taken up by water bodies within the spatial domain of NA landmass which we have not accounted for, as our simulation domain was the terrestrial biosphere. However only 0.03 and 3.2 % were offset by the terrestrial biosphere in 1988 and 2002 respectively, leaving almost all fossil fuel emissions to the atmosphere. Although the NA biosphere was modeled as a long-term sink, the significant drops in NEP during the drought years (1988 and 2002) offset 28% of the long-term carbon gains from the long-term mean over the last three decades.

4.3.4.2. Long-term Trends

Despite overall increases in long-term spatially averaged trends of NA modeled GPP (+0.12 Pg C decade⁻¹), NPP (+0.02 Pg C decade⁻¹) and NEP (+0.09 Pg C decade⁻¹) in recent decades (Fig. 4-5 (a1 - d1)), the impacts of the major droughts on these trends varied across regions. Although NEP dropped during droughts in 1988 and 2002 (Fig. 4-5a2), the northern ecosystems (north of 45° N) were stronger sinks with an average increase in NEP of +0.13 Pg C decade⁻¹ as a result of greater GPP (0.52 Pg C decade⁻¹) with longer growing season (Fig. 4-5a2). In regions south of 45° N NEP increased by 0.04 Pg C decade⁻¹ (Fig. 4-5a3), but this increase was mainly attributed to a relatively greater decline in R_e (-0.48 Pg C decade⁻¹) than in GPP (-0.45 Pg C decade⁻¹) (Fig. 4-5d3), as a result of greater increases in GPP than R_e in the eastern forests. The greater decline in GPP than R_e in the drought-affected southwest US resulted in increasing sources (Fig. 4-8c), indicating that projected increases in dryness (IPCC, 2013) in these parts of NA could enhance net carbon release and reduce net carbon sink of the continent.

4.4. Discussion

4.4.1. Major Drought Events and Long-term Trends in Productivity

The soil-plant-atmosphere hydraulic scheme in *ecosys* described in Section 4.2.1, and demonstrated at CA-Let (Fig. 4-1) was shown to capture modeled drought effects at site scale (Fig. 4-1) shown by the decline in LE (Eqs. B1b, c) relative to H (Eq. B1d) causing the grassland to change from a strong sink (modeled vs. EC-derived NEP = 204 vs. 295 g C m⁻² yr⁻¹) in 2002 to a smaller sink (modeled vs. EC-derived NEP = 10 vs. 18 g C m⁻² yr⁻¹) during the 2001 drought of (Table 4-1). At continental scale, these processes were shown to reduce modeled GPP both in 1988 and 2002 which were mainly attributed to the water stress observed in NARR (SPI < -1) in the drought affected regions (Fig. 4-2). We also have modeled a concurrent reduction in R_e in both

drought years (Fig. 4-5) which was caused by a reduction in the supply of labile carbon from a decline in GPP (van der Molen et al., 2011) and less moisture availability for microbial activity hence a decline in R_h . However, a reduction in precipitation observed with negative SPI in eastern forests of NA (Fig. 4-2) during 2002 was not shown to decrease modeled GPP (Fig. 4-3) and LAI (Fig. 4-4), and this was corroborated with the NDVI (Fig. 4-4). These responses of eastern forests to lower SPI could be attributed to deep-rooted trees that sustained water availability and to higher precipitation compared to potential evapotranspiration.

Overall, the drought events increased net carbon releases to the atmosphere shown by the declines in modeled NEP (Table 4-2) and these were mainly attributed to the greater sensitivity to water stress of GPP than R_e . A study (Schwalm et al., 2010b) using a global network of EC towers reported that GPP was 50% more sensitive to drought than was R_e across a wide range of biomes. Therefore, a reduction in GPP could be larger than a reduction in R_e during drought, resulting in a decline in NEP and consequently changing ecosystems to net sources (Novick et al., 2004; van der Molen et al., 2011). Spatially averaged trends of modeled NEP for the drought affected sub-regions of NA (Fig. 4-7a2) indicated that the declines in NEP continued after the drought years of 1988 and 2002, demonstrating carry-over effects to the next year of the drought events and indicating that drought can still affect the ecosystem carbon dynamics after the initial declines in GPP and R_e . This effects could be mainly due to drought-related depletion in reservoirs of soil moisture and plant carbohydrates (van der Molen et al., 2011) that were not completely replenished after the drought events. Consequently complete recovery of NEP to the pre-drought values could take up to 2 years (Fig. 4-7a2) as found by (Arnone Iii et al., 2008).

Although the NA terrestrial biosphere was modeled to be a carbon sink over the last three decades (Table 4-2), the major drought events such as those in 1988 and 2002 (Fig. 4-5a1)

adversely affected the continental carbon exchange by reducing the sink hence controlling much of the interannual variability. The drought affected regions such as the southwest and the Great Plains and northern Mexico had high interannual variability of modeled mid-August LAI, NARR precipitation and NDVI (Fig. 4-6) that could be a result of frequent occurrences in El Niño–Southern Oscillation (ENSO). Herweijer et al. (2007) reported that spatial variability of major droughts events reconstructed from networks of tree-ring chronologies were similar to ENSO patterns mainly in the southwest of US with an opposite effect on the Pacific Northwest. Similarly, Ropelewski and Halpert (1986) reported that patterns of NA precipitation departures from the long-term normal were associated with ENSO events for western and southeastern US and northern Mexico, suggesting that ENSO events could mainly control the major drought events in those regions. IPCC AR4 (2007) climate model projections had also shown that southwest US, similar to the subtropical dry zones of the world, will dry and expand to the north due to increasing warming (Cook et al., 2010) and this expansion can have a significant impact on the ecosystem productivity and carbon budget of NA.

4.4.2. Spatial and Temporal Patterns of NA Carbon Budget

The Great Plains, northern, eastern and southeastern regions of NA have mainly been carbon sinks over the last three decades, except where stand-replacing disturbances occurred (Fig. 4-8c). These effects of disturbances on NEP are explicitly modeled in *ecosys* and tested against EC measurements as described in Grant et al. (2010) and Wang et al. (2011). Regions dominated by forests and croplands were stronger sinks compared to non-forested regions, whereas drier regions such as the southwest were mainly carbon sources (Fig. 4-8c). This modeled result was consistent with some of the results reported in the North America Carbon Program (NACP) regional interim synthesis model intercomparison (Huntzinger et al., 2012) in which the Midwest

and southeast US were simulated as carbon sinks by some models. Boreal regions of NA were mainly sinks for most of the models in this intercomparison, as modeled here (Fig. 4-8c). Our result indicated that on an annual scale central and northern Mexico were net carbon sources which was consistent with some other studies that reported Mexico as a net carbon source. This source was partly attributed to land use changes as a result of the ongoing deforestation in Mexico reported in Cairns et al. (2000) and Pacala et al. (2007). Our model results for the spatial distributions of the carbon sinks were also consistent with another report (Peters et al., 2007) that estimated sinks mainly in the deciduous forests and the east coast. Xiao et al. (2011) calculated sources and sinks of conterminous US by integrating NEE estimates of EC towers and MODIS products, and found that most of the sinks were dominated by evergreen and deciduous forests and savannas.

Previous studies that used several approaches to estimate land-atmosphere carbon exchange across NA have presented a wide range of annual estimates of ecosystem productivity. Huntzinger et al. (2013) estimated average annual (2000 - 2005) NEP for 19 terrestrial biospheric models, with averages of +0.4 Pg C yr⁻¹ for prognostic models and +0.9 Pg C yr⁻¹ for diagnostic models. Our NEP estimate of +0.6 Pg C yr⁻¹ was close to the average of the prognostic and diagnostic models (Table 4-3). Our continental modeled NBP of +0.54 Pg C yr⁻¹ was close to an estimate of +0.505 Pg C yr⁻¹ from the first North American State of the Carbon Cycle Report by King et al. (2007) for 2003, which was computed based on a wide range of carbon inventories. Our NBP was also close to one of +0.57 Pg C yr⁻¹ from a study (Schuh et al., 2010) in which top-down atmospheric inversion modeling method was used to estimate carbon sources and sinks from atmospheric CO₂ concentrations and atmospheric transport in 2004. In another study using CarbonTracker, Peters et al. (2007) estimated an annual average (2000 - 2005) carbon sink of

+0.65 Pg C yr⁻¹, however the latest estimates of CarbonTracker CT2013B resulted in net carbon sink of +0.44 Pg C yr⁻¹ (Table 4-3). The smaller modeled carbon sink in 2002 (+0.05 Pg C yr⁻¹) was corroborated with a similar estimate of +0.05 Pg C yr⁻¹ from CarbonTracker CT2013B, an estimated decline of 88% (0.37 Pg C yr⁻¹) from the long-term (2000 - 2010) mean (0.42 Pg C yr⁻¹). A 31% (0.17 Pg C yr⁻¹) decline in modeled NEP from the long-term mean during the drought in 2008 was also corroborated with a 43% (0.18 Pg C yr⁻¹) decline in carbon sink estimated from Carbon Tracker in 2008. In a more recent study, King et al. (2015) summarized estimates from atmospheric inversion, inventory-based and TBMs and stated that NA was a carbon sink with annual average for 2000 – 2009 ranging from 0.27 Pg C yr⁻¹ to 0.89 Pg C yr⁻¹, and with the mean +0.47 Pg C yr⁻¹. These NEP in the model were driven by an average GPP of 14.44 Pg C yr⁻¹, similar to one of 13.4 Pg C yr⁻¹ from the MODIS MOD17 product (2000 - 2005) , which was slightly lower than our estimate of (Table 4-3).

Although NA terrestrial ecosystems are estimated collectively to be a net carbon sink, fossil fuel emissions are a much greater source of carbon to the atmosphere. Fossil fuel emissions in NA have been increasing at a rate of 0.017 Pg C yr⁻¹ which is greater than that of the modeled terrestrial sink in NA over the last three decades (0.009 Pg C yr⁻¹) (Fig. 4-9). This greater rate causes a net increase of 0.008 Pg C yr⁻¹ in net emissions without considering the carbon that could be taken up by the water bodies within the NA spatial domain. On an annual basis, only about half of the emission from fossil fuel and land cover change resides in the atmosphere and the rest is taken up by the oceans and terrestrial biospheres (Baker et al., 2006; IPCC, 2007). Our modeling result indicated that on average 30% of the total fossil fuel emission was taken up by the terrestrial biosphere of NA in 2000 – 2005 (0.54/1.8 Pg C yr⁻¹ in Table 4-3). This result agreed with King et

al. (2007) who estimated that 30% of the NA fossil fuel emission was offset by sink of the terrestrial biosphere in 2003.

4.5. Conclusions

We observed a significant decline in modeled GPP, R_e and NEP associated with major drought events in 1988 and 2002 in much of NA, particularly in the Great Plains, western and southwest of US. The frequent occurrences of drought in this part of the continent could be associated with patterns of ENSO and increases in global warming. The long-term annual average NEP have shown that most parts of the northern ecosystems and east and southeast US and the Midwest have been strong carbon sinks and these regions are mostly dominated by forest ecosystems and croplands. Some parts of Mediterranean California, NA deserts, northern Mexico and parts of western coastlines of Alaska were shown to be carbon sources. However, at continental scale, NA was shown to be a carbon sink, although interannual variability was mainly associated with climate extremes such as drought. Although NA remained a smaller carbon sink during the major drought years in 1988 and 2002, the significant drops in NEP offset 28% of the long-term carbon gains from the long-term mean over the last three decades, indicating that projected increases in the frequency of drought events under future climate change scenarios could turn ecosystems to carbon sources and may elevate the atmospheric CO₂ concentration. In this regard, understanding of the processes that control drought to better predict future impacts is crucial and process based ecosystem models can be coupled with climate models to develop early warning systems of drought occurrences that can support decision making.

List of Tables

Table 4-1. Annual precipitation and modeled vs. EC-derived carbon fluxes of mixed grass prairie EC flux tower site in Lethbridge (CA-Let) during the 2001 (drought) vs. 2002 (non-drought) year

Variables	2001		2002		% of change *	
	modeled	EC-derived	modeled	EC-derived	modeled	EC-derived
Annual precipitation (mm)	194	216	492	582	-61	-63
GPP (g C m ⁻² yr ⁻¹)	212	258	793	822	-73	-69
R _e (g C m ⁻² yr ⁻¹)	202	240	589	527	-65	-54
NEP (g C m ⁻² yr ⁻¹)	10	18	204	295	-95	-94
Mid-August LAI (m ² m ⁻²)	0.4	0.13	1.34	1.24	-70	-89

*the % of change in the drought year (2001) compared to 2002: $((2002 - 2001)/2002) \times 100$

Table 4-2. Changes in spatially averaged ecosystem carbon fluxes for different sub-regions of North America modeled in 1988 and 2002

Drought year	Flux component ^a	Annual total flux			Long-term annual average (1980 – 2010)			Flux change ^e			% change ^f		
		NA ^b	>45°N ^c	<45°N ^d	NA	>45°N	<45°N	NA	>45°N	<45°N	NA	>45°N	<45°N
1988	GPP	13.74	5.14	8.60	14.45	5.54	8.91	-0.71	-0.40	-0.31	-4.9	-7.2	-3.5
	NPP	5.88	2.49	3.39	6.34	2.73	3.61	-0.46	-0.24	-0.22	-7.3	-8.8	-6.1
	R _e	13.70	5.12	8.57	13.91	5.32	8.59	-0.21	-0.20	-0.02	-1.5	-3.8	-0.2
	NEP	0.04	0.014	0.026	0.54	0.23	0.31	-0.50	-0.22	-0.28	-92.6	-93.9	-91.6
2002	GPP	13.60	5.18	8.41	14.45	5.54	8.91	-0.85	-0.36	-0.50	-5.9	-6.5	-5.6
	NPP	5.71	2.46	3.25	6.34	2.73	3.61	-0.63	-0.27	-0.36	-9.9	-9.9	-10.0
	R _e	13.54	5.20	8.34	13.91	5.32	8.59	-0.37	-0.12	-0.25	-2.7	-2.3	-2.9
	NEP	0.05*	-0.02	0.074	0.54	0.23	0.31	-0.49	-0.25	-0.24	-90.7	-108.7	-76.1

^a annual total fluxes in Pg C yr⁻¹

^b spatial domain of terrestrial region of North America

^c spatial domain of terrestrial region of North America north of 45°N

^d spatial domain of terrestrial region of North America south of 45°N

^e changes in drought year flux from the long-term year(annual flux – long-term mean)

^f percentage of change in drought year flux from the long-term mean ((annual flux - long-term mean)/long-term mean)*100

*Equals CarbonTracker CT2013B estimate for 2002 = +0.05 Pg C yr⁻¹ and 2008 = +0.18 Pg C yr⁻¹

(<http://www.esrl.noaa.gov/gmd/ccgg/carbontracker>, accessed March, 10, 2015)

Table 4-3. Comparison of carbon budget estimates of different models for NA

Estimates	Time	GPP	NPP	Ra	Rh	NEP	NBP	Net emission ^f
ecosys	2000-2005	14.4	6.3	8.1	5.7	0.6	0.54	1.26
NACP ^a	2000-2005	12.2-32.9			5.6-13.2	-0.7-(+1.7) ^g		
MODIS ^b	2000-2005	13.4						
CarbonTracker ^c	2000-2005						0.65/ 0.44*	
CO ₂ Inversion ^d	2004						0.57	
SOCCR ^e	2003						0.51	1.35

^a North American Carbon Program regional interim synthesis:(Huntzinger et al., 2012): mean NEP of +0.4 Pg C yr⁻¹ for prognostic models and +0.9 Pg C yr⁻¹ for diagnostic models

^b Moderate Resolution Imaging Spectroradiometer MOD17 product:(Heinsch et al., 2006a):
<http://modis.gsfc.nasa.gov/>

^c CarbonTracker is a CO₂ measurement and modeling system: Net ecosystem exchange (NEE) = 0.65 Pg C yr⁻¹ (Peters et al., 2007)

^d Carbon flux inversion: (Schuh et al., 2010)

^e The first state of the carbon cycle report: (King et al., 2007)

^f Net emission (fossil fuel emission (1.8 Pg C (Boden et al., 2013)) – Net biome productivity (NBP))

^g Mean NEP of +0.4 Pg C yr⁻¹ for prognostic models and +0.9 Pg C yr⁻¹ for diagnostic models

* Latest CarbonTracker CT2013B estimate = 0.44 Pg C yr⁻¹ (<http://www.esrl.noaa.gov/gmd/ccgg/carbontracker/>)

List of Figures

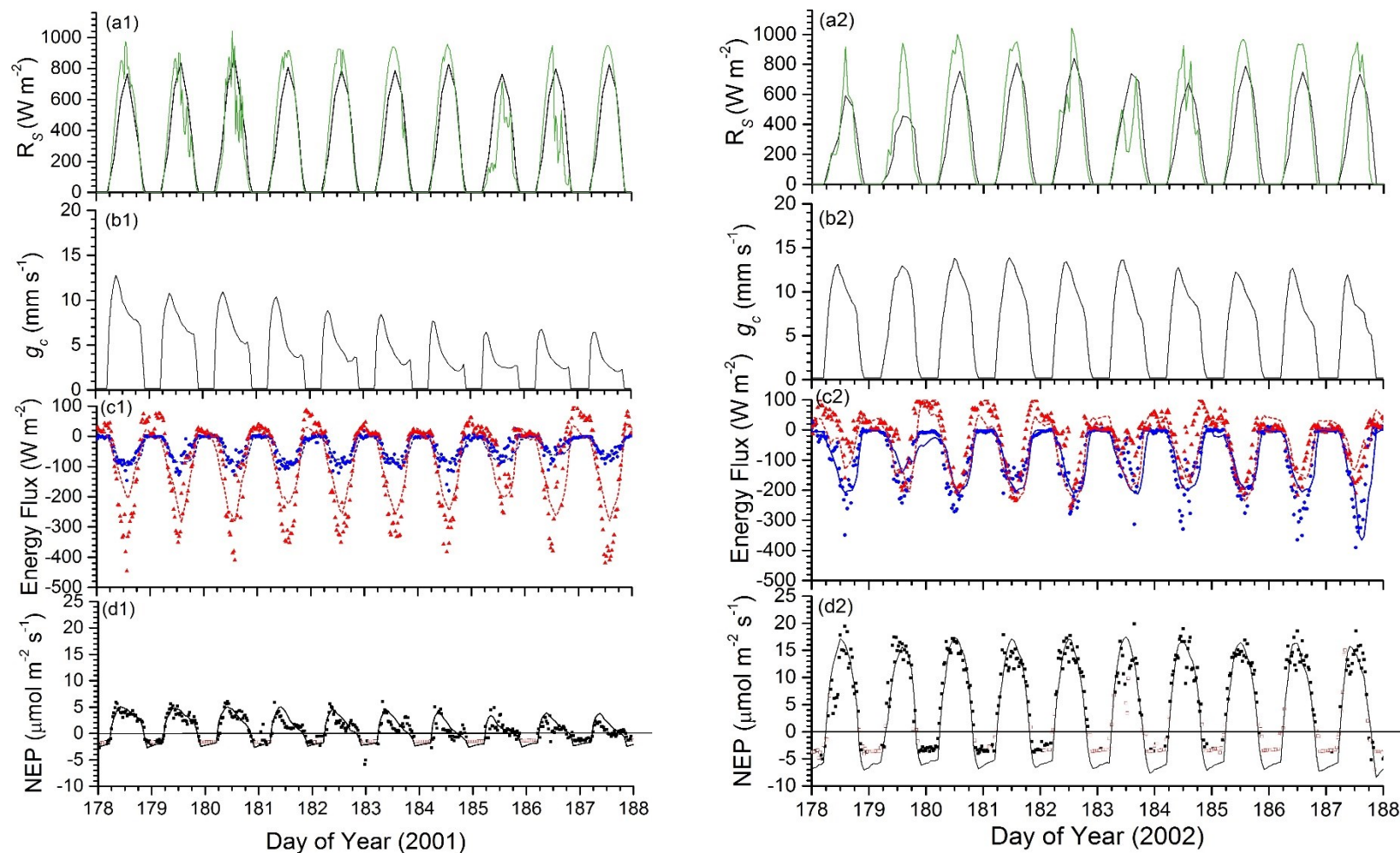


Figure 4-1. Mixed grass prairie in Lethbridge (CA-Let): comparison of hourly (a1, a2) incoming short wave radiation (R_s) from EC-measured (black) and NARR (green) and (b1, b2) canopy conductance (g_c), (c1, c2) energy fluxes (latent heat fluxes (blue), sensible heat fluxes (red)) and (d1, d2) CO₂ fluxes (modeled (black line), measured at EC (black closed dots), gap-filled from EC measurements (red open dots)) for drought year 2001(a1 – d1) vs. non-drought year 2002 (a2 – d2); +ve = influx, -ve = efflux. Measured fluxes source:(Flanagan and Adkinson, 2011)

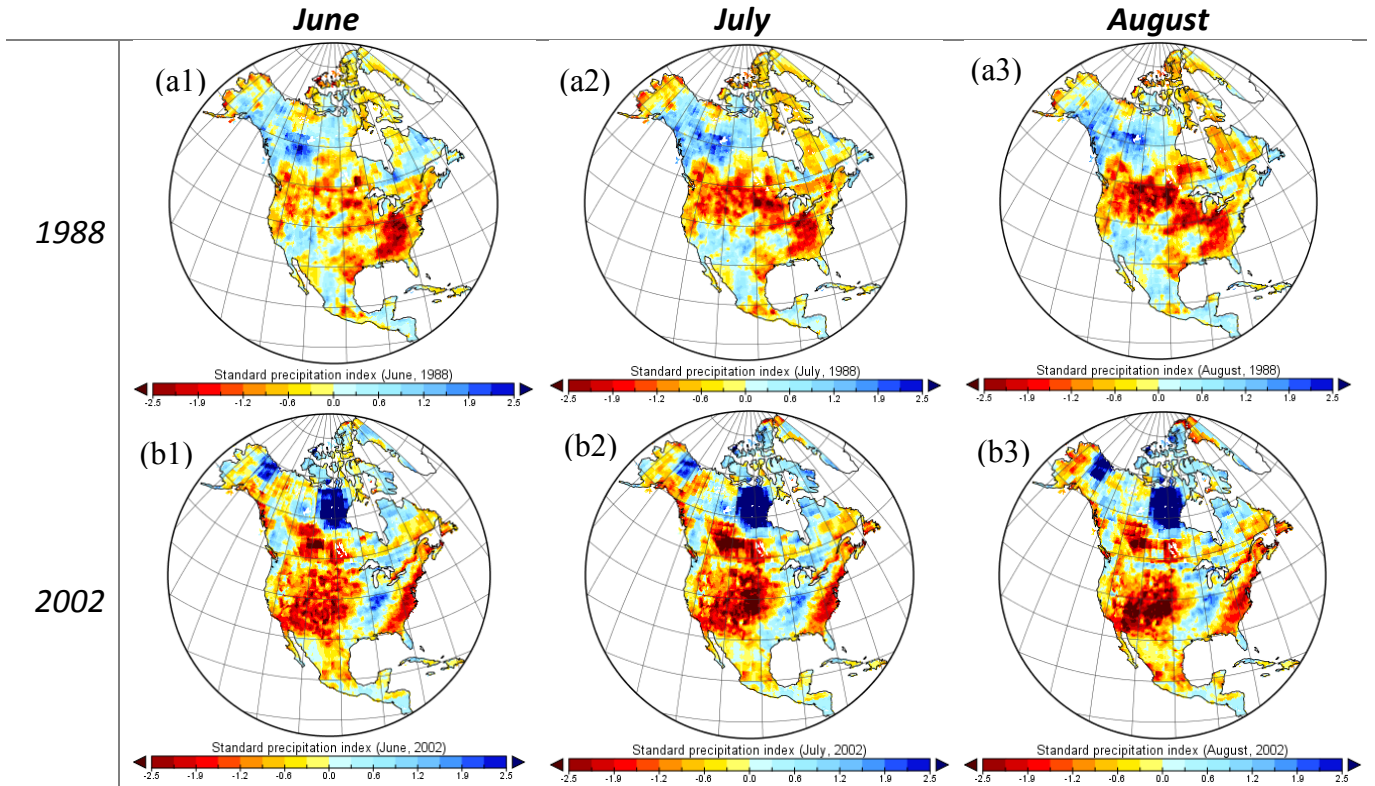


Figure 4-2. Spatial patterns in standard precipitation index (SPI) for June, July and August during major drought events (1988 and 2002) of North America: precipitation data range to calculate SPI 1979 – 2010

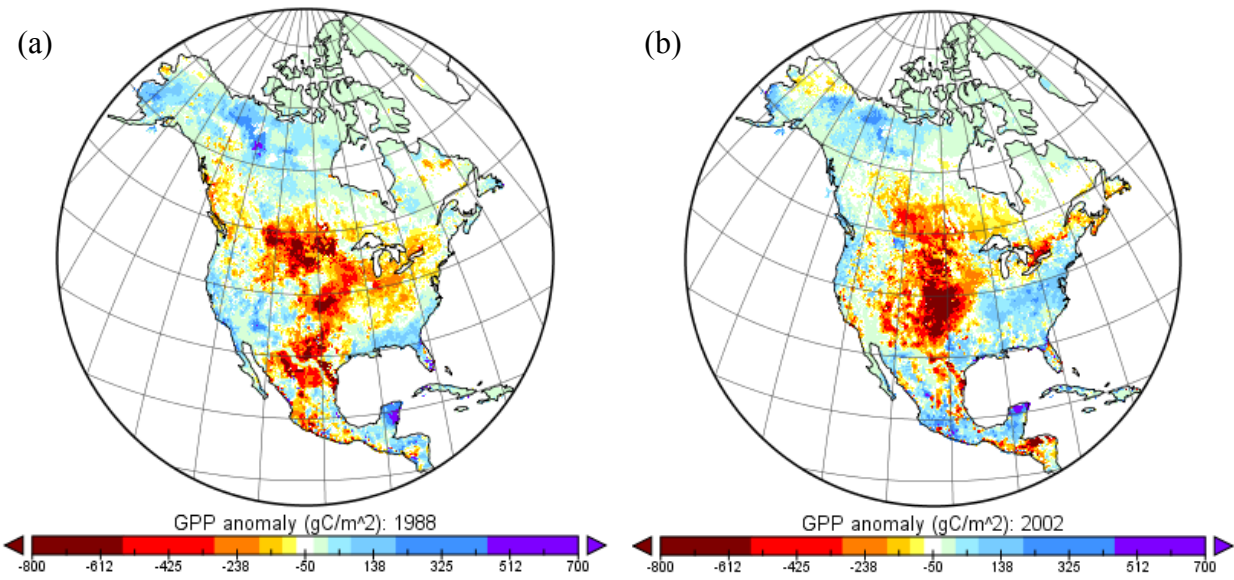


Figure 4-3. Spatial changes in modeled annual GPP: values obtained by subtracting the long-term (1980 – 2010) annual average GPP from annual GPP during the drought years (1988, 2002)

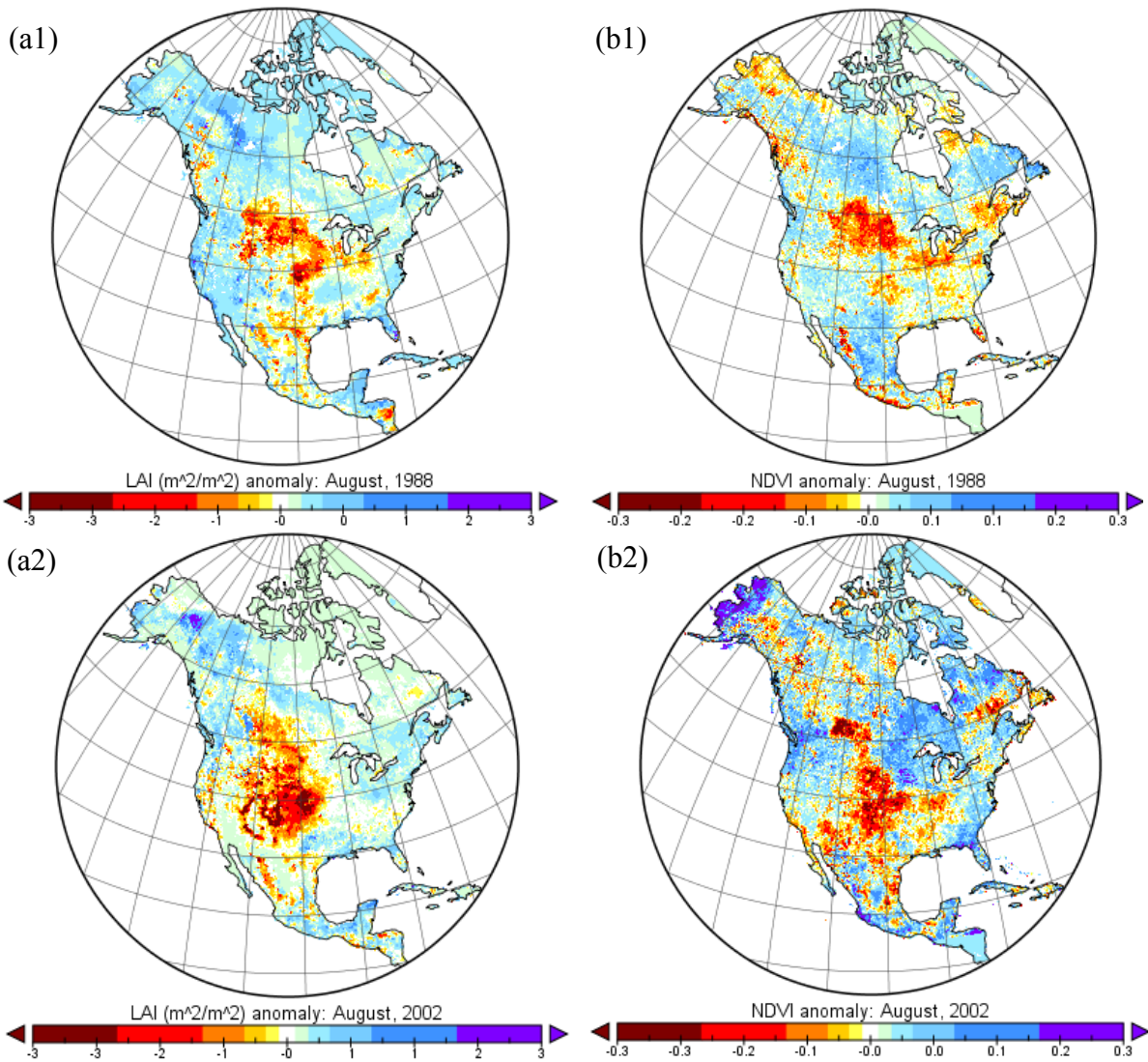


Figure 4-4. Spatial anomalies in modeled mid-August LAI vs. AHVRR NDVI from their long-term means (equals zero) for the major drought years (1988, 2002) in North America: GWR $R^2 = 0.84$ for 1988 and 0.71 for 2002

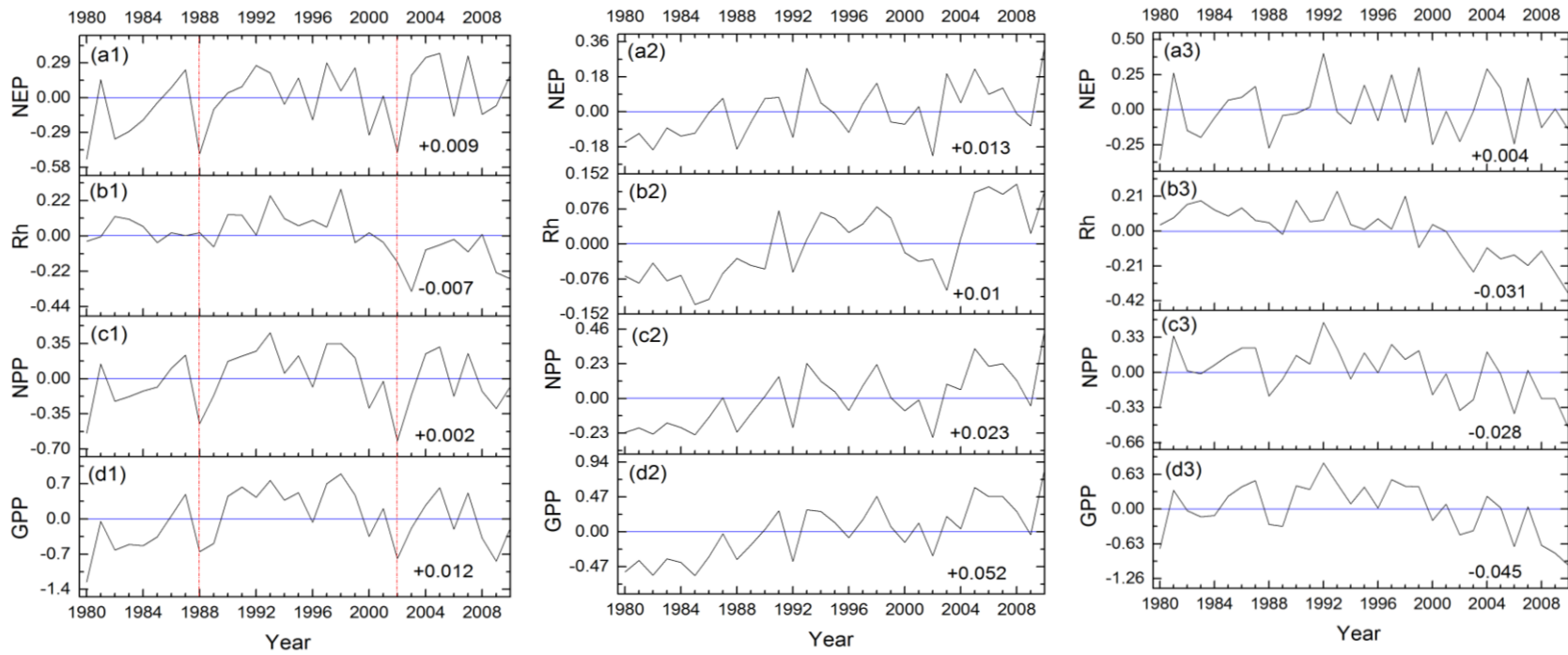


Figure 4-5. Long-term anomalies and trends in spatially averaged GPP, NPP, R_h and NEP (Pg C yr^{-1}) from the long-term mean (equals zero) across different sub-regions of North America: (a1 - d1) North America (a2 - d2) above 45°N (a3 - d3) below 45°N

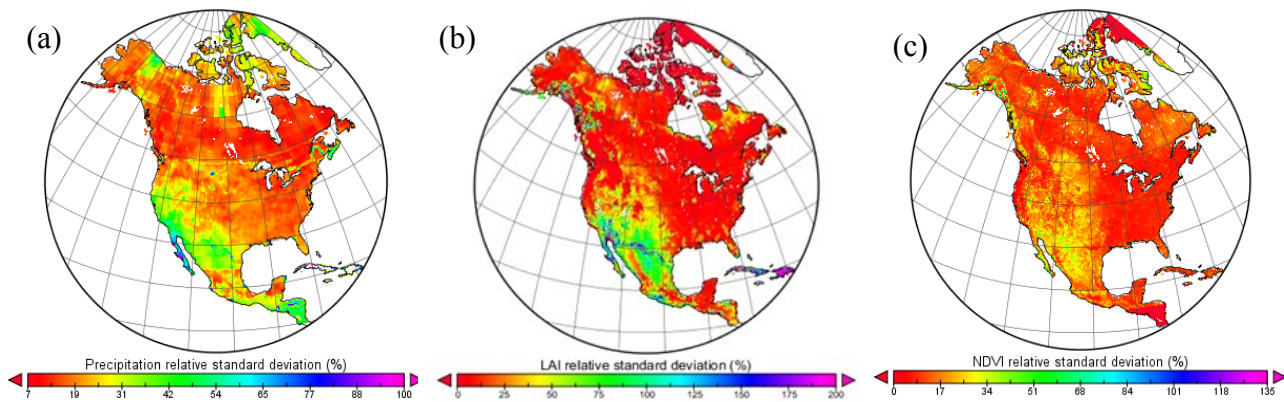


Figure 4-6. Relative standard deviation (%) for long-term (1980 – 2010) annual (a) NARR precipitation, (b) modeled mid-August LAI and (c) mid-August NDVI (1982 – 2006)

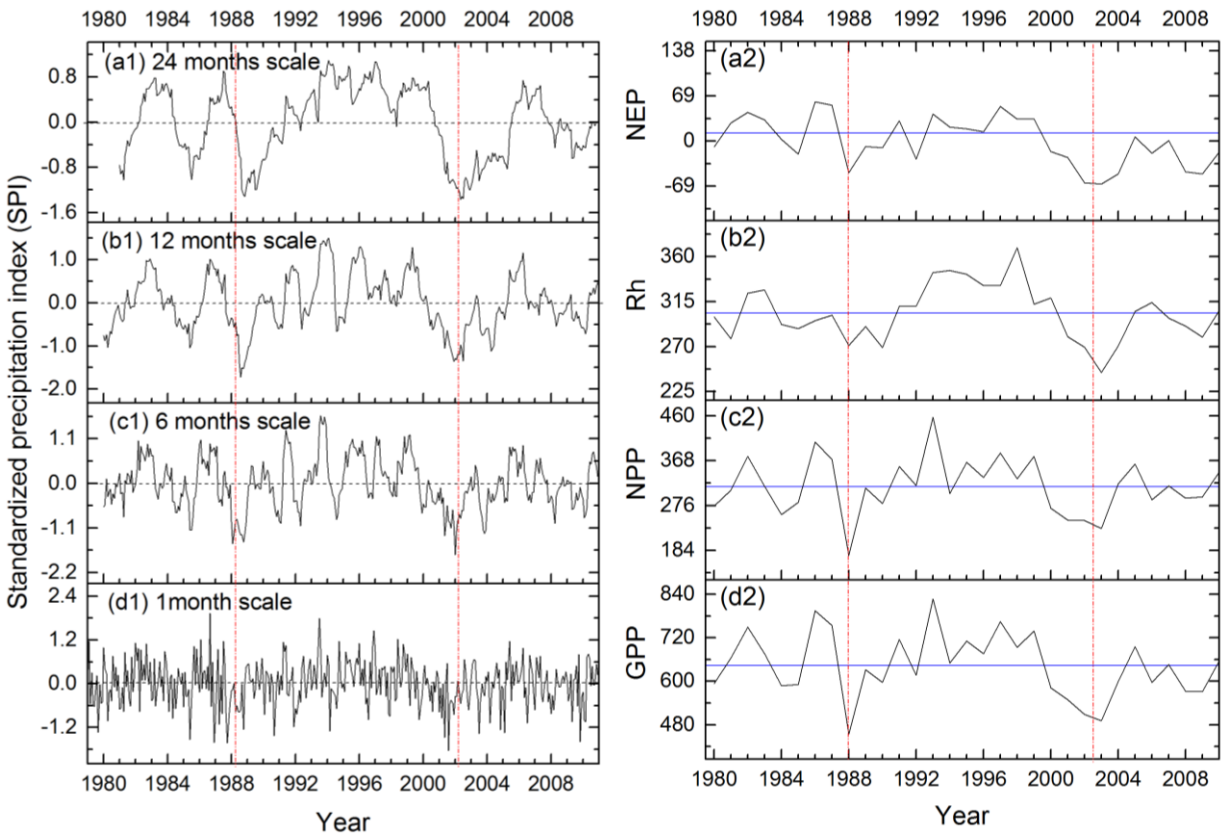


Figure 4-7. (a1 – d1) Standardized precipitation index (SPI) at different time scales (moving average for 3, 6, 12 and 24 months), and (a2 – d2) spatial average annual fluxes ($\text{g C m}^{-2} \text{ yr}^{-1}$) for drought affected sub-region of North America (Great Plains, southwest US and northern Mexico)

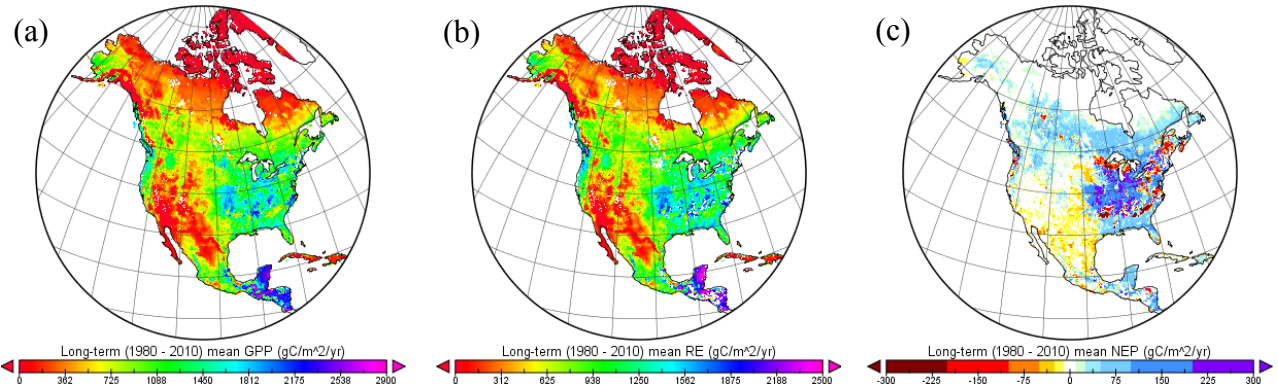


Figure 4-8. Long-term (1980 – 2010) modeled mean annual (a) GPP, (b) RE and (c) NEP of North America: positive NEP implies sinks and negative NEP sources. Localized red spots in (c) indicate carbon sources caused by severe disturbance effects on NEP during the modeled period

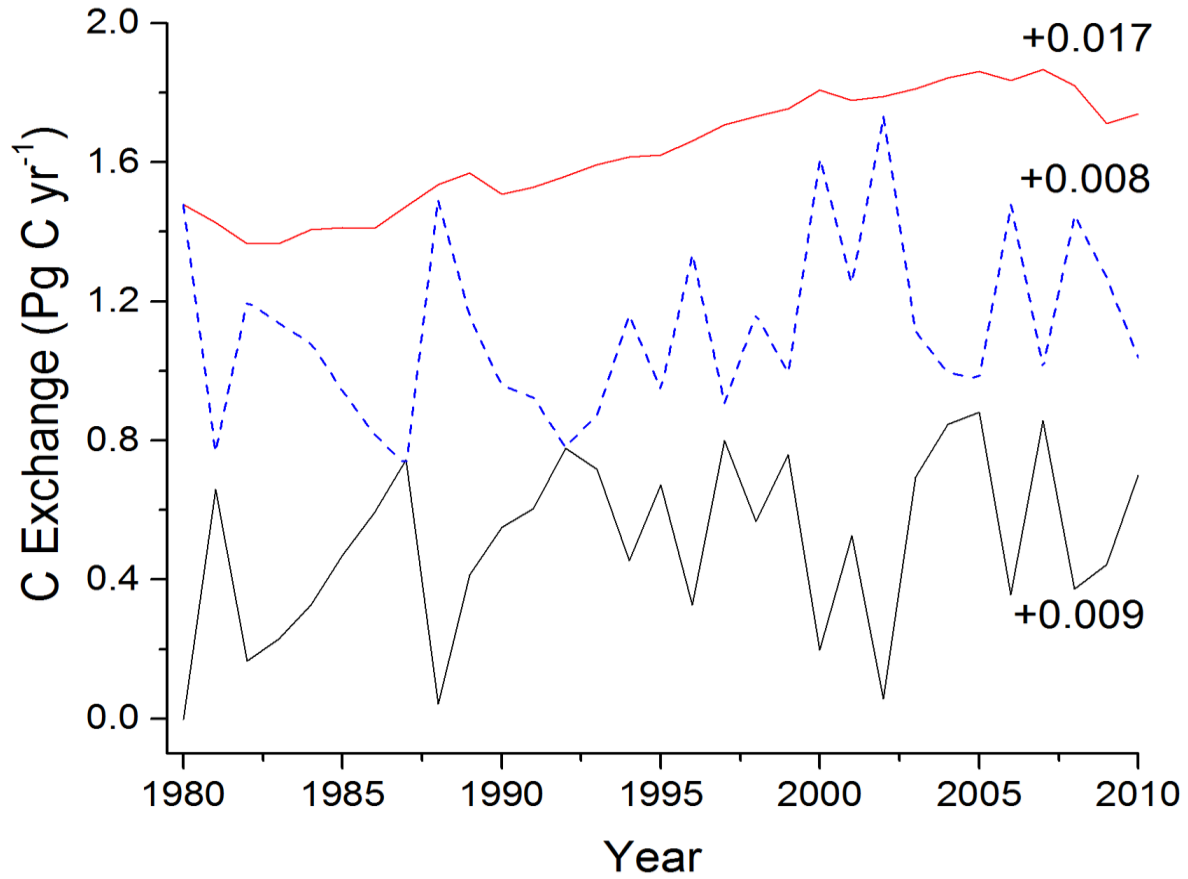


Figure 4-9. Long-term trends in modeled annual NEP (Black line), annual anthropogenic fossil fuel emissions (red line) and net carbon emissions (annual NEP subtracted from the annual fossil fuel emission) without considering the carbon that could be sequestered in water bodies in North America (blue line): North America fossil fuel emission data was obtained from Boden et al. (2013)

Appendix: A

Details of Eqs. B1, B2, B4, B6, B9 – B12 and B14 cited in the chapter are explained in Appendix B of Chapter 3

Appendix A: Soil C, N and P transformations

<i>Decomposition</i>		
$D_{S_{i,j,l,C}} = D'_{S_{i,j,l,C}} M_{i,d,l,C} f_{\text{vgl}} (S_{i,l,C} / G_{i,l,C})$	decomposition of litter, POC, humus	[A1a]
$D_{Z_{i,j,l,C}} = D'_{Z_{i,j,l,C}} M_{i,d,l,C} f_{\text{vgl}} (Z_{i,l,C} / G_{i,l,C})$	decomposition of microbial residues	[A1b]
$D_{A_{i,l,C}} = D'_{A_{i,l,C}} M_{i,d,l,C} f_{\text{vgl}} (A_{i,l,C} / G_{i,l,C})$	decomposition of adsorbed SOC	[A1c]
$M_{i,d,l,C} = M_{i,a,l,C} + \mathbf{q}_m (M_{i,a,l,C} G_{ix,l,C} - M_{ix,a,l,C} G_{i,l,C}) / (G_{ix,l,C} + G_{i,l,C})$	redistribution of active microbial biomass populations from each substrate-microbe complex i to other substrate-microbe complexes	[A3a]
$M_{i,a,l,C} = \sum_n M_{i,n,a,l,C}$	ix according to concentration differences (priming)	[A3b]
$f_{\text{vgl}} = T_{sl} \{ e^{[B - H_a / (R T_{sl})]} \} / \{ 1 + e^{[(H_{al} - ST_{sl}) / (R T_{sl})]} + e^{[(ST_{sl} - H_{ah}) / (R T_{sl})]} \}$	Arrhenius function for D and R_h	[A6]

Definition of Variables in Appendix A

Variable	Definition	Unit	Value	Reference
<i>subscripts</i>				
i	substrate-microbe complex: coarse woody litter, fine non-woody litter, POC, humus			
j	kinetic component: labile l , resistant r , active a			
l	soil or litter layer			
n	microbial functional type: heterotrophic (bacteria, fungi), autotrophic (nitrifiers, methanotrophs), diazotrophic, obligate aerobe, facultative anaerobes (denitrifiers), obligate anaerobes (methanogens)			
<i>variables</i>				
$A_{i,l,C}$	mass of adsorbed SOC	g C m^{-2}		
$D_{A_{i,l,C}}$	decomposition rate of $A_{i,l,C}$ by $M_{i,d,l,C}$ producing Q in [A13]	$\text{g C m}^{-2} \text{h}^{-1}$		
$D'_{A_{i,j,l,C}}$	specific decomposition rate of $S_{i,j,l,C}$ by $\sum_n M_{i,n,a,l}$ at 25°C	$\text{g C g C}^{-1} \text{h}^{-1}$		
$D_{S_{i,j,l,C}}$	decomposition rate of $S_{i,j,l,C}$ by $\sum_n M_{i,n,a,l}$ producing Q in [A13]	$\text{g C m}^{-2} \text{h}^{-1}$		
$D'_{S_{i,j,l,C}}$	specific decomposition rate of $S_{i,j,l,C}$ by $\sum_n M_{i,n,a,l}$ at 25°C	$\text{g C g C}^{-1} \text{h}^{-1}$		
$D_{Z_{i,j,l,C}}$	decomposition rate of $Z_{i,j,l,C}$ by $\sum_n M_{i,n,a,l}$ producing Q in [A13]	$\text{g C m}^{-2} \text{h}^{-1}$		
$D'_{Z_{i,j,l,C}}$	specific decomposition rate of $Z_{i,j,l,C}$ by $\sum_n M_{i,n,a,l}$ at 25°C	$\text{g C g C}^{-1} \text{h}^{-1}$		
f_{vgl}	temperature function for microbial growth respiration	dimensionless		
f_{uml}	temperature function for maintenance respiration	dimensionless		
$G_{i,l,C}$	total C in substrate-microbe complex	g C Mg^{-1}		
$[\text{H}_2\text{PO}_4^-]$	concentration of H_2PO_4^- in soil solution	g P m^{-3}		

H_a	energy of activation	J mol^{-1}	65×10^3	Addiscott (1983)
H_{dh}	energy of high temperature deactivation	J mol^{-1}	225×10^3	
H_{dl}	energy of low temperature deactivation	J mol^{-1}	195×10^3	
K_{NH_4}	M-M constant for NH_4^+ uptake at microbial surfaces	g N m^{-3}	0.40	
K_{NO_3}	M-M constant for NO_3^- uptake at microbial surfaces	g N m^{-3}	0.35	
K_{PO_4}	M-M constant for H_2PO_4^- uptake at microbial surfaces	g P m^{-3}	0.125	
$M_{i,d,l,C}$	heterotrophic microbial C used for decomposition	g C m^{-2}		
$M_{i,n,j,l,C}$	microbial C	g C m^{-2}		
$M_{i,n,j,l,N}$	microbial N	g N m^{-2}		
$M_{i,n,j,l,P}$	microbial P	g P m^{-2}		
$[\text{NH}_4^+_{i,n,j,l}]$	concentration of NH_4^+ at microbial surfaces	g N m^{-3}		
$[\text{NH}_4^+_{mn}]$	concentration of NH_4^+ at microbial surfaces below which $U_{\text{NH}_4} = 0$	g N m^{-3}	0.0125	
$[\text{NO}_3^-_{i,n,j,l}]$	concentration of NO_3^- at microbial surfaces	g N m^{-3}		
$[\text{NO}_3^-_{mn}]$	concentration of NO_3^- at microbial surfaces below which $U_{\text{NO}_3} = 0$	g N m^{-3}	0.03	
$[\text{H}_2\text{PO}_4^-_{i,n,j,l}]$	concentration of H_2PO_4^- at microbial surfaces	g N m^{-3}		
$[\text{H}_2\text{PO}_4^-_{mn}]$	concentration of H_2PO_4^- at microbial surfaces below which $U_{\text{PO}_4} = 0$	g N m^{-3}	0.002	
q_m	rate constant for reallocating $M_{i,a,l,C}$ to $M_{i,d,l,C}$	h^{-1}	0.5	
R	gas constant	$\text{J mol}^{-1} \text{K}^{-1}$	8.3143	
$R_{gi,n,l}$	growth respiration of $M_{i,n,a,l}$ on $Q_{i,l,C}$ under nonlimiting O_2 and nutrients	$\text{g C g C}^{-1} \text{h}^{-1}$		
R_h	total heterotrophic respiration of all $M_{i,n,a,l}$ under ambient DOC, O_2 , nutrients, θ and temperature	$\text{g C m}^{-2} \text{h}^{-1}$		
$R_{hi,n,l}$	heterotrophic respiration of $M_{i,n,a,l}$ under ambient DOC, O_2 , nutrients, θ and temperature	$\text{g C m}^{-2} \text{h}^{-1}$		
R_m	specific maintenance respiration at 25°C	$\text{g C g N}^{-1} \text{h}^{-1}$	0.0115	Barnes et al. (1998)
$R_{mi,n,j,l}$	maintenance respiration by $M_{i,n,j,l}$	$\text{g C m}^{-2} \text{h}^{-1}$		
S	change in entropy	$\text{J mol}^{-1} \text{K}^{-1}$	710	Sharpe and DeMichelle (1977)
T_{sl}	soil temperature	K		
$U_{\text{NH}_4i,n,j,l}$	NH_4^+ uptake by microbes	$\text{g N m}^{-2} \text{h}^{-1}$		
U'_{NH_4}	maximum U_{NH_4} at 25°C and non-limiting NH_4^+	$\text{g N m}^{-2} \text{h}^{-1}$	5.0×10^{-3}	
$U_{\text{NO}_3i,n,j,l}$	NO_3^- uptake by microbes	$\text{g N m}^{-2} \text{h}^{-1}$		
U'_{NO_3}	maximum U_{NO_3} at 25°C and non-limiting NO_3^-	$\text{g N m}^{-2} \text{h}^{-1}$	5.0×10^{-3}	
$U_{\text{PO}_4i,n,j,l}$	H_2PO_4^- uptake by microbes	$\text{g N m}^{-2} \text{h}^{-1}$		
U'_{PO_4}	maximum U_{PO_4} at 25°C and non-limiting H_2PO_4^-	$\text{g N m}^{-2} \text{h}^{-1}$	5.0×10^{-3}	
y	selected to give a Q_{10} for f_m of 2.25		0.081	

Chapter 5

General discussion and conclusions

5.1. Sensitivity of Modeled NEP to Gridded Climates and Soil

We observed that gridded vs. measured weather inputs correlated well allowing simulation of the impacts of weather on land-atmosphere carbon exchange under contrasting weather (warm vs. cool, dry vs. wet) for most of the EC sites. However, the degree of agreement varied, with generally good agreement for NARR and site T_a and poorer agreement for precipitation. We identified biases in NARR shortwave incoming radiation and precipitation at some sites that needed further improvements. Incoming shortwave radiation was slightly underestimated for most of the sites (Fig. 2-2). Deviations in precipitation intensity should also be improved (Fig. 2-3), as temporal distribution of precipitation determines water availability for plant growth and controlled the model response to extreme weather events such as drought. Most of the inaccuracies of the gridded weather were mainly attributed to sparse distribution of meteorological stations that were used to make the gridded layers. These inaccuracies were greater for higher latitude regions where sampling stations are sparse due to less accessibility and higher operational costs to maintain stations in remote areas. Therefore, increasing the number of observation stations to better represent the spatial heterogeneity is crucial to improve the accuracy of the weather datasets, thus minimize the uncertainties of model estimates associated with weather inputs.

Lack of detailed information on soil physical and hydraulic properties and vertical multi-layer profiles in UNASM affected simulation of sub-surface movement of water and of available soil water for plant uptake, hence CO_2 fixation. For instance, UNASM maximum soil depth were less than what was measured at CA-Oas site (Table 2-5) hence key responses of the model to extreme climate events such as drought was not well captured (Fig. 2-8). Lack of deeper soil

vertical profile in UNASM could especially affect modeled net ecosystem productivity (NEP) in higher latitudes where modeling NEP is highly controlled by the depth of the underlying permafrost. Deepening of the active layer depth as a result of warming is a key climate change feedback in permafrost regions that can release large volume of stored carbon to the atmosphere as a result of increasing R_e . Better representation of SOC through soil profiles is also crucial to better simulate climate change feedbacks in higher latitudes. Available soil nutrients, hence CO₂ fixation could be affected as a result of initial SOC in the soil inputs. For instance, total SOC content of UNASM varied from what were measured at the sites that resulted in under/over-estimation of SOC, hence available soil nutrients for most sites. Besides, UNASM did not have an attribute to SON and therefore, estimation of SON from SOC resulted in over/under estimations of available nitrogen, hence modeled NEP, as in the case of CA-Qfo site (Fig. 2-10). Therefore, incorporating this attribute in the database is important to better estimate available soil nitrogen and hence continental carbon exchange.

NEP differences attributed to gridded vs. measured model inputs varied among sites when tested against EC-derived values. Thus, under/overestimation of modeled NEP attributed to the gridded inputs could have compensating effects at continental scale that might reduce the deviations in modeled NEP by smoothing out the differences. Nevertheless, these differences in modeled NEP associated with the quality of gridded model drivers that we tested for the selected EC sites at grid cell level would certainly be reflected at regional level and could affect continental carbon budget estimates and need to be carefully examined.

Further improvement of these gridded datasets could increase the accuracy of model estimates hence our understanding of the continental and global scale carbon budget. These can be realized by ensuring better representations of the soil and weather attributes at pixel level. For

instance, implementing better techniques of interpolation/extrapolation of original soil datasets that were used to reconstruct UNASM is important to ensure the representation of the dominant soil characteristics in a pixel. Moreover, improving the spatial resolution of NARR and UNASM is essential to have a more realistic and accurate representation of the spatial heterogeneity that allows better model estimation of carbon exchange. In this regard, there is always a trade-off between higher computational resources requirements for simulations vs. better spatial representation of weather and soil characteristics. Alternatively, when data is unavailable improving Pedo-transfer functions that make use of multiple linear and non-linear functions to estimate soil hydraulic characteristics from soil physical properties could provide a better model inputs.

Testing uncertainties in modeled NEP related to gridded weather and soil provided valuable information on limitations on continental scale carbon budget estimates. This rigorous testing has provided a basis to examine the extent to which accuracies in the continental scale simulations of land-atmosphere carbon exchange were subject to the combined effects of gridded weather and soil, besides uncertainties in the inherent model characteristics. Such testing has a direct implications in simulating the impact of climate change on NEP over a wide range of biomes and have allowed us to see the limitations in NARR and UNASM. Moreover, it also provided confidence that key responses of the modeled NEP to changes in climate were reasonably maintained. For instance, the high correlation between 3-hourly measured vs. NARR T_a has provided a greater confidence on the accuracy of gridded T_a that we used to examined the spatial and temporal variability and model the impacts of warming on gross primary productivity (GPP) across NA that we had explored in Chapter 3.

5.2. Impacts of Long-term Warming on GPP

We implemented a multi-scale (site to continental) rigorous testing of the model outputs using data derived from EC and satellite products. At site scale, modeled annual GPP derived from 20 selected EC site measurements agreed well with modeled GPP from the corresponding pixels where the EC sites were located ($R^2 = 0.76$) demonstrating the ability of the model to simulate CO_2 exchange in a wide range of climates and ecosystems across NA (Fig. 3-2). Differences in modeled vs. EC derived GPP is partly attributed to inaccuracies in the gridded model divers that could be a major sources of uncertainty as noted in the Chapter 2. Validating model outputs at regional and continental scales has been difficult due to lack of gridded observed data (Houborg and Soegaard, 2004; Sasai et al., 2007). However, spatial patterns of satellite products such as MODIS GPP can be used to compare with the spatial patterns of modeled GPP at continental scale. Thus, long-term (2000 - 2010) annual modeled vs. MODIS GPP were shown to have similar spatial patterns (geographically weighed regression, GWR $R^2 = 0.8$) demonstration close similarities spatial clusters (Fig. 3-4). Interannual anomalies in modeled vs. MODIS GPP for NA have also agreed well showing adverse effects of mid-continental drought in 2002 and drought in the south in 2008 - 2009 (Fig. 3-5).

Spatial and temporal analyses of long-term NARR T_a and precipitation have shown contrasting regional patterns. These contrasting regional trends in NARR T_a were observed over the last three decades in NA with most rapid warming in higher latitudes, particularly in the high Arctic while some areas in the western part of NA experienced a slight cooling. But overall the average T_a for the entire NA landmass has increased by $+0.38 \text{ }^\circ\text{C decade}^{-1}$ from 1979 – 2010. Despite the lack of clear spatial trends in precipitation changes, most areas at higher latitudes were

shown to gain in annual precipitation over the last three decades. Mid and lower latitudes had more spatially variable changes in precipitation in recent decades.

Different ecosystems across NA did not respond similarly to similar trends of warming and changes in precipitation and the responses were spatially heterogeneous. These contrasting responses to warming were dependent on the initial conditions (Shaver et al., 2000) of the ecosystem mainly determined by the climate zone, precipitation and availability of nutrients. For instance, modeled GPP increased with warming in ecosystems with cooler climates due to an increase in the rate of carboxylation (Table 3-4; Fig. 3-8b). This is mainly due to temperature responses which are larger in cooler regions where Q_{10} values are larger, but which declined with increasing temperature and declining Q_{10} (Sjögersten and Wookey, 2002). In these climates warming was mostly coupled with an increase in precipitation (Fig. 3-7) which increased rates of CO_2 fixation through enhancing kinetics of carboxylation (Bernacchi et al., 2001; Grant et al., 2009a), while largely avoiding the indirect effects on CO_2 fixation through declining ψ_s . GPP modeled in NA eco-regions such as eastern temperate forests, northern forests and Taiga contributed 92% of the increases in NA GPP over the last three decades, demonstrating that much of the changes in these eco-regions had a strong control over the long-term changes in NA GPP thus, continental carbon budget.

In contrast, warming in warmer and drier regions such as southwest US (Cook et al., 2004b), especially when coupled with a decline in precipitation, resulted declines in CO_2 fixation (Table 3-4; Fig. 3-8b), through an indirect effect by hastening transpiration and soil drying (Grant et al., 1999). Southwestern regions of NA accounted >50% of the NA ecosystems with declining GPP implying that further warming and projected dryness (IPCC, 2013; Seager et al., 2007; Williams et al., 2013) in this region could further reduce NA carbon uptake. Such contrasting

responses of warming could have implications in long-term changes in species composition and biome shifts (Reich et al., 2015). It is unclear how ecosystems respond to further warming which is dependent on the complex interactions with changes in precipitation and other climatic and biophysical controls and thus need to be further examined.

5.3. North American Carbon Sources and Sinks Affected by Drought

We observed a significant decline in modeled GPP, ecosystem respiration (R_e), NEP and leaf area index (LAI) associated with major drought events in 1988 and 2002 in much of NA, particularly in the Great Plains, western and southwest of US. The spatial patterns of reductions in modeled LAI were corroborated by a similar pattern of reduction in mid-August AVHRR NDVI product of the corresponding years (Fig 4-5). A decline in R_e was less than in GPP both in 1988 and 2002, indicating that carbon assimilation tend to be more sensitive to drought than was respiration. As a result of this sensitivity, NEP declined by 92 % (1988) and 90% (2002) from the long-term mean resulting in only +0.04 Pg C yr⁻¹ and +0.05 Pg C yr⁻¹ carbon sink in 1988 and 2002 respectively (Table 4-2). The significant drops in NEP offset 28% of the long-term carbon gains from the long-term mean over the last three decades. The long-term modeled terrestrial carbon sink was estimated to offset only 0.03 and 3.2 % the fossil fuel emissions of NA in 1988 and 2002 respectively, leaving almost all fossil fuel emissions to the atmosphere, implying that projected increases in the intensity and frequency of drought (IPCC, 2013) could further reduce the NA carbon sink.

Greater interannual variability in precipitation, modeled mid-August LAI and NDVI that may be associated with frequent occurrences of El Niño–Southern Oscillation' events (Herweijer et al., 2007; Ropelewski and Halpert, 1986) which led to major droughts, occurred in much of Great Plains, southwest US and northern Mexico, indicating that major drought events control

much of continental scale interannual variability of carbon exchange. Water limitations during these drought years induced soil drying that raised ψ_c , r_c and r_l (Grant et al., 1999; Grant and Flanagan, 2007b-a), hence a decline in CO_2 diffusion and rate of carboxylation (Fig. 4-1). A reduction in R_e in both drought years could be as a result of a reduction in the supply of labile carbon due to a decline in GPP (van der Molen et al., 2011) and less moisture availability for microbial activity hence in a decline in heterotrophic respiration (R_h).

The spatial patterns of modeled long-term annual average NEP (Fig. 4-7c) indicated that higher latitudes of NA, east, southeast and the Great Plains have mainly been carbon sinks over the last three decades. Among the different eco-regions of NA, it was shown that regions dominated by forests and croplands were strong sinks compared to non-forested regions. Drier climate regions such as the south and the southwest were mainly carbon sources. However, at continental level long-term average modeled NEP has an increasing trend ($+0.009 \text{ Pg C decade}^{-1}$) indicating that long-term average NA has been an increasing carbon sink, despite a sharp drops in NEP during 1988 and 2002. Although terrestrial NA has been a net carbon sink, fossil fuel emission is biggest larger source of carbon that made NA a net source. The rate of increases in fossil fuel emission in NA had an increasing trend of $+0.017 \text{ Pg C yr}^{-1}$ resulting in net source of carbon from fissile fuel emission increasing with a trend of $+0.008 \text{ Pg C yr}^{-1}$ over the last three decades (Fig. 4-9), without considering the carbon that would be taken up by the water bodies within the NA landmass spatial domain. Thus, NA contribute to the increasing global atmospheric CO_2 concentration, as on long-term average only 30% of the fissile fuel emissions in NA was modeled to offset by the NA biosphere.

Projected increases in the frequency of drought events (Huntington, 2006; IPCC, 2013) under future climate change scenarios could turn ecosystems to carbon sources and may elevate

the atmospheric CO₂ concentration more rapidly. For instance, most climate projections for the 21st century have indicated that the southwestern US will get drier resulting in more severe droughts (Cayan et al., 2010; Seager et al., 2007). Climate projections are also showing that global warming is expected to continue as a result of increasing atmospheric CO₂ concentration. Impacts of future warming, under different climate scenarios, on ecosystem productivity are partly uncertain and determined by the concurrent changes in precipitation and need to be carefully examined. Gains in GPP modeled and observed as a result of recent warming may not be sustained (Grant et al., 2011a; Peters et al., 2007) indefinitely under further warming. Carbon release may be accelerated, particularly due to deepening of the active layer that exposes large volume of carbon pool beneath the permafrost layer. An increase of about 3⁰C in the temperature of the top of the permafrost layer since 1980s have been reported in the Arctic (IPCC, 2013). In this regard, TBMs provide the predictive capability needed to estimate gains and losses of GPP and R_e under future climate change scenarios. As drought is one of the most costly natural disasters in NA, understanding of the processes that control drought and better methods of prediction is important and process based ecosystem models can be coupled with climate models to develop early warning systems of drought occurrences that can support decision making. It is also imperative to test ecosystem model outputs under past and present meteorological drivers against observations to build confidence on models predictive capabilities. Although lack of continental scale observations, recent developments in a remote sensing satellite products such as Orbiting Carbon Observatory-2 (OCO-2) that measures atmospheric CO₂ (launched in July, 2014) globally can provide an opportunity to conduct a better and rigorous testing of continental-scale model outputs which is vital to our understanding of the impacts of climate change on regional to global carbon cycle.

References

- Aertsen, W., Kint, V., Muys, B. and Van Orshoven, J., 2012. Effects of scale and scaling in predictive modelling of forest site productivity. *Environmental Modelling & Software*, 31: 19-27.
- Aguilar, E. et al., 2005. Changes in precipitation and temperature extremes in Central America and northern South America, 1961–2003. *Journal of Geophysical Research*, 110(D23).
- Albert, K.R., Mikkelsen, T.N., Michelsen, A., Ro-Poulsen, H. and van der Linden, L., 2011. Interactive effects of drought, elevated CO₂ and warming on photosynthetic capacity and photosystem performance in temperate heath plants. *Journal of Plant Physiology*, 168(13): 1550-1561.
- Allen, M.R., Stott, P.A., Mitchell, J.F., Schnur, R. and Delworth, T.L., 2000. Quantifying the uncertainty in forecasts of anthropogenic climate change. *Nature*, 407(6804): 617-620.
- Alley, W.M., 1984. The Palmer drought severity index: limitations and assumptions. *Journal of climate and applied meteorology*, 23(7): 1100-1109.
- Anderson, M.C., Kustas, W.P. and Norman, J.M., 2003. Upscaling and downscaling—A regional view of the soil–plant–atmosphere continuum. *Agronomy Journal*, 95(6): 1408-1423.
- Anisimov, O.A. et al., 2007. Uncertainties in gridded air temperature fields and effects on predictive active layer modeling. *Journal of Geophysical Research*, 112(F2).
- Arain, M.A. and Restrepo-Coupe, N., 2005. Net ecosystem production in a temperate pine plantation in southeastern Canada. *Agricultural and Forest Meteorology*, 128(3): 223-241.
- Arnold, J.A. et al., 2008. Prolonged suppression of ecosystem carbon dioxide uptake after an anomalously warm year. *Nature*, 455(7211): 383-386.

- Aubinet, M., Vesala, T. and Papale, D., 2012. Eddy covariance: a practical guide to measurement and data analysis. Springer.
- Baker, D.F. et al., 2006. TransCom 3 inversion intercomparison: Impact of transport model errors on the interannual variability of regional CO₂ fluxes, 1988-2003. *Global Biogeochemical Cycles*, 20(1): n/a-n/a.
- Baker, I.T., Denning, A.S. and StÖckli, R., 2010. North American gross primary productivity: regional characterization and interannual variability. *Tellus B*, 62(5): 533-549.
- Baldocchi, D. et al., 2001. FLUXNET: A new tool to study the temporal and spatial variability of ecosystem-scale carbon dioxide, water vapor, and energy flux densities. *Bulletin of the American Meteorological Society*, 82(11): 2415-2434.
- Baldocchi, D.D., 2003. Assessing the eddy covariance technique for evaluating carbon dioxide exchange rates of ecosystems: past, present and future. *Global Change Biology*, 9(4): 479-492.
- Beck, P.S.A. et al., 2011. Changes in forest productivity across Alaska consistent with biome shift. *Ecology Letters*, 14(4): 373-379.
- Beer, C. et al., 2010. Terrestrial Gross Carbon Dioxide Uptake: Global Distribution and Covariation with Climate. *Science*, 329(5993): 834-838.
- Belkin, I.M., 2009. Rapid warming of Large Marine Ecosystems. *Progress in Oceanography*, 81(1-4): 207-213.
- Bergeron, O., Margolis, H.A., Coursolle, C. and Giasson, M.-A., 2008. How does forest harvest influence carbon dioxide fluxes of black spruce ecosystems in eastern North America? *Agricultural and Forest Meteorology*, 148(4): 537-548.

- Bernacchi, C., Pimentel, C. and Long, S., 2003. In vivo temperature response functions of parameters required to model RuBP-limited photosynthesis. *Plant, Cell & Environment*, 26(9): 1419-1430.
- Bernacchi, C., Singaas, E., Pimentel, C., Portis Jr, A. and Long, S., 2001. Improved temperature response functions for models of Rubisco-limited photosynthesis. *Plant, Cell & Environment*, 24(2): 253-259.
- Berrisford, P. et al., 2009. The ERA-Interim Archive. ERA report series(1): 1-16.
- Boden, T.A., Marland, G. and Andres, R.J., 2013. Global, Regional, and National Fossil-Fuel CO2 Emissions. Carbon Dioxide Information Analysis Center, Oak Ridge National Laboratory, U.S. Department of Energy, Oak Ridge, Tenn., U.S.A. DOI: 10.3334/CDIAC/00001_V2013.
- Bond-Lamberty, B., Peckham, S.D., Ahl, D.E. and Gower, S.T., 2007. Fire as the dominant driver of central Canadian boreal forest carbon balance. *Nature*, 450(7166): 89-92.
- Box, E.O., Holben, B.N. and Kalb, V., 1989. Accuracy of the AVHRR vegetation index as a predictor of biomass, primary productivity and net CO2 flux. *Vegetatio*, 80(2): 71-89.
- Breshears, D.D. et al., 2005. Regional vegetation die-off in response to global-change-type drought. *Proceedings of the National Academy of Sciences of the United States of America*, 102(42): 15144-15148.
- Caccamo, G., Chisholm, L., Bradstock, R.A. and Puotinen, M., 2011. Assessing the sensitivity of MODIS to monitor drought in high biomass ecosystems. *Remote Sensing of Environment*, 115(10): 2626-2639.

- Cairns, M.A., Haggerty, P.K., Alvarez, R., De Jong, B.H. and Olmsted, I., 2000. Tropical Mexico's recent land-use change: A region's contribution to the global carbon cycle. *Ecological Applications*, 10(5): 1426-1441.
- Carlson, T.N. and Ripley, D.A., 1997. On the relation between NDVI, fractional vegetation cover, and leaf area index. *Remote Sensing of Environment*, 62(3): 241-252.
- Cayan, D.R. et al., 2010. Future dryness in the southwest US and the hydrology of the early 21st century drought. *Proceedings of the National Academy of Sciences*, 107(50): 21271-21276.
- Chapman, W.L. and Walsh, J.E., 1993. Recent variations of sea ice and air temperature in high latitudes. *Bulletin of the American Meteorological Society*, 74(1): 33-47.
- Churkina, G., Schimel, D., Braswell, B.H. and Xiao, X., 2005. Spatial analysis of growing season length control over net ecosystem exchange. *Global Change Biology*, 11(10): 1777-1787.
- Ciais, P. et al., 2005. Europe-wide reduction in primary productivity caused by the heat and drought in 2003. *Nature*, 437(7058): 529-533.
- Comiso, J.C., 2003. Warming trends in the Arctic from clear sky satellite observations. *Journal of Climate*, 16(21): 3498-3510.
- Cook, B.D. et al., 2004a. Carbon exchange and venting anomalies in an upland deciduous forest in northern Wisconsin, USA. *Agricultural and Forest Meteorology*, 126(3): 271-295.
- Cook, E.R. et al., 2010. Megadroughts in North America: Placing IPCC projections of hydroclimatic change in a long-term palaeoclimate context. *Journal of Quaternary Science*, 25(1): 48-61.

- Cook, E.R., Woodhouse, C.A., Eakin, C.M., Meko, D.M. and Stahle, D.W., 2004b. Long-term aridity changes in the western United States. *Science*, 306(5698): 1015-1018.
- Dai, A., Trenberth, K.E. and Qian, T., 2004. A global dataset of Palmer Drought Severity Index for 1870–2002: relationship with soil moisture and effects of surface warming. *Journal of Hydrometeorology*, 5(6).
- Daly, C., Doggett, M., Gibson, W. and Smith, J., 2012. PRISM Climate Group Oregon State University. Data Set.
- Davidson, E.A. and Janssens, I.A., 2006. Temperature sensitivity of soil carbon decomposition and feedbacks to climate change. *Nature*, 440(7081): 165-173.
- Delpierre, N. et al., 2012. Quantifying the influence of climate and biological drivers on the interannual variability of carbon exchanges in European forests through process-based modelling. *Agricultural and Forest Meteorology*, 154-155: 99-112.
- Dentener, F., 2006. Global maps of atmospheric nitrogen deposition, 1860, 1993, and 2050. Data set. Available on-line(<http://daac.ornl.gov>) from Oak Ridge National Laboratory Distributed Active Archive Center, Oak Ridge, TN, USA.
- Dermody, O., Weltzin, J.F., Engel, E.C., Allen, P. and Norby, R.J., 2007. How do elevated [CO₂], warming, and reduced precipitation interact to affect soil moisture and LAI in an old field ecosystem? *Plant and Soil*, 301(1-2): 255-266.
- Dieleman, W.I.J. et al., 2012. Simple additive effects are rare: a quantitative review of plant biomass and soil process responses to combined manipulations of CO₂ and temperature. *Global Change Biology*, 18(9): 2681-2693.
- Dore, M.H., 2005. Climate change and changes in global precipitation patterns: what do we know? *Environment international*, 31(8): 1167-1181.

- Dutta, K., Schuur, E., Neff, J. and Zimov, S., 2006. Potential carbon release from permafrost soils of Northeastern Siberia. *Global Change Biology*, 12(12): 2336-2351.
- Easterling, D.R. et al., 1997. Maximum and minimum temperature trends for the globe. *Science*, 277(5324): 364-367.
- Elmendorf, S.C. et al., 2012a. Global assessment of experimental climate warming on tundra vegetation: heterogeneity over space and time. *Ecology Letters*, 15(2): 164-175.
- Elmendorf, S.C. et al., 2012b. Plot-scale evidence of tundra vegetation change and links to recent summer warming. *Nature Clim. Change*, 2(6): 453-457.
- Farquhar, G., Caemmerer, S. and Berry, J., 1980. A biochemical model of photosynthetic CO₂ assimilation in leaves of C₃ species. *Planta*, 149(1): 78-90.
- Flanagan, L.B. and Adkinson, A.C., 2011. Interacting controls on productivity in a northern Great Plains grassland and implications for response to ENSO events. *Global Change Biology*, 17(11): 3293-3311.
- Flanagan, L.B. and Syed, K.H., 2011. Stimulation of both photosynthesis and respiration in response to warmer and drier conditions in a boreal peatland ecosystem. *Global Change Biology*, 17(7): 2271-2287.
- Frankenberg, C. et al., 2014. Prospects for chlorophyll fluorescence remote sensing from the Orbiting Carbon Observatory-2. *Remote Sensing of Environment*, 147: 1-12.
- Gaumont-Guay, D. et al., 2006. Influence of temperature and drought on seasonal and interannual variations of soil, bole and ecosystem respiration in a boreal aspen stand. *Agricultural and Forest Meteorology*, 140(1-4): 203-219.

- Gough, C., Vogel, C., Schmid, H., Su, H.-B. and Curtis, P., 2008. Multi-year convergence of biometric and meteorological estimates of forest carbon storage. *Agricultural and Forest Meteorology*, 148(2): 158-170.
- Goulden, M.L., Munger, J.W., Fan, S.-M., Daube, B.C. and Wofsy, S.C., 1996. Exchange of carbon dioxide by a deciduous forest: response to interannual climate variability.
- Goulden, M.L. et al., 2006. An eddy covariance mesonet to measure the effect of forest age on land-atmosphere exchange. *Global Change Biology*, 12(11): 2146-2162.
- Goward, S.N., Markham, B., Dye, D.G., Dulaney, W. and Yang, J., 1991. Normalized difference vegetation index measurements from the advanced very high resolution radiometer. *Remote Sensing of Environment*, 35(2-3): 257-277.
- Grant, R., 1998. Simulation in ecosys of root growth response to contrasting soil water and nitrogen. *Ecological Modelling*, 107(2): 237-264.
- Grant, R., 2001. A review of the Canadian ecosystem model ecosys. in *Modeling Carbon and Nitrogen Dynamics for Soil Management*: pp. 173-264, CRC Press, Boca Raton, FL.
- Grant, R. et al., 2007d. Net ecosystem productivity of boreal jack pine stands regenerating from clearcutting under current and future climates. *Global Change Biology*, 13(7): 1423-1440.
- Grant, R. et al., 2010. Net ecosystem productivity of temperate and boreal forests after clearcutting—a Fluxnet-Canada measurement and modelling synthesis. *Tellus B*, 62(5): 475-496.
- Grant, R., Black, T., Humphreys, E. and Morgenstern, K., 2007c. Changes in net ecosystem productivity with forest age following clearcutting of a coastal Douglas-fir forest: testing

- a mathematical model with eddy covariance measurements along a forest chronosequence. *Tree Physiology*, 27(1): 115-131.
- Grant, R., Juma, N., Robertson, J., Izaurrealde, R. and McGill, W.B., 2001b. Long-Term Changes in Soil Carbon under Different Fertilizer, Manure, and Rotation. *Soil Science Society of America Journal*, 65(1): 205-214.
- Grant, R. et al., 2011b. Controlled warming effects on wheat growth and yield: field measurements and modeling. *Agronomy Journal*, 103(6): 1742-1754.
- Grant, R. et al., 1999. Crop water relations under different CO₂ and irrigation: testing of ecosys with the free air CO₂ enrichment (FACE) experiment. *Agricultural and Forest Meteorology*, 95(1): 27-51.
- Grant, R.F., 2004b. Modeling topographic effects on net ecosystem productivity of boreal black spruce forests. *Tree Physiology*, 24(1): 1-18.
- Grant, R.F., 2014. Nitrogen mineralization drives the response of forest productivity to soil warming: Modelling in ecosys vs. measurements from the Harvard soil heating experiment. *Ecological Modelling*, 288: 38-46.
- Grant, R.F. et al., 2007a. Net Biome Productivity of Irrigated and Rainfed Maize–Soybean Rotations: Modeling vs. Measurements. *Agronomy Journal*, 99(6): 1404.
- Grant, R.F., Baldocchi, D.D. and Ma, S., 2012. Ecological controls on net ecosystem productivity of a seasonally dry annual grassland under current and future climates: Modelling with ecosys. *Agricultural and Forest Meteorology*, 152: 189-200.
- Grant, R.F. et al., 2009a. Interannual variation in net ecosystem productivity of Canadian forests as affected by regional weather patterns – A Fluxnet-Canada synthesis. *Agricultural and Forest Meteorology*, 149(11): 2022-2039.

- Grant, R.F. et al., 2006a. Net ecosystem productivity of boreal aspen forests under drought and climate change: Mathematical modelling with Ecosys. *Agricultural and Forest Meteorology*, 140(1-4): 152-170.
- Grant, R.F. and Flanagan, L.B., 2007b-a. Modeling stomatal and nonstomatal effects of water deficits on CO₂ fixation in a semiarid grassland. *J Geophys Res-Biogeophys*, 112(G3): G03011.
- Grant, R.F. and Flanagan, L.B., 2007b-b. Modeling stomatal and nonstomatal effects of water deficits on CO₂ fixation in a semiarid grassland. *Journal of Geophysical Research*, 112(G3).
- Grant, R.F., Humphreys, E.R., Lafleur, P.M. and Dimitrov, D.D., 2011a. Ecological controls on net ecosystem productivity of a mesic arctic tundra under current and future climates. *Journal of Geophysical Research*, 116(G1).
- Grant, R.F. et al., 2008. Changes in net ecosystem productivity of boreal black spruce stands in response to changes in temperature at diurnal and seasonal time scales. *Tree Physiology*, 29(1): 1-17.
- Grant, R.F., Oechel, W.C. and Ping, C.L., 2003. Modelling carbon balances of coastal arctic tundra under changing climate. *Global Change Biology*, 9(1): 16-36.
- Grant, R.F. et al., 2006b. Intercomparison of techniques to model water stress effects on CO₂ and energy exchange in temperate and boreal deciduous forests. *Ecological Modelling*, 196(3-4): 289-312.
- Groisman, P.Y. et al., 1999. Changes in the probability of heavy precipitation: important indicators of climatic change. *Climatic Change*, 42(1): 243-283.

- Gu, L. et al., 2006. Direct and indirect effects of atmospheric conditions and soil moisture on surface energy partitioning revealed by a prolonged drought at a temperate forest site. *Journal of Geophysical Research: Atmospheres* (1984–2012), 111(D16).
- Gu, Y. et al., 2008. Evaluation of MODIS NDVI and NDWI for vegetation drought monitoring using Oklahoma Mesonet soil moisture data. *Geophysical Research Letters*, 35(22).
- Guanter, L. et al., 2014. Global and time-resolved monitoring of crop photosynthesis with chlorophyll fluorescence. *Proceedings of the National Academy of Sciences*, 111(14): E1327-E1333.
- Gurney, K.R. et al., 2002. Towards robust regional estimates of CO₂ sources and sinks using atmospheric transport models. *Nature*, 415(6872): 626-630.
- Harden, J.W. et al., 2000. The role of fire in the boreal carbon budget. *Global Change Biology*, 6(S1): 174-184.
- Hart, S.C., 2006. Potential impacts of climate change on nitrogen transformations and greenhouse gas fluxes in forests: a soil transfer study. *Global Change Biology*, 12(6): 1032-1046.
- Hatfield, J.L. et al., 2011. *Climate Impacts on Agriculture: Implications for Crop Production* All rights reserved. No part of this periodical may be reproduced or transmitted in any form or by any means, electronic or mechanical, including photocopying, recording, or any information storage and retrieval system, without permission in writing from the publisher. *Agron. J.*, 103(2): 351-370.
- Hayes, M.J., Svoboda, M.D., Wilhite, D.A. and Vanyarkho, O.V., 1999. Monitoring the 1996 drought using the standardized precipitation index. *Bulletin of the American Meteorological Society*, 80(3): 429-438.

- Heinsch, F., Reeves, M. and Votava, P., 2006a. others 2003 User's Guide: GPP and NPP (MOD17A2/A3) Products NASA MODIS Land Algorithm Version 20, December 2, 2003. University of Montana.
- Heinsch, F.A. et al., 2006b. Evaluation of remote sensing based terrestrial productivity from MODIS using regional tower eddy flux network observations. *Geoscience and Remote Sensing, IEEE Transactions on*, 44(7): 1908-1925.
- Held, I.M. and Soden, B.J., 2000. Water vapor feedback and global warming 1. *Annual review of energy and the environment*, 25(1): 441-475.
- Herweijer, C., Seager, R., Cook, E.R. and Emile-Geay, J., 2007. North American droughts of the last millennium from a gridded network of tree-ring data. *Journal of Climate*, 20(7): 1353-1376.
- Hill, G.B. and Henry, G.H.R., 2011. Responses of High Arctic wet sedge tundra to climate warming since 1980. *Global Change Biology*, 17(1): 276-287.
- Hinzman, L. et al., 2005. Evidence and Implications of Recent Climate Change in Northern Alaska and Other Arctic Regions. *Climatic Change*, 72(3): 251-298.
- Houborg, R.M. and Soegaard, H., 2004. Regional simulation of ecosystem CO₂ and water vapor exchange for agricultural land using NOAA AVHRR and Terra MODIS satellite data. Application to Zealand, Denmark. *Remote Sensing of Environment*, 93(1-2): 150-167.
- Houghton, J.T. et al., 2001. *Climate change 2001: the scientific basis*, 881. Cambridge university press Cambridge.
- Hudson, J.M.G. and Henry, G.H.R., 2009. Increased plant biomass in a High Arctic heath community from 1981 to 2008. *Ecology*, 90(10): 2657-2663.

- Huntington, T.G., 2006. Evidence for intensification of the global water cycle: review and synthesis. *Journal of Hydrology*, 319(1): 83-95.
- Huntzinger, D. et al., 2013. The North American Carbon Program multi-scale synthesis and terrestrial model intercomparison project–Part 1: overview and experimental design. *Geoscientific Model Development*, 6(6): 2121-2133.
- Huntzinger, D.N. et al., 2012. North American Carbon Program (NACP) regional interim synthesis: Terrestrial biospheric model intercomparison. *Ecological Modelling*, 232(0): 144-157.
- Hurt, G.C. et al., 2006. The underpinnings of land-use history: three centuries of global gridded land-use transitions, wood-harvest activity, and resulting secondary lands. *Global Change Biology*, 12(7): 1208-1229.
- Ineson, P. et al., 1998. Effects of climate change on nitrogen dynamics in upland soils. 2. A soil warming study. *Global Change Biology*, 4(2): 153-161.
- IPCC, 2007. *Climate Change 2007: The Physical Science Basis. Contribution of Working Group I to the Fourth Assessment Report of the Intergovernmental Panel on Climate Change* [Solomon, S., D. Qin, M. Manning, Z. Chen, M. Marquis, K.B. Averyt, M. Tignor and H.L. Miller (eds.)]. Cambridge University Press, Cambridge, United Kingdom and New York, NY, USA.
- IPCC, 2013. *Climate change 2013: The Physical Science Basis. Contribution of Working Group I to the fifth assessment report of the Intergovernmental Panel on Climate Change* [Stocker TF, Qin D, Plattner G-K, Tignor M, Allen SK, Boschung J, Nauels A, Xia Y, Bex V, Midgley PM, eds]. Cambridge, UK & New York, NY, USA: Cambridge University Press.

- Izaurrealde, R.C. et al., 2011. Climate Impacts on Agriculture: Implications for Forage and Rangeland Production All rights reserved. No part of this periodical may be reproduced or transmitted in any form or by any means, electronic or mechanical, including photocopying, recording, or any information storage and retrieval system, without permission in writing from the publisher. *Agron. J.*, 103(2): 371-381.
- Jain, A.K., Briegleb, B.P., Minschwaner, K. and Wuebbles, D.J., 2000. Radiative forcings and global warming potentials of 39 greenhouse gases. *Journal of Geophysical Research: Atmospheres* (1984–2012), 105(D16): 20773-20790.
- Jamieson, P., Martin, R., Francis, G. and Wilson, D., 1995. Drought effects on biomass production and radiation-use efficiency in barley. *Field Crops Research*, 43(2): 77-86.
- Jentsch, A., Kreyling, J. and Beierkuhnlein, C., 2007. A new generation of climate-change experiments: events, not trends. *Frontiers in Ecology and the Environment*, 5(7): 365-374.
- Jones, P.D., New, M., Parker, D.E., Martin, S. and Rigor, I.G., 1999a. Surface air temperature and its changes over the past 150 years. *Reviews of Geophysics*, 37(2): 173.
- Jones, P.D., New, M., Parker, D.E., Martin, S. and Rigor, I.G., 1999b. Surface air temperature and its changes over the past 150 years. *Reviews of Geophysics*, 37(2): 173-199.
- Jordan, D.B. and Ogren, W.L., 1984. The CO₂/O₂ specificity of ribulose 1, 5-bisphosphate carboxylase/oxygenase. *Planta*, 161(4): 308-313.
- Jung, M., Henkel, K., Herold, M. and Churkina, G., 2006. Exploiting synergies of global land cover products for carbon cycle modeling. *Remote Sensing of Environment*, 101(4): 534-553.

- Jung, M. et al., 2007a. Assessing the ability of three land ecosystem models to simulate gross carbon uptake of forests from boreal to Mediterranean climate in Europe. *Biogeosciences*, 4(4): 647-656.
- Jung, M. et al., 2007b. Uncertainties of modeling gross primary productivity over Europe: A systematic study on the effects of using different drivers and terrestrial biosphere models. *Global Biogeochemical Cycles*, 21(4).
- Kalfas, J.L., Xiao, X., Vanegas, D.X., Verma, S.B. and Suyker, A.E., 2011. Modeling gross primary production of irrigated and rain-fed maize using MODIS imagery and CO₂ flux tower data. *Agricultural and Forest Meteorology*, 151(12): 1514-1528.
- Karnieli, A. et al., 2010. Use of NDVI and land surface temperature for drought assessment: merits and limitations. *Journal of Climate*, 23(3): 618-633.
- Kasischke, E.S., Christensen Jr, N. and Stocks, B.J., 1995. Fire, global warming, and the carbon balance of boreal forests. *Ecological applications*: 437-451.
- Kim, Y., Kimball, J.S., Zhang, K. and McDonald, K.C., 2012. Satellite detection of increasing Northern Hemisphere non-frozen seasons from 1979 to 2008: Implications for regional vegetation growth. *Remote Sensing of Environment*, 121: 472-487.
- King, A. et al., 2015. North America's net terrestrial CO₂ exchange with the atmosphere 1990–2009. *Biogeosciences*, 12(2): 399-414.
- King, A.W. et al., 2007. The first state of the carbon cycle report (SOCCR): The North American carbon budget and implications for the global carbon cycle. The first state of the carbon cycle report (SOCCR): The North American carbon budget and implications for the global carbon cycle.

- Klady, R.A., Henry, G.H.R. and Lemay, V., 2011. Changes in high arctic tundra plant reproduction in response to long-term experimental warming. *Global Change Biology*, 17(4): 1611-1624.
- Kljun, N. et al., 2006. Response of net ecosystem productivity of three boreal forest stands to drought. *Ecosystems*, 9(7): 1128-1144.
- Knorr, W. and Heimann, M., 1995. Impact of drought stress and other factors on seasonal land biosphere CO₂ exchange studied through an atmospheric tracer transport model. *Tellus B*, 47(4): 471-489.
- Kolari, P., Lappalainen, H.K., Hänninen, H. and Hari, P., 2007. Relationship between temperature and the seasonal course of photosynthesis in Scots pine at northern timberline and in southern boreal zone. *Tellus B*, 59(3): 542-552.
- Korzukhin, M.D., Ter-Mikaelian, M.T. and Wagner, R.G., 1996. Process versus empirical models: which approach for forest ecosystem management? *Canadian Journal of Forest Research*, 26(5): 879-887.
- Koven, C.D. et al., 2011. Permafrost carbon-climate feedbacks accelerate global warming. *Proceedings of the National Academy of Sciences*, 108(36): 14769-14774.
- Krishnan, P. et al., 2008. Factors controlling the interannual variability in the carbon balance of a southern boreal black spruce forest. *Journal of Geophysical Research: Atmospheres* (1984–2012), 113(D9).
- Krishnan, P. et al., 2006. Impact of changing soil moisture distribution on net ecosystem productivity of a boreal aspen forest during and following drought. *Agricultural and Forest Meteorology*, 139(3): 208-223.

- Krishnan, P., Black, T.A., Jassal, R.S., Chen, B. and Nestic, Z., 2009. Interannual variability of the carbon balance of three different-aged Douglas-fir stands in the Pacific Northwest. *Journal of Geophysical Research: Biogeosciences* (2005–2012), 114(G4).
- Lafleur, P.M. and Humphreys, E.R., 2008. Spring warming and carbon dioxide exchange over low Arctic tundra in central Canada. *Global Change Biology*, 14(4): 740-756.
- Lawrence, D.M. and Slater, A.G., 2005. A projection of severe near-surface permafrost degradation during the 21st century. *Geophysical Research Letters*, 32(24).
- Lawrence, D.M., Slater, A.G., Tomas, R.A., Holland, M.M. and Deser, C., 2008. Accelerated Arctic land warming and permafrost degradation during rapid sea ice loss. *Geophysical Research Letters*, 35(11).
- Li, T., Grant, R.F. and Flanagan, L.B., 2004. Climate impact on net ecosystem productivity of a semi-arid natural grassland: modeling and measurement. *Agricultural and forest meteorology*, 126(1): 99-116.
- Lindroth, A. et al., 2009. Storms can cause Europe-wide reduction in forest carbon sink. *Global change biology*, 15(2): 346-355.
- Liu, S. et al., 2013. The Unified North American Soil Map and its implication on the soil organic carbon stock in North America. *Biogeosciences*, 10(5): 2915-2930.
- Ma, S., Baldocchi, D.D., Xu, L. and Hehn, T., 2007. Inter-annual variability in carbon dioxide exchange of an oak/grass savanna and open grassland in California. *Agricultural and Forest Meteorology*, 147(3): 157-171.
- Malcolm, J.R., Markham, A., Neilson, R.P. and Garaci, M., 2002. Estimated migration rates under scenarios of global climate change. *Journal of Biogeography*, 29(7): 835-849.

- Marcott, S.A., Shakun, J.D., Clark, P.U. and Mix, A.C., 2013. A reconstruction of regional and global temperature for the past 11,300 years. *science*, 339(6124): 1198-1201.
- McCaughey, J., Pejam, M., Arain, M. and Cameron, D., 2006. Carbon dioxide and energy fluxes from a boreal mixedwood forest ecosystem in Ontario, Canada. *Agricultural and Forest Meteorology*, 140(1): 79-96.
- McGowan, J.A., Cayan, D.R. and Dorman, L.M., 1998. Climate-ocean variability and ecosystem response in the Northeast Pacific. *Science*, 281(5374): 210-217.
- McKee, T.B., Doesken, N.J. and Kleist, J., 1993. The relationship of drought frequency and duration to time scales, *Proceedings of the 8th Conference on Applied Climatology*. American Meteorological Society Boston, MA, pp. 179-183.
- McKenney, D.W. and Pedlar, J.H., 2003. Spatial models of site index based on climate and soil properties for two boreal tree species in Ontario, Canada. *Forest Ecology and Management*, 175(1): 497-507.
- McManus, k.M. et al., 2012. Satellite-based evidence for shrub and graminoid tundra expansion in northern Quebec from 1986 to 2010. *Global Change Biology*, 18(7): 2313-2323.
- Melillo, J.M. et al., 2011. Soil warming, carbon–nitrogen interactions, and forest carbon budgets. *Proceedings of the National Academy of Sciences*, 108(23): 9508-9512.
- Mesinger, F. et al., 2006. North American Regional Reanalysis. *Bulletin of the American Meteorological Society*, 87(3): 343-360.
- Mesinger, F. et al., 2004. North American regional reanalysis, *Preprints AMS 2004 Annual meeting*, Seattle WA.

- Miller, J.R., Turner, M.G., SmithWick, E.A., Dent, C.L. and Stanley, E.H., 2004. Spatial extrapolation: the science of predicting ecological patterns and processes. *BioScience*, 54(4): 310-320.
- Monson, R.K. et al., 2005. Climatic influences on net ecosystem CO₂ exchange during the transition from wintertime carbon source to springtime carbon sink in a high-elevation, subalpine forest. *Oecologia*, 146(1): 130-147.
- Monteith, J.L., 1972. Solar Radiation and Productivity in Tropical Ecosystems. *Journal of Applied Ecology*, 9(3): 747.
- Moorcroft, P.R., 2006. How close are we to a predictive science of the biosphere? *Trends in Ecology & Evolution*, 21(7): 400-407.
- Murphy, D. et al., 2009. An observationally based energy balance for the Earth since 1950. *Journal of Geophysical Research: Atmospheres* (1984–2012), 114(D17).
- Myneni, R. et al., 2002. Global products of vegetation leaf area and fraction absorbed PAR from year one of MODIS data. *Remote sensing of environment*, 83(1): 214-231.
- Myneni, R.B., Keeling, C., Tucker, C., Asrar, G. and Nemani, R., 1997. Increased plant growth in the northern high latitudes from 1981 to 1991. *Nature*, 386(6626): 698-702.
- Natali, S.M., Schuur, E.A.G. and Rubin, R.L., 2012. Increased plant productivity in Alaskan tundra as a result of experimental warming of soil and permafrost. *Journal of Ecology*, 100(2): 488-498.
- Novick, K. et al., 2004. Carbon dioxide and water vapor exchange in a warm temperate grassland. *Oecologia*, 138(2): 259-274.

- Nowinski, N.S., Taneva, L., Trumbore, S.E. and Welker, J.M., 2010. Decomposition of old organic matter as a result of deeper active layers in a snow depth manipulation experiment. *Oecologia*, 163(3): 785-792.
- Oberbauer, S.F. et al., 2007. Tundra CO₂ fluxes in response to experimental warming across latitudinal and moisture gradients. *Ecological Monographs*, 77(2): 221-238.
- Olthof, I., Pouliot, D., Latifovic, R. and Wenjun, C., 2008. Recent (1986-2006) Vegetation-Specific NDVI Trends in Northern Canada from Satellite Data. *Arctic*, 61(4): 381-394.
- Oren, R. et al., 2006. Estimating the uncertainty in annual net ecosystem carbon exchange: Spatial variation in turbulent fluxes and sampling errors in eddy-covariance measurements. *Global Change Biology*, 12(5): 883-896.
- Pacala, S. et al., 2007. The North American carbon budget past and present.
- Palmer, T. and Räisänen, J., 2002. Quantifying the risk of extreme seasonal precipitation events in a changing climate. *Nature*, 415(6871): 512-514.
- Pan, Y. et al., 2011. Age structure and disturbance legacy of North American forests. *Biogeosciences*, 8(3): 715-732.
- Pan, Y., McGuire, A.D., Kicklighter, D.W. and Melillo, J.M., 2006. The importance of climate and soils for estimates of net primary production: a sensitivity analysis with the terrestrial ecosystem model. *Global Change Biology*, 2(1): 5-23.
- Parmesan, C. and Yohe, G., 2003. A globally coherent fingerprint of climate change impacts across natural systems. *Nature*, 421(6918): 37-42.
- Peng, C. et al., 2011. A drought-induced pervasive increase in tree mortality across Canada's boreal forests. *Nature climate change*, 1(9): 467-471.

- Peng, S., Piao, S., Wang, T., Sun, J. and Shen, Z., 2009. Temperature sensitivity of soil respiration in different ecosystems in China. *Soil Biology and Biochemistry*, 41(5): 1008-1014.
- Pereira, J.S. et al., 2007. Net ecosystem carbon exchange in three contrasting Mediterranean ecosystems -- the effect of drought. *Biogeosciences*, 4(5): 791-802.
- Peters, W. et al., 2007. An atmospheric perspective on North American carbon dioxide exchange: CarbonTracker. *Proceedings of the National Academy of Sciences*, 104(48): 18925-18930.
- Piao, S.L., Friedlingstein, P., Ciais, P., Viovy, N. and Demarty, J., 2007. Growing season extension and its impact on terrestrial carbon cycle in the Northern Hemisphere over the past 2 decades. *Global Biogeochemical Cycles*, 21(3).
- Pieper, S.J., Loewen, V., Gill, M. and Johnstone, J.F., 2011. Plant Responses to Natural and Experimental Variations in Temperature in Alpine Tundra, Southern Yukon, Canada. *Arctic, Antarctic, and Alpine Research*, 43(3): 442-456.
- Polyakov, I.V. et al., 2002. Observationally based assessment of polar amplification of global warming. *Geophysical Research Letters*, 29(18): 1878.
- Pouliot, D., Latifovic, R. and Olthof, I., 2009. Trends in vegetation NDVI from 1 km AVHRR data over Canada for the period 1985–2006. *International Journal of Remote Sensing*, 30(1): 149-168.
- Rastetter, E.B., Aber, J.D., Peters, D.P., Ojima, D.S. and Burke, I.C., 2003. Using mechanistic models to scale ecological processes across space and time. *BioScience*, 53(1): 68-76.
- Reich, P.B. et al., 2015. Geographic range predicts photosynthetic and growth response to warming in co-occurring tree species. *Nature Climate Change*.

- Reichstein, M. et al., 2013. Climate extremes and the carbon cycle. *Nature*, 500(7462): 287-295.
- Reichstein, M. et al., 2003. Modeling temporal and large-scale spatial variability of soil respiration from soil water availability, temperature and vegetation productivity indices. *Global biogeochemical cycles*, 17(4).
- Rigor, I.G., Colony, R.L. and Martin, S., 2000. Variations in surface air temperature observations in the Arctic, 1979-97. *Journal of Climate*, 13(5): 896-914.
- Ropelewski, C.F. and Halpert, M.S., 1986. North American precipitation and temperature patterns associated with the El Niño/Southern Oscillation (ENSO). *Monthly Weather Review*, 114(12): 2352-2362.
- Running, S.W. et al., 2004. A continuous satellite-derived measure of global terrestrial primary production. *BioScience*, 54(6): 547-560.
- Rustad, L. et al., 2001. A meta-analysis of the response of soil respiration, net nitrogen mineralization, and aboveground plant growth to experimental ecosystem warming. *Oecologia*, 126(4): 543-562.
- Sasai, T., Okamoto, K., Hiyama, T. and Yamaguchi, Y., 2007. Comparing terrestrial carbon fluxes from the scale of a flux tower to the global scale. *Ecological Modelling*, 208(2-4): 135-144.
- Schaefer, K. et al., 2012. A model-data comparison of gross primary productivity: Results from the North American Carbon Program site synthesis. *Journal of Geophysical Research: Biogeosciences* (2005–2012), 117(G3).
- Schmid, H.P., Grimmond, C.S.B., Cropley, F., Offerle, B. and Su, H.-B., 2000. Measurements of CO₂ and energy fluxes over a mixed hardwood forest in the mid-western United States. *Agricultural and Forest Meteorology*, 103(4): 357-374.

- Schuh, A.E. et al., 2010. A regional high-resolution carbon flux inversion of North America for 2004. *Biogeosciences*, 7(5): 1625-1644.
- Schuur, E.A. et al., 2008. Vulnerability of permafrost carbon to climate change: Implications for the global carbon cycle. *BioScience*, 58(8): 701-714.
- Schuur, E.A. et al., 2009. The effect of permafrost thaw on old carbon release and net carbon exchange from tundra. *Nature*, 459(7246): 556-559.
- Schwalm, C.R. et al., 2010a. A model-data intercomparison of CO₂ exchange across North America: Results from the North American Carbon Program site synthesis. *Journal of Geophysical Research: Biogeosciences (2005–2012)*, 115(G3).
- Schwalm, C.R. et al., 2010b. Assimilation exceeds respiration sensitivity to drought: A FLUXNET synthesis. *Global Change Biology*, 16(2): 657-670.
- Seager, R. et al., 2007. Model projections of an imminent transition to a more arid climate in southwestern North America. *Science*, 316(5828): 1181-1184.
- Seidl, R., Rammer, W., Scheller, R.M. and Spies, T.A., 2012. An individual-based process model to simulate landscape-scale forest ecosystem dynamics. *Ecological Modelling*, 231: 87-100.
- Serreze, M. and Francis, J., 2006. The Arctic Amplification Debate. *Climatic Change*, 76(3-4): 241-264.
- Serreze, M.C. et al., 2000. Observational Evidence of Recent Change in the Northern High-Latitude Environment. *Climatic Change*, 46(1-2): 159-207.
- Shaver, G.R. et al., 2000. Global Warming and Terrestrial Ecosystems: A Conceptual Framework for Analysis. *BioScience*, 50(10): 871-882.

- Siegenthaler, U. et al., 2005. Stable Carbon Cycle-Climate Relationship During the Late Pleistocene. *Science*, 310(5752): 1313-1317.
- Sjögersten, S. and Wookey, P.A., 2002. Climatic and resource quality controls on soil respiration across a forest–tundra ecotone in Swedish Lapland. *Soil Biology and Biochemistry*, 34(11): 1633-1646.
- Stocks, B.J. et al., 2002. Large forest fires in Canada, 1959–1997. *Journal of Geophysical Research*, 108(D1).
- Stott, P.A. and Kettleborough, J., 2002. Origins and estimates of uncertainty in predictions of twenty-first century temperature rise. *Nature*, 416(6882): 723-726.
- Sulman, B., Desai, A., Cook, B., Saliendra, N. and Mackay, D., 2009. Contrasting carbon dioxide fluxes between a drying shrub wetland in Northern Wisconsin, USA, and nearby forests. *Biogeosciences*, 6(6): 1115-1126.
- Sun, X. and Barros, A.P., 2010. An Evaluation of the Statistics of Rainfall Extremes in Rain Gauge Observations, and Satellite-Based and Reanalysis Products Using Universal Multifractals. *Journal of Hydrometeorology*, 11(2).
- Swann, A.L., Fung, I.Y., Levis, S., Bonan, G.B. and Doney, S.C., 2010. Changes in Arctic vegetation amplify high-latitude warming through the greenhouse effect. *Proceedings of the National Academy of Sciences*, 107(4): 1295-1300.
- Tagesson, T. et al., 2012. High-resolution satellite data reveal an increase in peak growing season gross primary production in a high-Arctic wet tundra ecosystem 1992–2008. *International Journal of Applied Earth Observation and Geoinformation*, 18: 407-416.
- Taylor, K.E., 2001. Summarizing multiple aspects of model performance in a single diagram. *Journal of Geophysical Research*, 106(D7): 7183.

- Thomas, C.K. et al., 2009. Seasonal hydrology explains interannual and seasonal variation in carbon and water exchange in a semiarid mature ponderosa pine forest in central Oregon. *Journal of Geophysical Research: Biogeosciences* (2005–2012), 114(G4).
- Thornton, P.E. et al., 2012. Daymet: Daily surface weather on a 1 km grid for North America, 1980-2008, Oak Ridge National Laboratory (ORNL).
- Tucker, C.J., 1979. Red and photographic infrared linear combinations for monitoring vegetation. *Remote Sensing of Environment*, 8(2): 127-150.
- Tucker, C.J., Newcomb, W.W., Los, S.O. and Prince, S.D., 1991. Mean and inter-year variation of growing-season normalized difference vegetation index for the Sahel 1981-1989. *International Journal of Remote Sensing*, 12(6): 1133-1135.
- Tucker, C.J. et al., 2001. Higher northern latitude normalized difference vegetation index and growing season trends from 1982 to 1999. *International Journal of Biometeorology*, 45(4): 184-190.
- Turner, D.P. et al., 2006. Evaluation of MODIS NPP and GPP products across multiple biomes. *Remote Sensing of Environment*, 102(3-4): 282-292.
- Turner, D.P. et al., 2005. Site-level evaluation of satellite-based global terrestrial gross primary production and net primary production monitoring. *Global Change Biology*, 11(4): 666-684.
- Urbanski, S. et al., 2007. Factors controlling CO₂ exchange on timescales from hourly to decadal at Harvard Forest. *Journal of Geophysical Research: Biogeosciences* (2005–2012), 112(G2).

- van Aardenne, J.A., Dentener, F.J., Olivier, J.G.J., Goldewijk, C.G.M.K. and Lelieveld, J., 2001. A 1°×1° resolution data set of historical anthropogenic trace gas emissions for the period 1890–1990. *Global Biogeochemical Cycles*, 15(4): 909-928.
- Van Bogaert, R. et al., 2011. A century of tree line changes in sub-Arctic Sweden shows local and regional variability and only a minor influence of 20th century climate warming. *Journal of Biogeography*, 38(5): 907-921.
- van der Molen, M.K. et al., 2011. Drought and ecosystem carbon cycling. *Agricultural and Forest Meteorology*, 151(7): 765-773.
- Van Mantgem, P.J. et al., 2009. Widespread increase of tree mortality rates in the western United States. *Science*, 323(5913): 521-524.
- van Nes, E.H. and Scheffer, M., 2005. IMPLICATIONS OF SPATIAL HETEROGENEITY FOR CATASTROPHIC REGIME SHIFTS IN ECOSYSTEMS. *Ecology*, 86(7): 1797-1807.
- Verbyla, D., 2008. The greening and browning of Alaska based on 1982–2003 satellite data. *Global Ecology and Biogeography*, 17(4): 547-555.
- Verma, S.B. et al., 2005. Annual carbon dioxide exchange in irrigated and rainfed maize-based agroecosystems. *Agricultural and Forest Meteorology*, 131(1): 77-96.
- Walker, M.D. et al., 2006. Plant community responses to experimental warming across the tundra biome. *Proceedings of the National Academy of Sciences of the United States of America*, 103(5): 1342-1346.
- Walther, G.-R. et al., 2002. Ecological responses to recent climate change. *Nature*, 416(6879): 389-395.

- Wan, Z., Wang, P. and Li, X., 2004. Using MODIS land surface temperature and normalized difference vegetation index products for monitoring drought in the southern Great Plains, USA. *International Journal of Remote Sensing*, 25(1): 61-72.
- Wang, Z. et al., 2013. Incorporating weather sensitivity in inventory-based estimates of boreal forest productivity: A meta-analysis of process model results. *Ecological Modelling*, 260: 25-35.
- Wang, Z. et al., 2011. Evaluating weather effects on interannual variation in net ecosystem productivity of a coastal temperate forest landscape: A model intercomparison. *Ecological Modelling*, 222(17): 3236-3249.
- Way, D.A. and Oren, R., 2010. Differential responses to changes in growth temperature between trees from different functional groups and biomes: a review and synthesis of data. *Tree Physiology*, 30(6): 669-688.
- Webster, M.D. et al., 2002. Uncertainty in emissions projections for climate models. *Atmospheric environment*, 36(22): 3659-3670.
- Wei, Y. et al., 2014. The North American Carbon Program Multi-scale Synthesis and Terrestrial Model Intercomparison Project–Part 2: Environmental driver data. *Geoscientific Model Development*, 7(6): 2875-2893.
- Westerling, A.L., Hidalgo, H.G., Cayan, D.R. and Swetnam, T.W., 2006. Warming and earlier spring increase western US forest wildfire activity. *science*, 313(5789): 940-943.
- White, M.A. et al., 2009. Intercomparison, interpretation, and assessment of spring phenology in North America estimated from remote sensing for 1982-2006. *Global Change Biology*, 15(10): 2335-2359.

- Williams, A.P. et al., 2013. Temperature as a potent driver of regional forest drought stress and tree mortality. *Nature Climate Change*, 3(3): 292-297.
- Williams, A.P. et al., 2010. Forest responses to increasing aridity and warmth in the southwestern United States. *Proceedings of the National Academy of Sciences*, 107(50): 21289-21294.
- Xiao, J. et al., 2011. Assessing net ecosystem carbon exchange of U.S. terrestrial ecosystems by integrating eddy covariance flux measurements and satellite observations. *Agricultural and Forest Meteorology*, 151(1): 60-69.
- Zha, T. et al., 2009. Carbon sequestration in boreal jack pine stands following harvesting. *Global Change Biology*, 15(6): 1475-1487.
- Zhang, K. et al., 2008. Satellite-based model detection of recent climate-driven changes in northern high-latitude vegetation productivity. *Journal of Geophysical Research*, 113(G3).
- Zhang, X. et al., 2014. Multi-scale geospatial agroecosystem modeling: A case study on the influence of soil data resolution on carbon budget estimates. *Science of The Total Environment*, 479: 138-150.
- Zhao, Y. et al., 2012. How errors on meteorological variables impact simulated ecosystem fluxes: a case study for six French sites. *Biogeosciences*, 9(7): 2537-2564.
- Zhu, W. et al., 2012. Extension of the growing season due to delayed autumn over mid and high latitudes in North America during 1982-2006. *Global Ecology and Biogeography*, 21(2): 260-271.